Investigation of wound characteristics and the force associated with skull fracture due to impact by a hammer

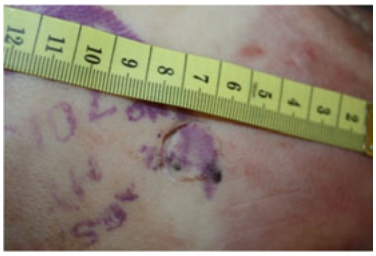

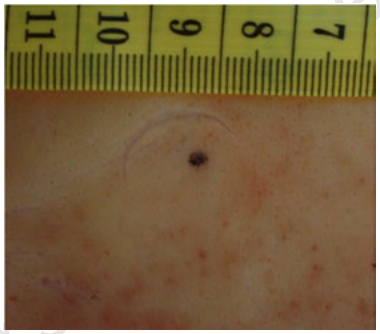

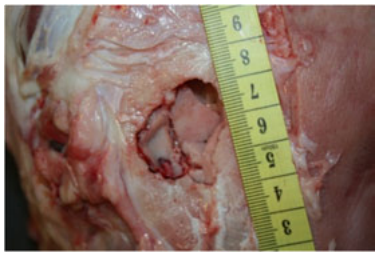

Calvin Gerald Mole (MLXCAL001)

MPhil Biomedical Forensic Science

Division of Forensic Medicine and Toxicology

Department of Clinical Laboratory Sciences

Faculty of Health Sciences

University of Cape Town

Dr. M. Heyns (supervisor)

May 2014

Plagiarism Declaration

I, Calvin Gerald Mole, hereby declare that this submission is my own work and that, to the best of my knowledge and belief, it contains no material previously published or written by another person nor material which to a substantial extent has been accepted for the award of any other degree or diploma of the university or other institute of higher learning, except where due acknowledgment has been made in the text.
I empower the university to reproduce for the purpose of research either the whole or any portion of the contents in any manner whatsoever.

Signed by candidate

Calvin Gerald Mole
MPhil Biomedical Forensic Sciences
MLXCAL001
University of Cape Town
Medical Campus
10 May 2014

Abstract

Death due to cranial blunt force trauma is a major issue not just in South Africa but worldwide. The vast majority of studies conducted on cranial blunt force trauma have analysed trauma to the frontal portion of the head. This is due to the involvement of the frontal portion of the head in automotive accidents. The lateral portion of the head is however no less important and is often impacted during homicidal assault.

In cases involving cranial blunt force trauma, a common question asked of experts relates to the amount of force involved with a particular trauma. The goal of forensic science in general is to provide objective, repeatable results. At present, however, answering this question relies on a subjective rating scale of mild, moderate or severe force. Determining the severity of the force is also subjective, in that it relies heavily on the experience of the expert. Forensic anthropology by its nature is often subjective; however there is a need to move away from conducting analyses based predominantly on the experience of the investigator.

With this in mind, this dissertation offers background information on fracture mechanics and impact biomechanics and provides a current review of the literature surrounding lateral impact to the skull. The research conducted as part of this dissertation attempts to quantify the force and energy involved with lateral impact to the skull due to a blow by a hammer, as well as describes the wound morphology associated with such impacts.

Human tissue for experimentation is becoming increasingly difficult to acquire. There is therefore a need to determine suitable models for use in such testing. In the current study whole porcine heads were impacted on the fronto-parietal portion of the cranium. Half of the specimens were impacted with an implement resembling the shape and weight of a hammer. These hammer tests were conducted primarily to determine the type of trauma associated with such impacts and determine if a correlation exists between velocity or energy of impact and the level of trauma sustained.

The remaining specimens were impacted with a Hopkinson pressure bar of the same diameter as the striker in the hammer tests. The Hopkinson pressure bar apparatus allows for the determination of the force of impact. The use of the Hopkinson pressure bar to determine fracture forces in whole specimens is novel.

The fracture forces obtained in the current study agree considerably with the literature previously published on lateral, cranial blunt force trauma to both human and porcine specimens. The fractures produced, however, are atypical and may indicate a need to conduct further tests on other animal models.

Contents

Chapter 1:

Foreword

1.1. Acknowledgements

I am eternally indebted to the following people, without whom this project would not have been possible:

- **Dr Marise Heyns:** For her tireless supervision of this project.
- **Mr Trevor Cloete:** Of the Blast Impact and Survivability Research Unit (BISRU), Department of Mechanical Engineering, University of Cape Town, for his supervision and expertise in the engineering aspects of the study and for the use of the BISRU facilities.
- **Mr Rudi Harmse:** Of Winelands Pork for supplying the porcine specimens utilised in the study.
- **Mr Charles Harris:** For the construction of the suspension rig utilised in the study.
- **Mr Victor Twala:** Of the Western Cape Government, Department of Agriculture for supporting the project.
- **Mr John Frost, Ms Natasha Kloppers and Mr Sean Langton:** For their assistance with the design and drawing process of the suspension rig.
- **My colleagues:** Ms Danielle Cupido**,** Mr Mohaimin Kasu and Ms Rolanda Londt for all their help and encouragement when I needed it.
- **University of Cape Town Postgraduate Office:** For funding.

1.2. List of abbreviations

AP: Antero-posterior

DIHB: Direct impact Hopkinson bar

N.A: Neutral axis

SHB: Split Hopkinson bar

1-D: One-dimensional

3-D: Three-dimensional

Notations used in calculations

(Note: standard units of measurement in brackets)

a: Acceleration (m/s^2)

A: Area (m^2)

c: Speed of sound (m/s)

E_y: Young's modulus (N/m^2)

F: Force (N)

g: Gravitational acceleration (9.8 m/s^2)

I: Second moment area (m^4)

J: Joules

KE: Kinetic energy (J)

Kg: Kilograms

K_G: Gauge factor

M: Mass (kg)

N: Newtons

P: Pressure (Pa)

Pa: Pascals

t: time (s)

v: Velocity (m/s^1)

ε: Strain

σ: Stress (Pa)

Δ: Deflection (m)

τ : Time it takes a stress wave to travel the length of a bar

ρ: Density (Kg/m^3)

1.3. List of figures

1.4. List of tables

Chapter 2:
Proposal

Proposal for Masters Dissertation:

Investigation of wound characteristics and the energy associated with skull fracture due to impact by a hammer

Calvin Gerald Mole (MLXCAL001)

MPhil Biomedical Forensic Science

Division of Forensic Medicine and Toxicology

Department of Clinical Laboratory Sciences

Faculty of Health Sciences

University of Cape Town

Supervisor: Dr Marise Heyns

2.1. Background

The human skull is a complex three-dimensional structure made up of several bones. The bones of the cranial vault are made up of three layers. The inner and outer layers consist of high density compact bone while the central layer has a porous structure similar to cancellous bone. The geometry of each skull bone is unique both internally and externally. The thickness of the skull as well as the curvature of the skull varies in different regions. The temporal region has a concave (medial) curve and the parietal region has a convex curve and the temporal region is much thinner than the parietal region [1]. Furthermore the frontal region is unique in that it contains the frontal sinus making it structurally different to other regions of the cranial vault. All of these factors contribute to the complexity of studying how a skull fractures and the force involved with a fracture.

The composition of bone allows for it to be strong but flexible, however a fracture can occur when a force is applied in such a way as to exceed the strength or maximum threshold of elasticity of the bone. The size, shape, speed of impact and degree of force of an impacting mass as well as the impacting energy will determine the resulting fracture. An impacting mass causes compression on the side of impact (outer cortex) and tension on the inner cortex directly opposite the site of impact. Bone fails first in the area of tension and the fracture spreads to the outer cortex. A fracture will follow the path of least resistance along a bone radiating outwards from the site of impact. As the fracture moves secondary sites of compression and tension are created which causes the formation of concentric fractures which transect the radiating fractures [2].

The majority of studies looking at fracture tolerance of the skull have focussed on the frontal bone due to the attention of researchers to frontal impact in vehicle accidents [1]. However more research needs to be conducted on the lateral side of the skull because of its importance in homicidal blunt force trauma. The left lateral aspect of the skull, particularly the parietal region, has been shown to be the most commonly fractured region of the skull in cases of head trauma due to a blunt instrument [3].

2.2. Introduction

Previously conducted studies relating to the energy and force of impact causing cranial bone to fail (fracture) have used a number of different methods to impart a blow of a given energy to various areas of the skull. These methods include the use of free-fall methods (a whole body or head is dropped from a height and impacts with a surface), drop tests (a mass is dropped from a height using a modified tower to impact with a head), pistons (hydraulic/pneumatic piston impacts with a head) and modified pendulums (a mass attached to a pendulum impacts with a head) [1, 4]. Although drop tests are the most common method used to impart a force, the inertial effects of the dropped mass may result in the crushing of the skull between the impacting component

and the floor of the drop tower. This results in parameters which differ from a normal blow to the head.

The use of different methods has also led to a range of results being published. In 1880, Messerer was the first to begin conducting studies on the force involved with trauma to the head. Messerer conducted compression tests in the lateral direction using 13 unembalmed human cadaver heads and reported fracture forces ranging from 400kg to 800kg [1]. In 1968 Nahum and colleagues conducted a study using an impacting mass to deliver blows to the temporo-parietal region of embalmed and unembalmed cadaver heads [5]. From this study it was concluded that the minimum tolerance level for the temporo-parietal region was 2450N for males and 2000N for females. In a follow up study to this Schneider and Nahum [6] performed drop tests using varying weights at known velocities (3-6m/s) and found a tolerance level of 3630N for the temporo-parietal region. In 1977 a pneumatic piston was used to produce lateral impacts to the heads of unembalmed cadavers seated in an upright position [7]. This study showed peak forces ranging from 4210N to 9590N and concluded the lateral part of the skull can withstand forces of approximately 5000N without fracturing.

More recently studies by Baumer et al. [8] and Powell et al. [9] have performed impact studies using porcine specimens. These studies demonstrated that an increased energy of impact is needed to initiate skull fracture in older specimens compared to younger specimens and it was also demonstrated that a greater amount of fracturing occurred at higher impact energies.

However, relatively few studies have focussed on the tolerance level of skulls to impact by specific implements. Raymond and colleagues [10, 11] investigated the tolerance of the temporo-parietal region to blunt ballistic impact (impact by a low velocity projectile) by performing impact studies with a 38mm projectile at velocities ranging from 18m/s – 37m/s. The peak fracture force in the temporo-parietal region was found to be approximately 5600N and the authors observed an initial force tolerance level of 2346N. It was also noted that the energy of the impact played a role in the type of fracture caused by the impact, with linear fractures occurring at lower energies (~27 J) compared to depressed, comminuted fractures (~58 J) [10]. Another study designed a drop rig to allow for the attachment of different implements and performed drop tests on the fronto-parietal region of pig heads [12]. Two implements used in this study to demonstrate different blunt force impacts were a hammer and a wooden broom handle. Sharkey and colleagues [12] found that the minimum force associated with laceration of the skin by these implements was approximately 4000N and that the shape of the lacerations produced was indicative of the implement used. In terms of skull fractures, for both the hammer and broom handle the most common skull damage observed was in the form of diastatic fractures (suture separation); the incidence of which increased as

the force of impact increased. Suture separation was first observed at a force of 4150N with the hammer and 6524N with the broom handle.

2.3. Rationale behind study

When confronted with a case involving trauma to the head, forensic pathologists are often asked questions such as: “What instrument could have been used to cause this trauma?” and “How much force is associated with these types of injuries?”

Even though blunt and sharp force homicides have been considered some of the most common forms of homicide [13], there are relatively few studies which have set out to document the types of injuries associated with blunt or sharp force trauma from specific weapons. Even fewer studies have set out to determine the impacting energy involved with trauma from specific implements. As such answering the aforementioned questions becomes a complex task often relying on subjective assessments, such as experience gained from previous cases, and the use of arbitrary, subjective, rating scales such as mild, moderate or severe force.

It is therefore imperative that further studies be conducted to accurately document wound characteristics and the energy associated with trauma due to specific implements.

2.4. Aims and objectives

The primary objective of this study is therefore to determine the energy and force involved with trauma to the head due to blows with a hammer.

The secondary objectives of this study are to describe the wound morphology:

a) In soft tissue (skin laceration) caused by blows to the head with a hammer.
b) In hard tissue (cranial fracture patterns) caused by blows to the head with a hammer.

2.5. Materials and methods

2.5.1. Test rig

A gas gun test rig (Fig. 2.1), stabilised on a metal I-beam, will be used to deliver an impact to the centre of the parietal region of the pig head by each implement of interest. These implements will be two hammer heads of differing size and mass. A gas gun is an apparatus which uses pressurised gas to propel a projectile down a barrel.

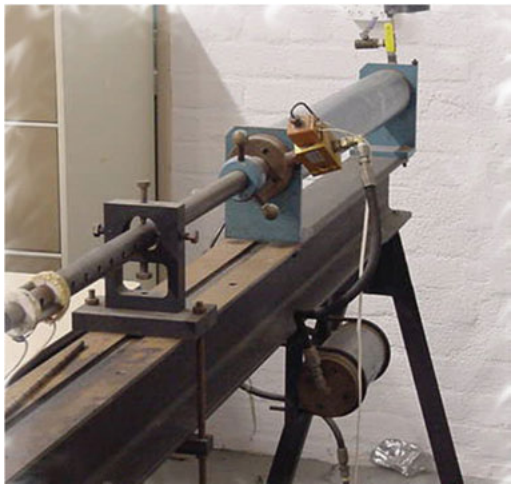

Fig. 2.1 A gas gun

2.5.2. Specimen preparation

Porcine head specimens (n=30) which have previously been approved for human consumption will be obtained from a local supplier (Winelands Pork). Specimens will be placed in a leak proof body bag for transportation. Upon delivery until testing commences, specimens will be stored in fridges at -20ºC. The fridges to be used run independently with their own cooling systems and will be used specifically for the porcine specimens of this project. Two different fridges will be utilised; one for storage of fresh specimens and one for storage of used specimens prior to disposal. Prior to testing the specimens will be thawed at room temperature for 24hrs and will be visually inspected for any signs of head injury. Specimens with visible head injury before testing will be excluded from the study. All tests will be performed on the porcine heads with the skin and skull contents intact. All areas to be utilized in this project, including the fridge, thawing, testing and processing areas, are access controlled.

For testing, thawed specimens will be transported to the department of Engineering BISRU (Blast Impact and Survivability Research Unit) lab located at Upper Campus, University of Cape Town.

The porcine head will be suspended in netting in front of the test rig by means of a pendulum, to allow for movement of the specimen after impact. This is to provide a more realistic outcome of impact to the head than if the specimen were to be rigidly restrained prior to impact.

2.5.3. Analysis

Impact tests will be performed using each implement at three different impact velocities in a range of approximately 10m/s – 30m/s (in increments of 10m/s). The velocity of each impact will be adjusted by increasing or decreasing the pressure in the gas gun

and each impact will be repeated five times. Each specimen will be subjected to a single impact. This will result in a total of 30 impact tests on 30 porcine specimens.

During each impact the final velocity and the time of flight of the projectile will be measured. As the mass of each implement is known the following data can be calculated:

- Energy of impact [$KE = \frac{1}{2}MV^2$; where KE denotes kinetic energy/energy of impact (J), M denotes impacting mass (kg) and V denotes velocity at impact (m/s)]
- Acceleration [V= U + AT; where V denotes velocity at impact (m/s), U denotes initial velocity (m/s), A denotes acceleration (m/s^2) and T denotes time (s)]
- Force of initial impact [F = M.A; where F denotes the impacting force (N), M denotes the impacting mass (Kg) and A denotes acceleration (m/s^2)]

Following impact the skin of the specimen will be inspected for laceration. Any soft tissue damage will be documented and photographed. The site of impact will then be cleaned by removing the soft tissue and periosteum. This will be followed by a visual inspection for any fracture of the skull.

Specimens showing fracture of the skull after initial visual inspection shall be thoroughly cleaned by means of dissection. Fractures will be documented and photographed.

2.6. Work plan

Activity	Week1 (Jan 1-6)	2	3	4	5	6	7	8	9	10	11	12	13	14	15	16	17	18	19	20	21	22
Proposal																						
Ethics																						
Lit Review																						
Intro and methods (thesis)																						
Experiments																						
Results (thesis)																						
Write up																						

Activity	Week23 (June 3-9)	24	25	26	27	28	29	30	31	32	33	34	35	36	37	38	39	40	41	42	43	44
Experiments																						
Results (thesis)																						
Write up																						
Discussion (thesis)																						
Drafts and completion of Thesis																						

2.7. References

1. Yoganandan NA, Pintar FA (2004) Biomechanics of temporo-parietal skull fracture. Clin Biomech 19:225 – 239.

2. Kroman A, Kress T, Porta D (2011) Fracture propagation in the human cranium : A re-testing of popular theories. Clin Anat 24:309 – 318.

3. Kremer C, Racette S, Dionne C, Sauvageau A (2008) Discrimination of falls and blows in blunt head trauma: Systematic study of the hat brim line rule in relation to skull fractures. J Forensic Sci 53:716 – 719.

4. Verschueren P, Delye H, Depreitere B, Van Lierde C, Haex B, Berckmans D, Verpoest I, Goffin J, Vander Sloten J, Van der Perre G (2007) A new test set-up for skull fracture characterisation. J Biomech 40:3389 – 3396.

5. Nahum AM, Gatts JD, Gadd CW, Danforth J (1968) Impact tolerance of the skull and face. Proc Stapp Car Crash Conf 12:302 – 316.

6. Schneider DC, Nahum AM (1972) Impact studies of facial bones and skulls. Proc Stapp Car Crash Conf 16:186 – 203.

7. Stalnaker R, Melvin J, Nuscholtz G, Alem N, Benson J (1977) Head impact response. Proc Stapp Car Crash Conf 21:305 – 335.

8. Baumer TG, Passalacqua N V, Powell BJ, Newberry WN, Fenton TW, Haut RC (2010) Age dependent fracture characteristics of rigid and compliant surface impacts on the infant skull—A porcine model. J Forensic Sci 55:993 – 997.

9. Powell BJ, Passalacqua N V, Baumer TG, Fenton TW, Haut RC (2012) Fracture patterns on the infant porcine skull following severe blunt impact. J Forensic Sci 57:312 – 317.

10. Raymond D, Van Ee C, Crawford G, Bir C (2009) Tolerance of the skull to blunt ballistic temporo-parietal impact. J Biomech 42:2479 – 2485.

11. Raymond D, Crawford G, Van Ee C, Bir C (2009) Development of biomechanical response corridors of the head to blunt ballistic temporo-parietal impact. J Biomech Eng. doi: 10.1115/1.3194751.

12. Sharkey E, Cassidy M, Brady J, Gilchrist M, NicDaeid N (2011) Investigation of the force associated with the formation of lacerations and skull fractures. Int J Leg Med 126:835 – 834.

13. Ambade VN, Godbole HV (2006) Comparison of wound patterns in homicide by sharp and blunt force. Forensic Sci Int 156:166 – 70.

2.8. Addendum

Since writing this proposal, some of the methodology has been slightly altered. This addendum provides an explanation for these changes.

It was decided that calculating the force involved with an impact using Newton's second law would be inaccurate and open to criticism. It was therefore decided that in addition to conducting the impact tests described in the proposal, impact tests using the Hopkinson pressure bar apparatus would also be conducted. The Hopkinson pressure bar allows for a far more accurate determination of the force of impact.

Due the addition of Hopkinson pressure bar tests, it was decided to conduct the experiments using an implement of only one size (mass: 200g, diameter: 20mm).

Finally, it was decided not to use specimens which had been frozen and subsequently thawed prior to testing. The effects of conducting impact tests on previously frozen specimens are unknown and warrant further study. However, attempting to determine if prior freezing of specimens has any effect on the results produced during impact tests was beyond the scope of this study. Therefore, specimens were obtained fresh on the day of testing.

Chapter 3
Review:

Fracture Mechanics and Lateral Impact Biomechanics of the Skull

3.1. Trauma analysis in forensic anthropology

The analysis of trauma in forensic anthropology often requires a multidisciplinary approach, including but not limited to anatomy, biomechanics, pathology and physics. As such the following review will provide basic information relating to bone: its structure, basic biomechanics, and how it fractures. This will be followed by a critical review of the literature surrounding the biomechanics of lateral head impact.

The study of forensic anthropology has grown considerably over the years and today specialists in forensic anthropology are often called upon to garner as much information as they can from skeletal material in the pursuit of justice. In cases of blunt trauma forensic anthropologists may be asked, among other things, to determine the number and sequence of blows, the point of impact(s), the direction and angle of impact(s), the shape and type of implement used and the amount of energy or force used.

The interpretation of trauma as seen in the skeleton is however a difficult task [1]. Bone trauma is generally divided into three categories, namely; sharp, blunt and ballistic trauma. Each of these categories have markers or signs which are usually characteristic of that type of trauma, however problems can arise when sharp trauma produces characteristics of blunt trauma or ballistic trauma resembles typical blunt trauma. These traumas are often classified as sharp-blunt and blunt-ballistic trauma which can be confusing and misleading. It is therefore best to view these categories as a continuum rather than a set of discreet characteristics [2]. It is also important to distinguish between trauma which is old and healing, perimortem trauma (inflicted around the time of death) and postmortem trauma due to taphonomic factors. Such information may form an important part of criminal proceedings where an accurate interpretation of trauma is of paramount importance. It is therefore not only essential to understand the boundaries and limitations of trauma analysis but also to continually push the envelope of research to improve what we are capable of discerning from trauma inflicted upon bones, as well as to refine and validate what we already know.

3.2. Basic biomechanics of bone

Biomechanics is a multidisciplinary field combining the knowledge of mechanics, as applied to physics and engineering, with the biological knowledge of the human body [3]. More succinctly, biomechanics is the application of engineering principles to biological systems [4]. The mechanical properties and anatomical structure of bone will play a role in how a bone will react to both natural and unnatural forces which are applied to it. Disease states can affect the mechanical properties of bone; as such the disease state of a bone also performs a role in determining if a fracture will occur after a traumatic incident.

3.2.1. Histology of bone

Bone is composed of bone cells and an extracellular matrix. The extracellular matrix is primarily made up of inorganic material (60% w/w) consisting mostly of calcium and phosphate in the form of impure hydroxyapatite crystals. This inorganic component is what gives bone its hardness and rigidity but also makes it brittle. The organic component (30% w/w) of the extracellular matrix, called osteoid, is predominantly made up of type I collagen and various proteoglycans and glycosaminoglycans which give bone its flexibility and elasticity. The remaining 10% w/w of the extracellular matrix is made up of water [3].

Bone has a hierarchical structural organisation which consists of macroscopic and microscopic structures [5]. Macroscopically there are two different types of bone which can be identified in humans. These are compact (cortical) bone and spongy (cancellous) bone. A typical long bone has a shaft (diaphysis) which consists of a central marrow cavity surrounded by spongy bone and an outer layer (cortex) of compact bone. The epiphysis or head of long bones consists of spongy bone surrounded by a thin layer of compact bone. The bones of the skull however, are different in that they consist of a layer of spongy bone (diploë) sandwiched between two

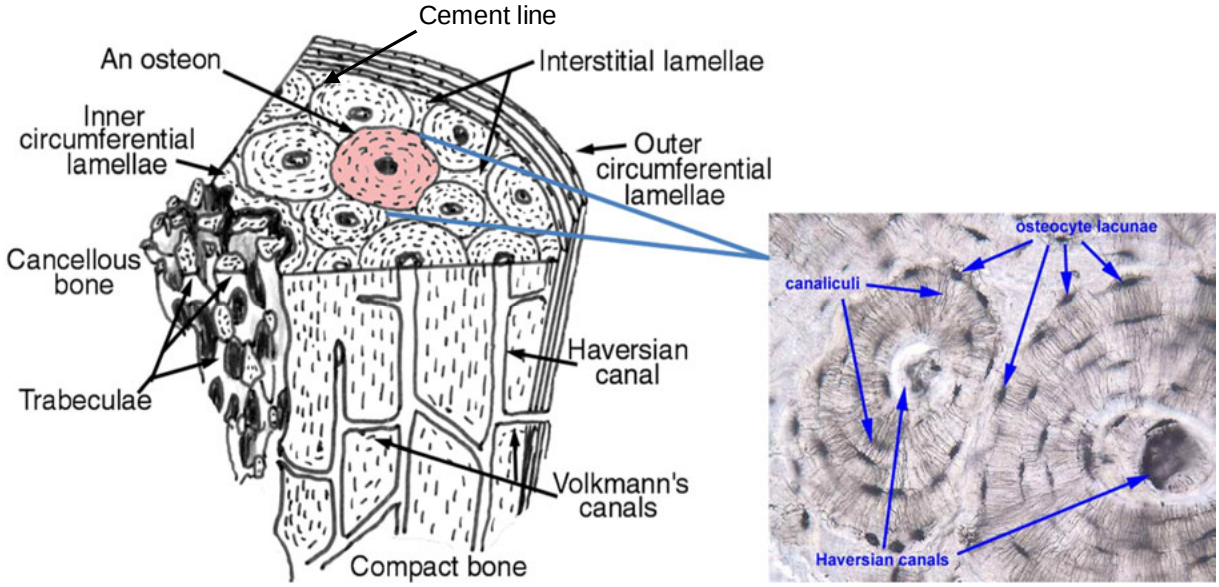

Fig. 3.1 Section through a long bone (adapted from [58])

layers of cortical bone. Cancellous bone is made up of bony trabecular struts and marrow filled cavities making it more porous and less dense than cortical bone. Cancellous bone is also more metabolically active than cortical bone.

Microscopically the structural unit of cortical bone is the osteon or Haversian system (fig. 3.1). Osteons are not present in spongy bone. Osteons are long cylindrical

structures which run roughly parallel to the long axis of the diaphysis. The longitudinal arrangement of osteons is what makes long bones very strong in compression. At the centre of every osteon is a canal, the Haversian canal, which contains blood vessels, lymph vessels and nerves. A number of concentric circles can be found around each Haversian canal called lamellae. Blood vessels, lymph vessels and nerves also run perpendicular to the Haversian canals in what are called Volkmann's canals. Interstitial systems, which are the remnants of old osteons, can be found in the area between adjacent osteons. The junction between an osteon and the interstitial bone is known as the cement line. The cement line is a highly mineralised, collagen free layer. Surrounding the inner and outer layers of cortical bone are circumferential lamellae.

The structure of bone is directly related to its functions, which include: providing structural support, the protection of internal organs, providing an attachment site for muscles and facilitating muscle actions and body movements. Bone may also act as a storage well for certain nutrients such as calcium, as well as housing marrow which is responsible for producing blood and stem cells. Bone is metabolically active throughout life and can react to stresses and strains placed upon it. For example the body can lay down more bone in areas which experience regular stress and can remove bone after periods of disuse (Wolff's Law). It is believed that 10% - 15% of the bone in the body is replaced every year [4]. This production and remodelling of bone is achieved at a cellular level by specialised cells called osteoblasts and osteoclasts.

3.2.2. Terminology

There are a number of concepts which are fundamental to the study of biomechanics. Following is a list of these concepts and their definitions as applicable to the study of biomechanics.

Load and stress (σ): A load is a force or a combination of forces which are borne by an object. There are a number of different modes of loading which can affect bone (Fig.3.2). These modes of loading are often referred to as stress. Stress may be defined as force per unit area and is measured in newtons per metre squared (N/m^2) or pascals (Pa).

$$\text{Stress} = \text{Force}/\ \text{Area}$$

Tension is the pulling apart of an object by equal and opposite loads and it causes a structure to lengthen and narrow. Compression is the opposite of tension. During compression equal and opposite loads are applied toward the surface of a structure causing it to shorten and widen. Shear stress causes angular deformation in a structure, for example when a structure is loaded in shear, lines which were originally orthogonal will become acutely or obtusely angled. Bending occurs when loads act on a structure in such a way to cause the structure to bend about an axis. Bending causes a bone to be subjected to a combination of compression and tension in various areas on either side of the bending. Because cortical bone is weaker in tension than compression, a fracture usually initiates on the side subjected to tension [3, 6]. Torsion occurs when a load is applied to a structure in such a way as to cause it to twist about an axis. This twisting action causes shear stress to occur throughout the structure.

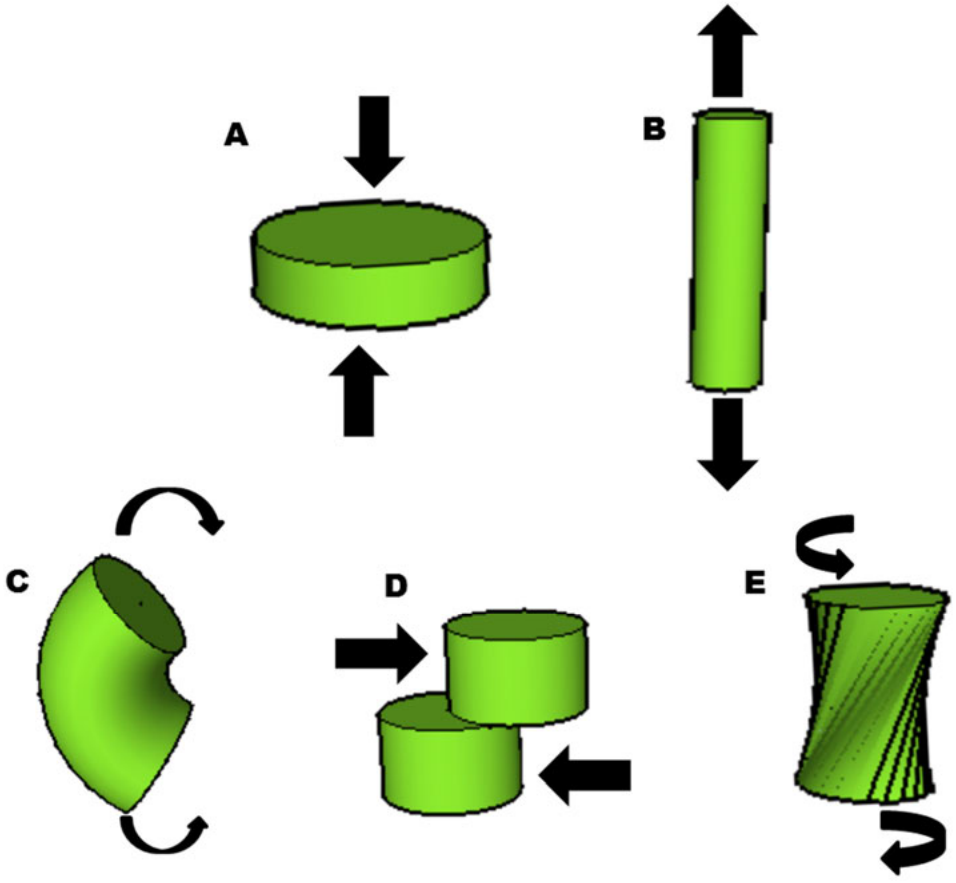

Fig. 3.2 Different modes of loading. A: Compression. B: Tension. C: Bending. D: Shear. E: Torsion.

Anisotropy: Bone is an anisotropic material which means it has different properties when it is loaded in different directions. For example bone is stronger in compression than in tension and is able to withstand a greater stress in compression compared to stress in tension and in shear respectively [3]. The modulus of elasticity of human bone is also greater in longitudinal loading compared to transverse and shear loading respectively (Table 3.1). In real life, forms of loading rarely occur in isolation. Loading usually occurs as a combination of different loading forms across a bone which has been subjected to a force, as described in bending. These differences in properties noted during loading in different directions are as a result of the anatomical structure of bone.

Table 3.1 Summary of the properties of human cortical bone [59]

Parameter	Value (MPa)
Modulus of elasticity	
Longitudinal	17 000
Transverse	11 500
Shear	3 300
Ultimate strength (longitudinal loading)	
Tension	133
Compression	193
Shear	68
Ultimate strength (transverse loading)	
Tension	51
Compression	133

Strain (ε): Strain is a measure of the degree of deformation [7] (distortion) and can be expressed as the ratio of change in length.

Strain = change in length/ original length.

Young's Modulus (E_y): Also known as the modulus of elasticity is the ratio of stress to strain in the elastic region of a material. It is often used to demonstrate the stiffness of a material [7].

$$E_y = \frac{Stress}{Strain} = \frac{\sigma}{\varepsilon}$$

Deformation: If a bone is placed under strain there are two types of deformation which a bone will go through before it fails (fractures). These two types of deformation are elastic and plastic deformation. Elasticity is defined as the property of a material to return to its normal shape and size after the removal of a load [3]. Elastic deformation is

therefore not permanent. The deformation occurs when a load is placed on the bone, however when the load is removed the bone returns to its normal shape and size. However, if a load is applied to bone which exceeds the elastic limit of the bone, plastic deformation will occur. Plastic deformation is permanent. If plastic deformation occurs the bone will not return to its normal shape and size after the load has been removed. For plastic deformation to occur, a visible fracture of the bone need not be present.

Viscoelasticity: Bone is a viscoelastic structure. This means it has both fluid and solid properties. Viscoelastic materials have a unique response to loading which is dependent on how quickly a load is applied or removed. Under high rates of loading (e.g. a bullet fired from a gun) bone may behave as a brittle material and fracture quickly under the load [3]. This can be seen histologically where fractures induced by low strain rate propagate around the osteons through the interstitial lamellae while fractures induced by high strain rate propagate indiscriminately through the bone [3]. In other words bone is capable of withstanding a greater load if the load is applied at a slow rate.

Force: Force is defined as a mechanical disturbance or load [3]. A force has direction and has the ability to alter the state of motion of an object [6]. Force can be found in numerous forms, for example an object can be pushed or pulled in a direction and weight is the force of gravity on an object. The body is subjected to various forces at any given time; however when these forces exceed the tolerance levels of certain tissues, injury can occur. In the case of bone, these injuries may be in the form of a fracture. The force of an impact plays an important role in the propagation of a fracture and the extent of damage which will be seen. It is believed that, provided all other factors are constant, a blunt impact to the head with a greater force will result in numerous radiating and concentric fractures, while a blunt impact with less force may result in the production of only a small linear fracture [8].

Newton's first law of motion states that an object will remain at rest or an object will move in a straight line at a constant velocity provided the net force acting on that object is zero. This law indicates that a force must be applied to an object in order to change its velocity or direction.

Newton's second law of motion states that an object with nonzero net force acting upon it will accelerate in the direction of the applied force and that the magnitude of acceleration will be proportional to the magnitude of the applied force. Using this law, if the mass and acceleration of an impacting object are known, an approximation of the force of impact can be calculated using the following equation:

$$\text{Force} = \text{mass} \times \text{acceleration}$$

$$F = m.a$$

Where force is measured in Newtons (N), mass in kilograms (Kg) and acceleration in metres per second squared (m/s^2).

Energy of impact: The amount of energy transferred in an impact also plays an important role in determining the extent of damage which may be caused by an impact. Kinetic energy is the energy associated with motion [6]. The amount of energy absorbed will be dependent on the surface which is impacted. A harder surface will dissipate a greater amount of energy. Therefore in an impact to the skull, kinetic energy is related to the amount of bone displacement. A greater transfer of energy will result in more damage to the skull. Kinetic energy can be calculated as follows:

$$KE = \frac{1}{2}MV^2$$

Where KE denotes kinetic energy measured in joules (J) or Newton metres (Nm), M denotes mass measured in kilograms (Kg) and V denotes velocity measured in metres per second (m/s).

3.3. Cranial blunt force trauma

3.3.1. Fracture mechanics

There are a number of extrinsic and intrinsic factors which contribute to the formation of a fracture. Extrinsic factors include the speed and magnitude of the impact as well as the size and shape of the impacting object. Intrinsic factors which will contribute to the formation of a fracture are the elasticity, plasticity, density and the health state of the bone. Certain diseases such as osteoporosis and osteitis deformans (Paget's disease) or congenital defects such as osteogenesis imperfecta structurally weaken bone making them more susceptible to fracture.

A fracture occurs when the limits of elasticity of a bone are reached. An accurate interpretation of fractures of the skull is vital and can provide a wealth of information including the origin of impact, the number and sequence of blows, and the implement used. Pathologists or anthropologists are often asked to gather such information in the course of an investigation. However with the advent of new technologies, much of the previous literature has been shown to be out-dated and incorrect and therefore further research in this area is warranted to ensure accurate interpretation of trauma.

Historically, most of what we know about how a human skull fractures comes from the work of Gurdjian and colleagues [9–12]. In summary these studies concluded that an impact to the skull will cause distortion of the shape of the skull. At the point of impact there will be an in-bending of the skull and this causes a compensatory out-bending of

other regions of the skull. The greatest area of out-bending could even be diagonally opposite the point of impact. This out-bending causes areas of high tensile force which causes the initiation of a fracture. For this reason it was believed that cranial fractures initiate from a location remote to the impact site and travel back to the point of impact following lines of structural weakness. This theory has been published in a number of well-known texts [13–15]. However this theory was not seen in actual cases and has therefore recently been challenged [8].

Using high speed video, Kroman et al. [8] demonstrated that fractures initiate at the point of impact and radiate outward. The videos of the tests showed no areas of out-bending, as previously described, on the skull during impact. This study however demonstrated that a fracture can occur remote to the site of impact if the skull is impacted against a rigid surface. A practical example of this would be if a victim's head were to be stamped on; fractures would occur at the point of impact of the boot and the head and at the point of contact between the head and the ground.

It is important to understand that the mechanism of fracture propagation is different in blunt trauma and ballistic trauma and will result in different fracture patterns [16–19]. The mechanism of fracture propagation due to blunt force trauma in the skull can be seen in figure 3.3. An impacting mass causes compression on the side of impact (outer cortex) and tension on the inner cortex directly opposite the site of impact. Bone fails first in tension and the fracture spreads to the outer cortex (site of compression). A fracture will follow the path of least resistance along a bone radiating outwards from the site of impact until its energy is dispelled. Regions of low resistance include sutures, sinuses and foramina [20]. Points of high resistance which seem to inhibit fracture propagation are buttressed areas of the skull where the bone is thicker and therefore stronger [21]. As the bone continues to bend inwards secondary sites of compression and tension are created causing the formation of concentric fractures which intersect the radiating fractures. In blunt force trauma the secondary sites of tension are found on the outer table of the skull causing concentric fractures to first fracture on the outer table and travel inward [17, 19].

An impact to the head may not produce a visible fracture. In some cases a low energy impact will only cause a fracture on the inner table of the skull. On the other hand high energy impacts may cause depressed fractures and it is believed that the depressed fracture may resemble the shape of the impacting object, making identification of a weapon possible [11, 14, 22–24]. However, a number of authors suggest that accurate identification of a weapon by the shape of a fracture is not possible and such attempts at identifying a weapon should be avoided [1, 25]. It is however possible to determine the number and sequence of impacts in cases involving multiple blows to the skull. reconstructing the sequence of impacts is achieved by applying Puppe's rule which states that if two or more fracture lines produced by different impacts intersect, the

fracture line which occurred later will terminate in the fracture line which occurred earlier [14, 26].

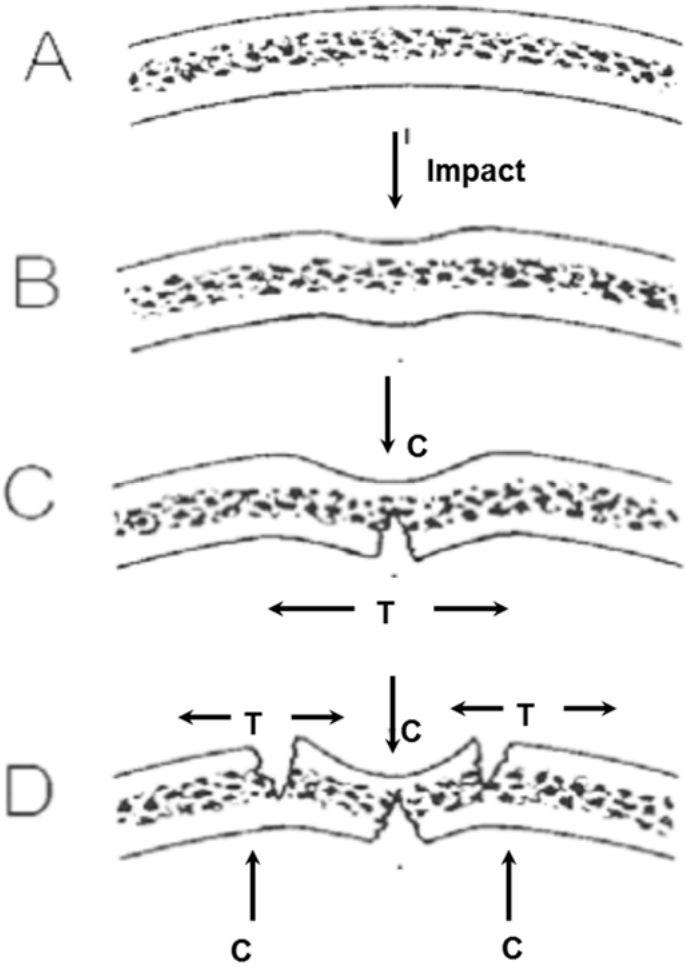

Fig. 3.3 Sequence of events in blunt force fracture propagation (adapted from [60])

3.3.2. Types of skull fracture

There are a number of different categories which skull fractures fall into according to the extent and pattern of the fracture. Following is a list of fracture types which are applicable to blunt force trauma of the head. This list is by no means extensive or complete but represents the most commonly occurring fracture patterns in blunt force trauma of the head [14]. It is also important to note that these fracture types are not mutually exclusive and they often present as a combination of two or more fracture patterns.

Linear fracture: These are common fractures which radiate out from the point of impact. Linear fractures generally occur as a result of low velocity impact with a large contact area [13]. As the name implies linear fractures form lines which can be straight or curved [14]. A specific type of linear fracture is a hinge fracture. Hinge fractures run across the base of the cranium in the middle fossa, anterior to the foramen magnum splitting the cranial base in two. A hinge fracture usually occurs due to a blunt force impact of high energy or high energy ballistic trauma to the lateral part of the head [2, 13, 27].

Diastatic fracture: A diastatic fracture also known as suture separation is the major separation of two bones along the suture line. This most frequently occurs along the sagittal suture and is more commonly seen in children [13, 14].

Depressed fracture: A depressed fracture occurs when the impact causes part of the outer cortex of the skull to be pushed inwards. Depressed fractures generally occur as a result of impact with a high kinetic energy but a small area of impact [13]. These fractures can intrude into the cranial cavity or they may be absorbed by the diploë of the skull. The size of the depression is dependent on the size of the contact area of the impacting object and energy of the impact. Greater impact energy will result in a greater displacement of bone.

Comminuted fracture: These fractures are commonly found in combination with depressed fractures. Comminuted fractures exhibit extensive fragmentation of the bone often in a web like pattern. Because of their appearance, comminuted fractures of the skull are also sometimes referred to as mosaic or spider's web fractures [14].

3.4. Biomechanical studies conducted on the lateral aspect of the skull

A large amount of funding and research has gone into the study of impact biomechanics of the frontal bone and bones of the face, owing to their involvement in automotive accidents [28]. Far fewer studies have been conducted on the force and energy associated with fracture of the lateral part of the skull, however this region is of no less importance. Lateral impacts of the skull do occasionally occur in vehicular accidents, particularly when the head impacts one of the side pillars of the vehicle. In terms of homicide, the left parietal bone is found to be the most commonly fractured area of the skull in homicidal blunt force trauma [29–31].

Studies have been conducted using a variety of methods to impart a blow of given energy or force on a specific area of the skull. The most common method employed has been the use of drop tests whereby a mass is dropped from a height, using a modified tower, to impact with a head. Other approaches employed include the use of free-fall methods (a whole body or head is dropped from a height and impacts with a surface), pistons (hydraulic/pneumatic piston impacts with a head) and modified pendulums (a

mass attached to a pendulum impacts with a head) [28, 32]. Following is a synopsis of previously conducted research around the biomechanics of the lateral part of the skull. A summary of the results from these studies can be seen in table 3.2 and figure 3.4.

3.4.1. Early studies (1800 – 1960)

Historically, studies on the biomechanics of head injuries have been conducted since the early 1800's. Bruns in 1854 performed compression tests using a vice made of two planks of wood. Undamaged human heads were used and changes in the diameter of the skull were measured [33]. In 1880 an attempt was made to measure the force associated with skull fracture [34]. Using seven male and six female unembalmed human cadaver heads, Messerer conducted static compression tests in the lateral direction and found mean peak fracture forces of 4792N in males and 5507N in females. The same tests were also conducted in the antero-posterior (AP) plane on a further 12 specimens to simulate frontal loading. These results demonstrated that under static loading the human skull appeared to be stronger in the AP direction as opposed to the lateral direction [28].

In the 1940's and 1950's Gurdjian and colleagues extensively studied the biomechanics of injury to the human skull [9–12, 35]. These studies used a free-fall method whereby embalmed intact human cadaver heads and dry human skulls coated with a strain sensitive lacquer were dropped from a height onto a solid steel slab. The energy of the impacts to the left or right posterior parietal region were calculated and ranged from 653J to 1230J. The impact velocities ranged from 5.0m/s to 6.3 m/s. This energy was found to be greater than the energy threshold for fracture in both the frontal and occipital bone suggesting that under impact loading the parietal bone was the strongest bone followed by the frontal bone and occipital bone respectively [10].

3.4.2. Recent studies (1960 – present)

The 1960's and 1970's saw a surge in biomechanical studies conducted primarily or in part on the lateral aspect of the skull. In 1968, Nahum and colleagues used a drop tower to allow a mass to impact the temporo-parietal region of five embalmed and five unembalmed human cadaver heads [36]. The velocity of the impacts was not measured but the study revealed a mean fracture force of 3123N ± 623N and 3944N ± 1287N for the temporo-parietal region of female and male specimens respectively. This was found (in contrast to the results by Gurdjian and colleagues [10]) to be less than the forces measured for the frontal bone and the study concluded by suggesting a minimum fracture tolerance level for the temporo-parietal region of 2000N for females and 2450N for males [36].

This was followed up with a study conducted by Schneider and Nahum in 1972 [37]. Intact cadavers and isolated head specimens were subjected to impacts by dropped weights. The weights ranged from 1.1kg to 3.8kg resulting in impact velocities ranging

from 3m/s to 6m/s. The mean fracture force of the temporo-parietal region was found to be 3630N ± 969N for all specimens in this study. The study also revealed overlap in the data between intact cadaver specimens and isolated head specimens. These results suggest that the use of either whole or isolated specimens are acceptable for future studies [37].

Hodgson and Thomas (1971) [38] conducted free fall tests on intact human cadavers. Specimens were hung upside down and raised to a specific height from where the cadaver was dropped to impact the surface of a flat plate. A cord was attached to the head of the cadavers to ensure impact with the desired region of the head. Drop heights ranged from 12.7cm to 114.3cm which resulted in impact velocities ranging from 1.6m/s to 4.7m/s. Cadavers were dropped multiple times, increasing the height each time until fracture of the skull occurred. A load cell was mounted underneath the impact surface to record the impact force. The mean peak impact force for the lateral part of the head was found to be 10151N ± 4928N, with a range of 5560N – 17792N. These peak forces were greater than those seen for the frontal region but less than those seen for the occipital region of the skull [38]. This study recorded far greater forces necessary to cause fracture than many other studies. This may be as a result of performing free fall tests with intact cadavers, as the mass of the entire body is behind the force (Newton's second law). The impact with the floor provides a large contact area during impact which will also cause larger forces.

In 1977, Stalnaker and colleagues [39] performed impact tests on five unembalmed intact human cadavers using a pneumatic piston. The cadavers were strapped to a chair seated in an upright position and subjected to impacts to the left lateral aspect of the head. The impactor had a diameter of 15.2cm and a striker surface with a load cell attached. The entire assembly of the impacting piston had a mass of 10kg. Impact velocities for the tests ranged from 6m/s to 9m/s. Three padded and two rigid impacts were performed. For the padded impacts, the striker surface was covered with a 25mm ensolite foam pad. None of the padded impacts resulted in a fracture however both rigid impacts did at forces of 7150N and 9600N. The peak forces of the padded impacts ranged from 4200N to 4800N. These results suggested that the lateral aspect of the head is able to withstand approximately 5000N of force without causing skull fracture.

In 1978, Got and colleagues [40] performed free fall tests on fresh, unembalmed, perfused cadavers which were either helmeted or not helmeted. Tests were designed to provide impacts to the frontal, temporo-parietal and fronto-facial regions. Force was measured using a force transducer placed under the impact surface. Five unhelmeted cadavers were used for impact tests on the temporo-parietal region. Two rigid impact tests were performed from drop heights of 1.8m and 2.5m. This resulted in impact velocities of 5.99m/s and 7m/s and peak forces of 12200N and 12500N respectively. Both the rigid impact tests produced fractures. These results are again greater than

results seen in other studies possibly as a result of performing free fall tests with whole cadavers. The three tests performed using a padded impact were all dropped from a height of 3m, resulting in an impact velocity of 7.67m/s. The range of peak forces produced was 5000N – 10100N and no fractures were noted in the padded impacts.

Allsop and colleagues (1991) [41] performed drop tests on 31 unembalmed cadaver heads using either a 12kg flat rectangular plate (5 x 10cm) or a 10.6kg flat circular plate (diameter: 2.54cm). The rectangular plate was used to deliver an impact to the parietal region at a velocity of 4.3m/s and the circular plate was used to deliver an impact to the temporo-parietal region at a velocity of 2.7m/s. Piezoelectric transducers were placed behind the impactors to measure force and an acoustic emission sensor was placed on the skull near the point of impact to detect any fracture. A mean fracture force of 12390N ± 3654N was found for the parietal region and 5195N ± 1010N for the temporo-parietal region. The authors also concluded that the mineral content of the bone did not significantly affect the fracture force. However, a larger contact area during impact was found to significantly increase peak forces.

A few years later, Yoganandan and colleagues [42] used an electrohydraulic testing device to deliver quasistatic and dynamic loads to various regions of intact cadaver heads. Quasistatic loading was performed on the parietal region at a rate of 2.5mm/s Specimens were rigidly attached to a structure via the auditory miatii. The impactor had a diameter of 48mm. The failure forces for the parietally loaded specimens ranged from 4464N to 5915N and energy of impact ranged from 14.07J to 18.88J. Only one specimen was loaded temporally and the failure force was found to be 6182N. These regions of the head did not undergo dynamic loading tests.

More recently (2004) Yoganandan and colleagues [43] performed free fall tests using intact, unembalmed, cadaver heads. Specimens were orientated in such a way as to allow impact to the lateral side of the head. A load cell was placed under the impact surface (50mm thick, 40-durometer padding) to measure force. Each specimen was repeatedly dropped, increasing the velocity of impact until fracture occurred. Impact velocities ranged from 4.9m/s to 7.7m/s. Four of the ten specimens sustained fractures while another four out of ten tests were stopped because the rated limit of the load cell (10KN) was about to be reached. The peak forces for these tests ranged from 5556N to 9917N and the energy of impact ranged from 16J to 73J. The results demonstrated that an increased impact severity (increased velocity of impact) resulted in an increased force and energy.

Table 3.2 Summary of studies previously conducted on the biomechanics of the lateral part of the skull

Study	Test	Skull Region	Fracture force	Energy	Velocity	Load Type	Impactor type	Specimen type
Messerer, 1880	Compression test	Lateral	3971N – 7247N			Static		Unembalmed, human heads
Gurdjian et al., 1949	Free fall test	Parietal		653J – 1230J	5m/s – 6.3m/s	Dynamic	Solid steel slab	Dry human skulls
Nahum et al., 1968	Drop test	Temporo-parietal	2215N – 5930N		Not measured	Dynamic	Steel weights (1.1kg – 3.8kg)	Embalmed and unembalmed, human heads
Hodgson and Thomas, 1971	Free fall test	Lateral	5560N – 17792N		1.6m/s – 4.7m/s	Dynamic	Solid steel slab	Intact human cadavers
Schneider and Nahum, 1972	Drop test	Temporo-parietal	2110N – 5200N		3m/s – 6m/s	Dynamic	Steel weights (1.1kg – 3.8kg)	Intact human cadavers
Stalnaker et al., 1977	Pneumatic piston	Lateral	7150N – 9600N		6m/s – 9m/s	Dynamic	10kg steel piston (unpadded)	Intact human cadaver
Got et al., 1978	Free fall test	Temporo-parietal	12200N – 12500N		5.9m/s – 7m/s	Dynamic	Solid steel slab	Intact human cadaver
Allsop et al., 1991	Drop test (circular disk 5cm^2)	Temporo-parietal	2500N – 10000N		4.3m/s	Dynamic	10.6kg flat circular plate (diameter: 2.5cm)	Unembalmed human heads
Allsop et al., 1991	Drop test (rectangular plate 50cm^2)	Temporo-parietal	5800N – 17000N		2.7m/s	Dynamic	12kg flat rectangular plate (5 x 10cm)	Unembalmed human heads
Yoganandan et al., 1995	Electrohydraulic piston	Parietal	4464N – 5915N	14J – 19J	2.5mm/s	Static	Steel piston. Diameter: 48mm	Unembalmed human heads
Yoganandan et al., 2004	Free fall test	Lateral	5556N – 9918N	16J – 73J	4.9m/s – 7.7m/s	Dynamic	50mm thick, 40-durometer padding	Unembalmed human heads
Raymond et al., 2009a,b	Gas gun (38.1mm rigid projectile)	Temporo-parietal	3547N – 9529N	54.1J -63.8J	20m/s and 35m/s	Dynamic	Rigid aluminium projectile. 0.103kg, 38mm diameter	Unembalmed human heads
Sharkey et al., 2011	Drop test (hammer)	Fronto-parietal	4150N – 8137N		7.4m/s	Dynamic	Hammer 2cm diameter	Porcine heads
Sharkey et al., 2011	Drop test (wooden broom handle)	Fronto-parietal	6524N – 8676N		7.4m/s	Dynamic	Wooden broom handle (30cm length, 2.2cm diameter	Porcine heads

In 2009 Raymond and colleagues set out to determine the tolerance of the skull to blunt ballistic impacts [44, 45]. Less-lethal projectiles deliver a blunt, ballistic impact at a high energy, generally through the use of rubber or plastic ammunitions. Muzzle energies for these weapons have a reported range of 160J to approximately 700J [46]. Although these weapons are designed to be “less-lethal”, severe injury is possible. In the United States of America between 1985 and 2000, 2% (19/768) of case reports for less-lethal weapon use accounted for head injuries of which 37% were lacerations and 26% were fractures [47]. Using a gas gun, Raymond and colleagues subjected the temporo-parietal region of unembalmed, isolated cadaver heads to impacts by a rigid aluminium projectile (diameter: 38mm; mass: 0.103kg). The projectile was hollow to allow for placement of an accelerometer. Strain gauges were also placed around the proposed area of impact of the skull to determine the time of fracture. Impact force was calculated by applying Newton’s second law. Specimens were impacted at a velocity of 20m/s on one side of the skull and 35m/s on the other side. At an impact velocity of 20m/s two of the seven impacts resulted in fracture: a linear fracture at a peak force of 6347N and energy of 27.4J and a depressed, comminuted fracture at a peak force of 3376N and energy of 19.6J. At an impact velocity of 35m/s only two of the seven impacts did not result in a fracture. All the fractures were depressed, comminuted fractures. The peak forces for these impacts ranged from 3547N – 9529N and the energies ranged from 54.1J – 63.8J. However, this data may be skewed due to impacting the same head on two different occasions. Even though opposite sides of the heads were used the initial impact could possibly have decreased the structural integrity of the skull as a whole, causing the data obtained from the second impact to be unreliable.

Sharkey et al., (2011) [48] performed drop tests on the fronto-parietal region of pig heads. A drop rig was designed to allow for the attachment of different implements. Two implements used in this study to demonstrate different blunt force impacts were a hammer (2cm diameter) and a wooden broom handle (30cm length, 2.2cm diameter). These weapons were dropped from a height of 2.8m and the attached weight was varied to increase or decrease the force of impact. An accelerometer attached to the drop rig measured data. Eighteen impact experiments were performed for each implement. The authors found that the minimum force associated with laceration of the skin by these implements was approximately 4000N and that the shape of the lacerations produced was indicative of the implement used. In terms of skull fractures, for both the hammer and broom handle the most common skull damage observed was in the form of diastatic fractures; the incidence of which increased as the force of impact increased. Suture separation was first observed at a force of 4150N with the hammer and 6524N with the broom handle.

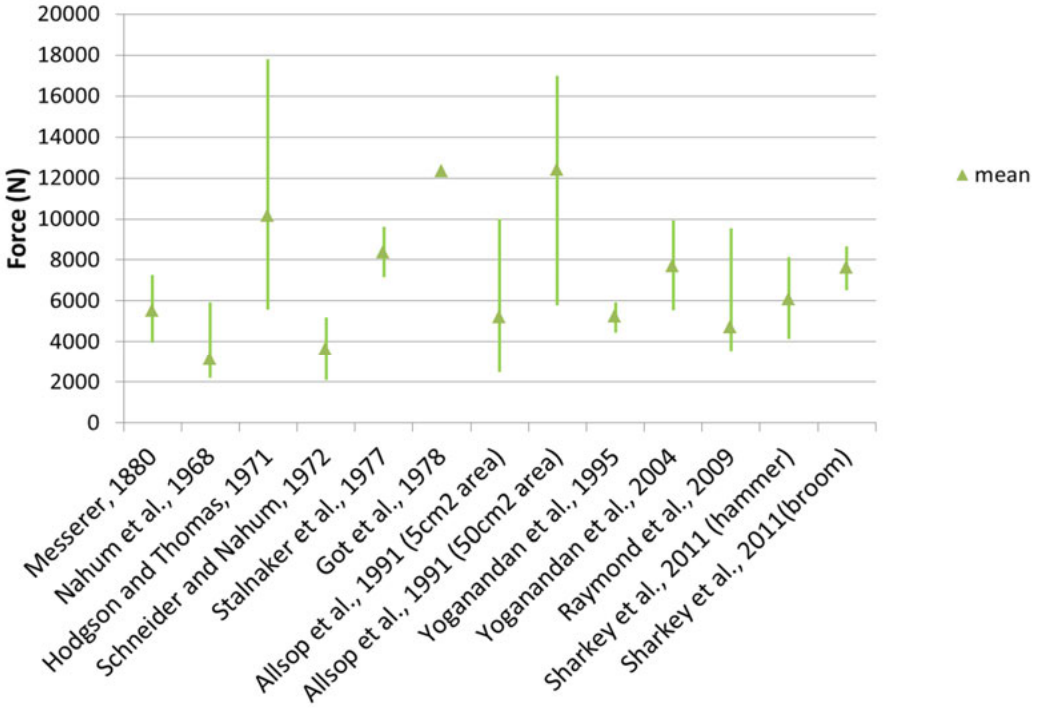

Fig. 3.4 Comparison of fracture force of lateral part of skull between studies

In an attempt to study the biomechanics of skull fracture in infants, Baumer et al., (2010) [49] and Powell et al., (2012) [50] conducted drop tests on isolated intact heads of infant porcine specimens. Specimens between the ages of 2 – 28 days were subjected to impacts to the centre of the parietal bone by either a compliant (deformable aluminium cylinder) or rigid (solid aluminium cylinder) interface with an impact surface area of 16cm^2 and a mass of 1.67kg. A load transducer placed behind the impactor measured force over time. The moment of fracture was determined by a sudden drop in the force – time plot of a specific impact. Baumer and colleagues [49] demonstrated that the energy and force needed to fracture the skull increased with the age of the specimen which was attributed to an increase in parietal bone thickness with age. It was also noted that the compliant interface caused more damage than the rigid interface to skulls less than 17 days of age, the opposite of which was found for specimens aged between 24 and 28 days. The follow up study conducted by Powell and colleagues [50] doubled the impact energies (3.1J – 22.6J) by doubling the drop heights used in the experiments. It was again found that the impact force increased with the age of the specimen for both the compliant and rigid interfaces. However, in contrast to the previous study the rigid interface caused more damage than the compliant interface at all ages demonstrating how bone is sensitive to the rate of loading, acting more brittle at a greater rate of loading. In terms of fracture propagation this study was in agreement with the theories proposed by Gurdjian and colleagues [9–12], noting the origination of fractures distant

to the site of impact. It was also found that a greater energy of impact resulted in more areas of fracture remote to the impact site, notably fracture of the occipital bone.

3.5. Summation

In the United Kingdom it has been shown that skull fractures account for approximately 6% of cases of fractures seen in hospitals, with a far greater incidence of skull fracture in men compared to women [51, 52]. A study in India showed that 41% of homicides over a period of three years were due to blunt force trauma; an overwhelming 80% of which involved the head [53]. A review of blunt force trauma cases in Ireland over a period of nine years demonstrated that 70% of blows resulted in both fracture of the skull and laceration of the scalp [48]. Cape Town, South Africa has one of the highest homicide rates in the world and homicide/ assault is the second leading cause of premature death in the city [54, 55]. Blunt force trauma is the third leading form of homicide after sharp force trauma and ballistic trauma respectively, making up 13% of homicides [56]. Clearly an understanding of blunt force trauma to the head is a critical tool in the analysis of forensic cases.

As can be seen in this review a number of studies have been conducted on lateral impacts to the head, however the results of these studies vary greatly. This may be due to the wide range of methodologies employed. For example, studies which repeatedly impacted a specimen until a fracture occurred [38, 43] may have inaccurate results, because with each successive impact the structural integrity and therefore the properties of the bone may have changed.

It is also interesting to note, with the exception of the studies conducted by Raymond and colleagues [44, 45], no studies have examined impacts at velocities greater than 10m/s. This is because the majority of tests conducted have utilised drop rigs and free fall tests where the attainable impact velocity is limited by the height of the drop. This however leaves a whole area of higher velocity blunt impacts with no discernable data.

The controversy surrounding the Gurdjian theories is another issue of concern. Not only does the rigid restraint of heads during impact tests not reflect the reality of head movement during impact, but it has also been shown to cause fractures remote to the sight of impact, which may lead to confusion [2]. It has also been noted that restraint of the specimen resulted in more fracturing of the paediatric porcine skull than free fall tests of the same energy [57].

It is clear that direct one to one comparison between the studies in this review are nearly impossible and all the variables need to be taken into account if a comparison is to be made. However, there is evidently a need to conduct further research in this area and any future research should attempt to address some of these issues.

3.6. References

1. Dirkmaat DC, Cabo LL, Ousley SD, Symes SA (2008) New perspectives in forensic anthropology. Yearb Phys Anthr 51:33 – 52.

2. Kroman A (2007) Fracture biomechanics of the human skeleton. University of Tennessee, Knoxville

3. Nordin M, Frankel VH (2012) Basic biomechanics of the musculoskeletal system, 4th Ed. Lippincott Williams and Wilkins, Philadelphia.

4. Ethier CR, Simmons CA (2007) Introductory biomechanics. From cells to organisms. Cambridge University Press, Cambridge.

5. Rho J, Kuhn-Spearing L, Zioupos P (1998) Mechanical properties and the hierarchical structure of bone. Med Eng Phys 20:92 – 102.

6. Low J, Reed A (1996) Basic biomechanics explained. Butterworth Heinemann, Oxford.

7. Hearn EJ (1997) Mechanics of Materials 1: An introduction to the mechanics of elastic and plastic deformation of solids and structural materials, 3rd Ed. Butterworth Heinemann, Oxford.

8. Kroman A, Kress T, Porta D (2011) Fracture propagation in the human cranium : A re-testing of popular theories. Clin Anat 24:309 – 318.

9. Gurdjian ES, Webster JE, Lissner HR (1947) The mechanism of production of linear skull fractures. Surg Gyn Obst 85:195 – 210.

10. Gurdjian ES, Webster JE, Lissner HR (1949) Studies on skull fracture with particular reference to engineering factors. Am J Surg 78:736 – 742.

11. Gurdjian ES, Webster JE, Lissner HR (1950) The mechanism of skull fracture. J Neurosurg 2:106 – 114.

12. Gurdjian ES, Webster JE, Lissner HR (1953) Observations on prediction of fracture site in head injury. Radiology 60:226 – 235.

13. DiMaio VJ, DiMaio D (2001) Forensic pathology, 2nd Ed. CRC Press, London.

14. Saukko P, Knight B (2004) Knight's forensic pathology, 3rd Ed. Arnold, London.

15. Shkrum MJ, Ramsay DA (2007) Forensic pathology of trauma: Common problems for the pathologist. Humana Press, New Jersey.

16. Smith O, Berryman H, Lahren C (1987) Cranial fracture patterns and estimate of direction from low velocity gunshot wounds. J Forensic Sci 32:1416 – 1421.

17. Berryman HE, Haun SJ (1996) Applying forensic techniques to interpret cranial fracture patterns in an archaeological specimen. Int J Osteoarchaeol 6:2 – 9.

18. Berryman HE, Symes SA (1998) Recognising gunshot and blunt cranial trauma through fracture interpretation. In: Reichs K (ed) Forensic osteology: Advances in the identification of human remains. Charles C Thomas, Springfeild, Il, pp 333 – 352.

19. Hart GO (2005) Fracture pattern interpretation in the skull: Differentiating blunt force from ballistics trauma using concentric fractures. J Forensic Sci 50:1276 – 1281.

20. Fenton TW, Stefan VH, Wood LA, Sauer NJ (2005) Symmetrical fracturing of the skull from midline contact gunshot wounds : Reconstruction of individual death histories from skeletonized human remains. J Forensic Leg Med 50:274 – 285.

21. Moritz A (1954) The pathology of trauma, 2nd Ed. Lea and Febiger, Philadelphia.

22. Clark EG, Sperry KL (1992) Distinctive blunt force injuries caused by a crescent wrench. J Forensic Sci 37:1172 – 1178.

23. Delannoy Y, Becart A, Colard T, Delille R (2012) Skull wounds linked with blunt trauma (hammer example). A report of two depressed skull fractures–Elements of biomechanical explanation. Leg Med 14:258 – 262.

24. Grassberger M, Gehl A, Püschel K, Turk EE (2011) 3D reconstruction of emergency cranial computed tomography scans as a tool in clinical forensic radiology after survived blunt head trauma - Report of two cases. Forensic Sci Int 207:e19 – 23.

25. Passalacqua N, Fenton T (2012) Developments in skeletal trauma : Blunt-force trauma. In: Dirkmaat DC (ed) A companion to forensic anthropology. Blackwell, Oxford, pp 400 – 411.

26. Viel G, Gehl A, Sperhake J (2009) Intersecting fractures of the skull and gunshot wounds . Case report and literature review. Forensic Sci Med Pathol 5:22 – 27.

27. Betz P, Stiefel D, Hausmann R, Eisenmenger W (1997) Fractures at the base of the skull in gunshots to the head. Forensic Sci Int 86:155 – 161.

28. Yoganandan NA, Pintar FA (2004) Biomechanics of temporo-parietal skull fracture. Clin Biomech 19:225 – 239.

29. Kremer C, Racette S, Dionne C, Sauvageau A (2008) Discrimination of falls and blows in blunt head trauma: Systematic study of the hat brim line rule in relation to skull fractures. J Forensic Sci 53:716 – 719.

30. Kremer C, Sauvageau A (2009) Discrimination of falls and blows in blunt head trauma: Assessment of predictability through combined criteria. J Forensic Sci 54:923 – 926.

31. Guyomarc'h P, Campagna-vaillancourt M, Kremer C, Sauvageau A (2010) Discrimination of falls and blows in blunt head trauma: A multi-criteria approach. J Forensic Sci 55:423 – 427.

32. Verschueren P, Delye H, Depreitere B, Van Lierde C, Haex B, Berckmans D, Verpoest I, Goffin J, Vander Sloten J, Van der Perre G (2007) A new test set-up for skull fracture characterisation. J Biomech 40:3389 – 3396.

33. Sances AJ, Yoganandan N (1988) The societal impact of biomechanics. Biomedical Engineering Proceedings of a special symposium on maturing technologies and emerging horizons in IEEE . pp115 – 122.

34. Messerer O (1880) Über Elasticität and Festigkeit der menschlichen Knochen. J G Cottaschen Buchhandling, Stuttgart.

35. Gurdjian ES, Webster JE (1946) Deformation of the skull in head injury studied by stress coat technique. Surg Gyn Obst 83:219 – 233.

36. Nahum AM, Gatts JD, Gadd CW, Danforth J (1968) Impact tolerance of the skull and face. Proc Stapp Car Crash Conf 12:302 – 316.

37. Schneider DC, Nahum AM (1972) Impact studies of facial bones and skulls. Proc Stapp Car Crash Conf 16:186 – 203.

38. Hodgson VR, Thomas LM (1971) Breaking strength of the human skull vs. impact surface curvature. DOT HS–800–583.

39. Stalnaker R, Melvin J, Nuscholtz G, Alem N, Benson J (1977) Head impact response. Proc Stapp Car Crash Conf 21:305 – 335.

40. Got C, Patel A, Fayon A, Tarriere C, Walfisch G (1978) Results of experimental head impacts on cadavers: The various data obtained and their relations to some measured physical parameters. Proc Stapp Car Crash Conf 22:57 – 97.

41. Allsop D, Perl TR, Warner CY (1991) Force/deflection and fracture characteristics of the temporo-parietal region of the human head. Proc Stapp Car Crash Conf 35:269 – 278.

42. Yoganandan NA, Pintar FA, Sances A, Walch PR, Ewing CL, Thomas DJ, Snyder RG (1995) Biomechanics of skull fracture. J Neurotrauma 12:659 – 668.

43. Yoganandan N, Zhang J, Pintar F (2004) Force and Acceleration Corridors from Lateral Head Impact. Traffic Inj Prev 5:368 – 373.

44. Raymond D, Crawford G, Van Ee C, Bir C (2009) Development of biomechanical response corridors of the head to blunt ballistic temporo-parietal impact. J Biomech Eng. doi: 10.1115/1.3194751.

45. Raymond D, Van Ee C, Crawford G, Bir C (2009) Tolerance of the skull to blunt ballistic temporo-parietal impact. J Biomech 42:2479 – 2485.

46. Wahl P, Schreyer N, Yersin B (2006) Injury pattern of the Flash-ball, a less-lethal weapon used for law enforcement: Report of two cases and review of the literature. J Emergency Med 31:325 – 330.

47. Hubbs K, Klinger D (2004) Impact munitions: Data base of use and effects. NCJ 204433.

48. Sharkey E, Cassidy M, Brady J, Gilchrist M, NicDaeid N (2011) Investigation of the force associated with the formation of lacerations and skull fractures. Int J Leg Med 126:835 – 834.

49. Baumer TG, Passalacqua N V, Powell BJ, Newberry WN, Fenton TW, Haut RC (2010) Age dependent fracture characteristics of rigid and compliant surface impacts on the infant skull—A porcine model. J Forensic Sci 55:993 – 997.

50. Powell BJ, Passalacqua N V, Baumer TG, Fenton TW, Haut RC (2012) Fracture patterns on the infant porcine skull following severe blunt impact. J Forensic Sci 57:312 – 317.

51. Van Staa TP, Dennison EM, Leufkens HGM, Cooper C (2001) Epidemiology of fractures in England and Wales. Bone 29:517 – 522.

52. Currey JD (2003) How well are bones designed to resist fracture ? J Bone Min Res 18:591 – 598.

53. Ambade VN, Godbole HV (2006) Comparison of wound patterns in homicide by sharp and blunt force. Forensic Sci Int 156:166 – 70.

54. Groenewald P, Bradshaw D, Daniels J, Matzopoulos R, Bourne D, Blease D, Zinyakatira N, Naledi NT (2008) Cause of death and premature mortality in Cape Town, 2001 - 2006. South African Medical Research Council, Cape Town.

55. Seedat M, Van Niekerk A, Jewkes R, Suffla S, Ratele K (2009) Violence and injuries in South Africa: Prioritising an agenda for prevention. Lancet 374:1011 – 1022.

56. Lerer LB, Matzopoulos RG, Phillips R (1997) Violence and injury mortality in the Cape Town metropole. S Afr Med J 87:298 – 301.

57. Powell B, Passalacqua N, Fenton T, Haut R (2013) Fracture characteristics of entrapped head impacts versus controlled head drops in infant porcine specimens. J Forensic Sci 58:678 – 683.

58. Haversion system. (2013) http://www.aokainc.com/haversian-system/. Accessed 8 Jan 2014

59. Reilly DT, Burstein AH (1975) The elastic and ultimate properties of compact bone tissue. J Biomech 8:393 – 405.

60. Gordon I, Shapiro HA, Berson SD (1988) Forensic medicine: A guide to principles, 3rd Ed. Churchill Livingstone, Edinburgh.

Chapter 4
Hopkinson pressure bar theory

4.1. Background

The Hopkinson pressure bar, first described by Bertram Hopkinson in 1914 [1], is an apparatus most commonly utilised in material testing to determine the properties of a material. Hopkinson used this technique to measure the pressures produced during dynamic loading of materials. Essentially, the Hopkinson bar apparatus consists of a gas gun and two or three bars. The bars are typically made of the same material. The two main bars utilised in this method are a shorter striker bar and a longer input bar. Depending on the configuration used, a third output bar may be used. The input and output bars have diametrically mounted strain gauges placed equidistant from the specimen to record stresses placed on the bars. The bar ends are accurately machined to be orthogonal to the bar axis, ensuring good contact between two bars, as well as between the bar and the specimen [2].

One configuration, introduced by Kolsky in 1949 [3], is known as the Split Hopkinson Bar (SHB). The SHB has become the standard apparatus for conducting compression tests at strain rates between 10^2 s^{-1} and 10^4 s^{-1} [4]. In this configuration the specimen is placed between the input bar and output bar (figure 4.1.). The original tests used detonators to launch compressive waves, however more recently a striker bar is launched from a gas gun which impacts with the input bar [5]. This generates a stress wave which travels along the input bar. Impedance is a measure of how much a structure resists motion when subjected to a given force. The input bar and specimen are of different materials, therefore an impedance mismatch exists at the specimen interface which causes a partially reflected wave to travel back along the length of the input bar. The remainder of the stress wave moves through into the output bar. The strain gauges placed on the input and output bars record these waves.

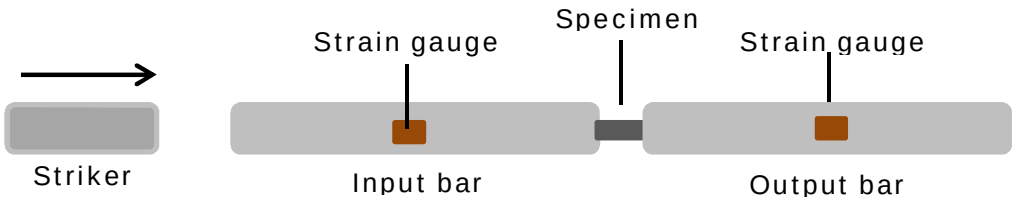

Fig. 4.1 Schematic representation of a split Hopkinson bar configuration

A modification to the SHB was proposed by Dharan and Hauser in 1970, named the direct impact Hopkinson bar (DIHB) [6]. In this configuration no input bar is used (figure 4.2). The striker impacts the specimen directly and stress waves are recorded in the output bar. However, the lack of an input bar results in an inability to calculate the strain rate. Therefore, direct strain measurements need to be made on the specimen, which have proved to be problematic [4].

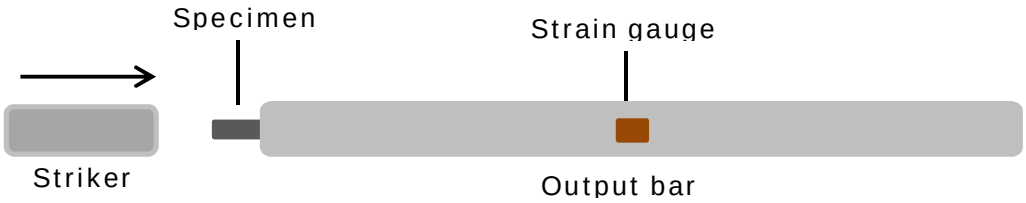

Fig. 4.2 Schematic representation of a direct impact Hopkinson bar configuration

In the current study, the Hopkinson pressure bar tests were configured in such a way as for the striker to impact the input bar directly (figure 4.3). The gauged input bar then impacted with the specimen, in this case a suspended porcine head. Teflon bushels are used to keep the input bar axially aligned with the striker bar, while maintaining near frictionless motion of the bar after impact. With this configuration it is possible to calculate the stress wave history at any point along the input bar from the gauge signals using one-dimensional (1-D) stress wave theory.

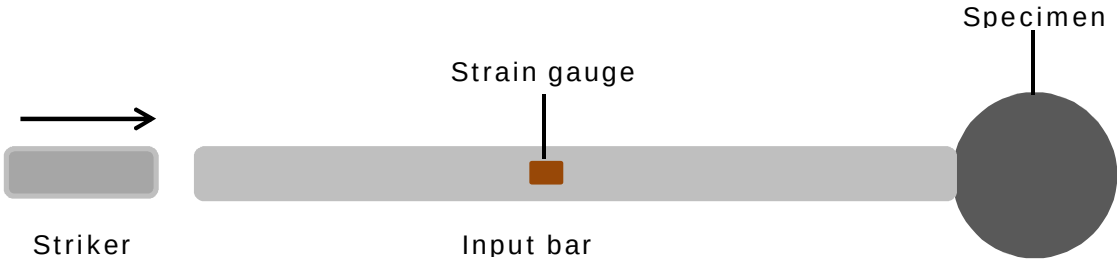

Fig. 4.3 Schematic representation of Hopkinson bar configuration utilised in the current study

4.2. Calculations

As previously mentioned, it is possible to calculate the stress wave history at any point along the input bar from the gauge signals. Following is a guide to performing these calculations. The equations below are derived from the works of Gama et al. [2], Gray [4], Spotts [7] and from personal communication with Cloete (2013).

Consider an input bar of length "L". The time it takes a stress wave to traverse the length of this bar may be calculated as follows:

$$\tau = \frac{L}{c} \tag{1}$$

Where τ is the amount of time it takes the stress wave to travel the length of the bar, L is the length of the bar, and c is the constant speed of sound in the bar. The constant speed of sound in a material may also be calculated:

$$c = \sqrt{\frac{E_y}{\rho}} \tag{2}$$

Where E_y is the Young's modulus of the bar and ρ is the density of the bar.

In the Hopkinson bar configuration utilised in the current study, the striker bar impacts directly with the input bar and the input bar then impacts with the specimen. The two ends of the input bar will be referred to as the impact end and the specimen end respectively. Upon impact between the striker and input bar, a compressive stress wave is generated which travels along the length of the input bar at the constant speed of sound of the bar and interacts with the specimen. Due to an impedance mismatch, the stress wave is partially reflected back down the length of the bar. The strain gauges situated in the middle of the bar record these waves. The stress state of the bar at any time is therefore represented by the superposition of these two stress waves travelling in opposite directions. Consider the right running wave σ_R to originate at the impact end (x=0) and the left running wave σ_L to originate at the specimen end (x=L).

Therefore the wave signal at the impact end (σ_i) will be equal to the sum of the left and right waves at that point on the bar. Keeping in mind that the waves run in opposite directions, if it takes a time of "t" for σ_R to reach a point on the bar it will take a time of "t – τ" for σ_L to reach that same point.

$$\boldsymbol{\sigma_i = \sigma_R \quad , \quad 0 < t < \tau} \tag{3}$$

$$\boldsymbol{\sigma_i(t) = \sigma_R(t) + \sigma_L(t - \tau)} \tag{4}$$

Similarly the signal at the gauge, σ_G, (Strain gauges are placed at the midpoint of the bar) and the signal at the specimen end, σ_S, can be determined at any given time.

$$\boldsymbol{\sigma_G(t) = \sigma_R\left(t - \frac{1}{2}\tau\right) + \sigma_L\left(t - \frac{1}{2}\tau\right)} \tag{5}$$

$$\boldsymbol{\sigma_S(t) = \sigma_R(t - \tau) + \sigma_L(t - \tau)} \tag{6}$$

It is also important to note that the signal at the midpoint of the bar is recorded by the strain gauges and for $t < \tau$ the gauge signal will equal the impact signal, but for $t > \tau$ the impact signal will be zero.

$$\boldsymbol{\sigma_i(t) = \begin{cases} \sigma_G\left(t + \frac{1}{2}\tau\right), & t < \tau \\ 0 \ , & t > \tau \end{cases}} \tag{7}$$

From equation (5) it is possible to determine σ_G at the midpoint of the bar.

$$\boldsymbol{\sigma_G(t - \frac{1}{2}\tau) = \sigma_R(t - \tau) + \sigma_L(t - \tau)} \tag{8}$$

Subtracting equation (8) from equation (4) and solving for σ_R (t) results in:

$$\boldsymbol{\sigma_i(t) - \sigma_G(t - \frac{1}{2}\tau) = \sigma_R(t) - \sigma_R(t - \tau)}$$

$$\therefore \boldsymbol{\sigma_R(t)} = \boldsymbol{\sigma_i(t)} - \boldsymbol{\sigma_G\left(t - \frac{1}{2}\tau\right)} + \boldsymbol{\sigma_R(t-\tau)} \tag{9}$$

By substituting equation (7) into equation (9) σ_R can be calculated at any given time.

$$\boldsymbol{\sigma_R(t)} = \begin{cases} \boldsymbol{\sigma_G\left(t + \frac{1}{2}\tau\right) - \sigma_G\left(t - \frac{1}{2}\tau\right) + \sigma_R(t-\tau)}, & \boldsymbol{t < \tau} \\ \boldsymbol{-\sigma_G\left(t - \frac{1}{2}\tau\right) + \sigma_R(t-\tau)}, & \boldsymbol{t > \tau} \end{cases} \tag{10}$$

From equation (4) we are able to calculate σ_L at any given time.

$$\boldsymbol{\sigma_L(t)} = \boldsymbol{\sigma_i(t+\tau) - \sigma_R(t+\tau)} \tag{11}$$

Because σ_G (t) is measured by the strain gauges, using the previous equations it is possible to determine the σ_i, σ_R, σ_L, and σ_S at any given time. By calculating the signal at the specimen end it is possible to determine what is occurring to the specimen. For example the force of impact with the specimen may be determined by converting the specimen signal into pressure. This is accomplished by multiplying the specimen signal with a calibration factor (K_c). The calibration factor is calculated as follows:

The output signal from the strain gauge using strain gauge theory is:

$$\boldsymbol{V_{out}} = \frac{\boldsymbol{K_G N \varepsilon V_{in}}}{\boldsymbol{4}} \tag{12}$$

Where K_G is the gauge factor, N is the number of active arms in the Wheatstone bridge, ε is the strain, and V_{in} is the bridge voltage.

$$But: \quad \boldsymbol{V_{out}} = \frac{\boldsymbol{V_{read}}}{\boldsymbol{G_{amp}}} \tag{13}$$

$$And: \quad \boldsymbol{\varepsilon} = \frac{\boldsymbol{\sigma}}{\boldsymbol{E_y}} \tag{14}$$

Where G_{amp} is the gain

Substituting equations (13) and (14) into equation (12) results in:

$$\boldsymbol{\sigma} = \frac{\boldsymbol{4E_y}}{\boldsymbol{G_{amp}K_G N V_{in}}} \boldsymbol{V_{read}} \tag{15}$$

This can be expressed as:

$$\boldsymbol{\sigma = K_C V_{read}}$$

$$\therefore \boldsymbol{K_C} = \frac{\boldsymbol{4E_y}}{\boldsymbol{G_{amp}K_g N V_{in}}} \tag{16}$$

Multiplying the specimen signal (equation 6) with the calibration factor (equation 16) gives the pressure of the bar impacting the specimen. The force of the impact at any given time can then be calculated by multiplying the impact pressure with the cross sectional area of the bar.

$$\boldsymbol{Force = Pressure\ X\ Area} \tag{17}$$

The velocity of the impact between the input bar and the specimen, i.e. the velocity at the specimen end (V_S), may also be calculated.

Each stress wave has a velocity change associated with it, namely:

$$\Delta \boldsymbol{V_R} = \frac{\boldsymbol{\sigma_R}}{\boldsymbol{\rho c}} \tag{18}$$

$$And: \ \Delta \boldsymbol{V_L} = -\frac{\boldsymbol{\sigma_L}}{\boldsymbol{\rho c}} \tag{19}$$

Where ΔV_R is the change in velocity associated with the right running wave and ΔV_L is the change in velocity associated with the left running wave. These velocities are summed to determine the velocity at any point along the bar:

$$\boldsymbol{V(t) = \Delta V_R(t) + \Delta V_L(t-\tau)} \tag{20}$$

Substituting equations (18) and (19) into equation (20) results in:

$$\boldsymbol{V(t) = \frac{\sigma_R(t)}{\rho c} - \frac{\sigma_L(t-\tau)}{\rho c}} \tag{21}$$

The velocity at the specimen end (impact velocity) is therefore:

$$\boldsymbol{V_S = \begin{cases} 0, & t < \tau \\ \frac{\sigma_R(t-\tau)}{\rho c} - \frac{\sigma_L(t-\tau)}{\rho c}, & t > \tau \end{cases}} \tag{22}$$

The displacement caused by the impact at any time can be calculated as follows:

$$\boldsymbol{V_S = \frac{\Delta S}{\Delta t}} \tag{23}$$

$$\boldsymbol{\therefore \Delta S = V_S \times \Delta t} \tag{24}$$

$$\boldsymbol{\therefore S(t) = S(t-1) + \left(\frac{V_S(t-1)+V_S(t)}{2} \times \Delta t\right)} \tag{25}$$

Where S is the displacement, V_S is the impact velocity, and Δt is the change in time.

The work energy or energy of impact can then be calculated by using the work – energy principle:

$$W = FD = \frac{1}{2}MV^2 \quad (26)$$

Where W is the work done measured in joules, F is the force , D is the displacement, M is the mass of the striker, and V is the impact velocity.

4.3. References

1. Hopkinson B (1914) A method of measuring the pressure produced in the detonation of high explosives or by the impact of bullets. Proc R Soc London, A 213:437 – 456.

2. Gama BA, Lopatnikov SL, Gillespie JWJ (2004) Hopkinson bar experimental technique : A critical review. Appl Mech Rev 57:223–250.

3. Kolsky H (1949) An investigation of the mechanical properties of materials at very high rates of loading. Proc Phys Soc, B 62:676 – 700.

4. Gray GT (2000) Classic split hopkinson pressure bar technique. In: Kuhn H, Medlin D (eds) ASM Handbook , vol . 8 , Mechanical testing and evaluation. ASM International, Materials Park, OH 44073, pp 462 – 476.

5. Al-Mousawi MM, Reid SR, Deans WF (1997) The use of the split Hopkinson pressure bar techniques in high strain rate materials testing. Proc Instn Mech Engrs, C 211:273 – 292.

6. Dharan CKH, Hauser FE (1970) Determination of stress-strain characteristics at very high strain rates. Exp Mech 10:370 – 376.

7. Spotts MF (1964) Mechanical design analysis. Prentice-Hall inc., New Jersey.

Chapter 5
Publication Ready Journal Article

How hard is hard enough? An investigation into the force associated with lateral blunt force trauma to the cranium

Calvin Gerald Mole[1], Marise Heyns[1], Trevor Cloete[2]

1. Division of Forensic Medicine and Toxicology, Department of Clinical Laboratory Sciences, Faculty of Health Sciences, University of Cape Town, Observatory, South Africa

2. Blast Impact and Survivability Research Unit (BISRU), Department of Mechanical Engineering, Faculty of Engineering and Built Environment, University of Cape Town, Rondebosch, South Africa

*Correspondence to: Dr. Marise Heyns, Department of Clinical Laboratory Sciences, Faculty of Health Sciences, University of Cape Town, P.O. Box 13914, Mowbray, 7705, South Africa. E-mail: marise.heyns@uct.ac.za. Tel: +27 214066604, Fax: +27 214481249

May 2014.

Abstract

Cranial blunt force trauma forms a substantial portion of deaths worldwide. However, only a few studies have attempted to determine the forces involved with blunt force trauma to the lateral side of the head. Nor have many studies been conducted at velocities exceeding 10m/s. The acquisition of human tissue for experimental studies is becoming increasingly difficult. As such, the current study investigates the types of trauma and the forces involved with cranial blunt force trauma in a porcine model. Thirty whole porcine heads were subjected to single impact tests on the fronto-parietal region at velocities ranging from 10m/s to 25m/s. Half of the specimens were subjected to impact by an implement resembling a hammer and the other half were subjected to impact with the Hopkinson pressure bar apparatus. The Hopkinson pressure bar is an apparatus commonly used in material testing. Its use to determine fracture forces in whole specimens is however, novel. Fractures appeared similar in both the hammer tests and Hopkinson pressure bar tests. The majority of lacerations and fractures resembled the shape of the striker surface with the most common fracture observed being a semi-circular depressed fracture. The mean peak fracture force was 7760N (±4150N), with a mean displacement of 3.1mm (±1.1mm). The peak fracture forces concur well with previous studies although no clear trend appears to exist between level of trauma and peak impact force. The types of fractures produced in the porcine specimens differ from those seen in blunt force trauma to the human skull.

Keywords: blunt force trauma; applied force; Hopkinson pressure bar; fracture; laceration

Introduction

Blunt force trauma, next to sharp force and ballistic trauma, is considered one of the most common forms of homicide worldwide. A study conducted in India revealed that 41% of homicides recorded over a three year period (1998 - 2000) involved blunt force trauma and an overwhelming 80% of these involved the head [1]. Similarly a study conducted in London, England demonstrated that 26% of non-firearm related homicides involved blunt force trauma, 88% of which involved multiple blows to the head [2]. Another review of blunt force trauma cases over a period of nine years (2000 – 2009) in Ireland demonstrated that 70% of blows resulted in both fracture of the skull and laceration of the scalp [3]. In Cape Town, South Africa homicide/ assault is the second leading cause of premature death [4, 5] and blunt force trauma forms a substantial portion of these deaths [6]. Clearly an understanding of blunt force trauma to the head is a critical tool in the analysis of forensic cases, not just in South Africa but worldwide.

Questions asked of experts investigating forensic cases involving cranial blunt force trauma commonly relate to:

- The number and sequence of blows
- The point of impact(s)
- The implement used to inflict the trauma
- The amount of force and energy used
- The ability of the type of trauma to threaten life

Yet very few studies have attempted to document the types of trauma inflicted by blunt instruments on the head. Nor have many studies attempted to relate the level of trauma seen to the amount of force or energy involved in blunt force trauma. This

lack of documented evidence makes answering some of the aforementioned questions extremely perilous, as the answering of these questions therefore becomes a complex task often relying upon subjective assessments, such as experience gained from previous cases, and the use of subjective rating scales such as mild, moderate or severe force. This contradicts the main purpose of forensic science which is to eliminate bias opinion of any kind by providing objective, repeatable results.

The majority of studies conducted on the biomechanics of head injury have focussed on impacts to the frontal bone and fronto-facial region of the skull as these regions are often involved in automotive accidents. [7]. The lateral side of the skull is however of no less importance. Lateral impacts on the skull do occasionally occur in automotive accidents and in terms of blunt force homicide the parietal bone is a commonly fractured area [8–10].

Those studies which have investigated lateral impact biomechanics have utilized a variety of different methodologies including: static compression tests [11], drop tests [3, 12–17], free fall tests [18–20], impacts with a pneumatic/ hydrolic piston [21, 22], gas gun tests [23, 24] and pendulum set ups [25]. Specimens utilized in these tests have also varied greatly, comprising intact human cadavers, intact cadaver heads, dry human skulls and porcine specimens. These variations in study methodology have not surprisingly resulted in studies with hugely varying results as well as making comparisons between studies somewhat difficult. However, in many parts of the world human specimens for studies are expensive and difficult to acquire. It has therefore become necessary to perform tests on synthetic or animal models and it is essential to compare the results of such studies with those previously conducted on human specimens.

Even fewer studies have attempted to document the biomechanics of blunt force cranial trauma with regards to specific implements such as a hammer. Generally case studies merely describe the wound morphology due to specific weapons [26–31]. Only a limited number of studies have attempted to analyse the associated force behind an impact due to a specific blunt instrument [3, 23, 32, 33].

It is therefore important that further research be conducted in this area. As such the primary objective of this study was to determine the amount of energy and force involved with blunt force trauma to the head by an implement resembling the shape and weight of a common household hammer. The second objective was to examine and describe the wound morphology in both soft and hard tissue caused by this implement with the aim of comparing the type and level of trauma to the amount of force involved.

Materials and Methods

Porcine bone is believed to be a suitable human bone substitute in fracture research and has been used as a model in many forensic studies [3, 15–17, 34, 35]. The use of isolated heads or intact bodies in biomechanical studies have been shown to produce similar results [13]. As such isolated porcine heads were used in the current study. A total of 30 whole porcine heads (each approximately 5kg in mass) were obtained from a local supplier. All tests were performed on the same day as the specimens were collected. The specimens were visually inspected and palpated prior to testing to determine if any head injury was present. Any specimens found with head injury prior to testing were discarded from the experiments.

During testing each porcine specimen was suspended upside down by means of an adjustable suspension system (fig. 5.1). It has previously been shown that rigid restraint of specimens during impact testing alters the stress distribution which results in a greater amount of fractures occurring as well as more fractures occurring remote to the site of impact [17, 25, 36]. The suspension system utilised in this study allowed for the free movement of the head after impact, limiting the chance of false fractures occurring due to restraint and thus ensuring that any trauma inflicted upon the specimen was due specifically to the impact. This system also allowed for easy adjustment of the specimen to ensure a perpendicular impact to the fronto-parietal region of the porcine specimen.

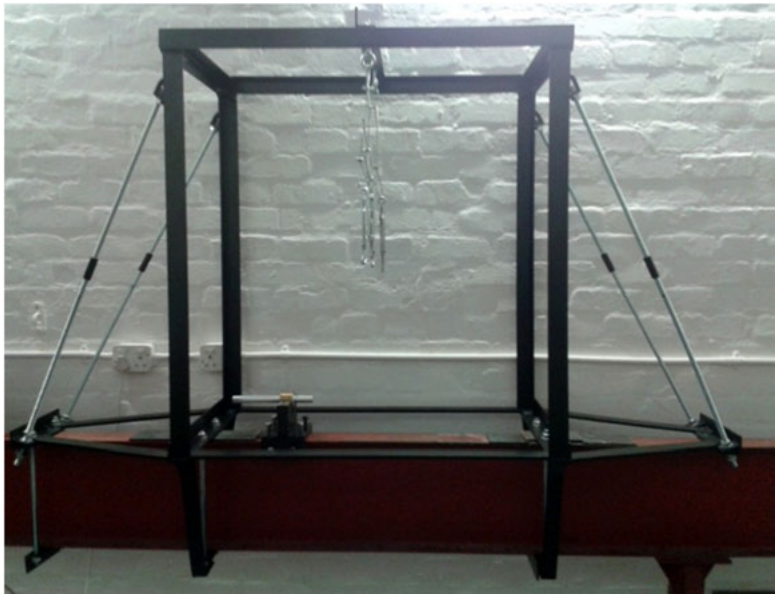

Fig. 5.1 The suspension system utilised in the tests. The specimen hangs upside down in a net suspended by the cables. Turnbuckles allow for easy adjustment of the specimen position.

Hammer tests

A rigid, cylindrical striker (fig. 5.2) with a diameter 20mm and mass of 200g was machined from aluminium. The size, shape and weight of the striker resemble the size and weight of a common household hammer. A gas gun was used to propel the striker into a specimen using compressed commercial air. The velocity of the striker

is easily adjusted by increasing or decreasing the pressure of the compressed air in the gas gun.

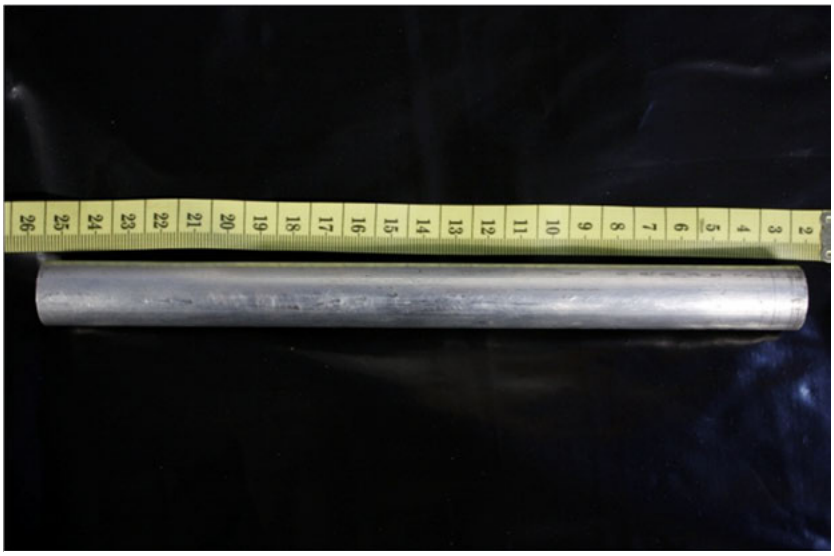

Fig. 5.2 The aluminium striker utilised in the hammer tests

Hammer tests were performed under three different impact conditions: Condition A was performed at a velocity of approximately 10m/s, condition B was performed at approximately 15m/s, and condition C was performed at approximately 25m/s. Each condition was tested four times on specimens with the skin intact and once on a specimen with the skin removed. Each specimen was subjected to a single impact resulting in a total of 15 impact experiments.

The striker velocity of each impact was recorded using a light based velocity trap. Following impact the skin of each specimen was investigated for the presence of laceration. Any soft tissue damage was documented and photographed. Following this any remaining soft tissue was carefully removed by dissection.

The specimens were then visually inspected for the presence of any fracture. Fractures were documented and photographed. Measurements were taken using a flexible measuring tape so as to follow the contours of the skull.

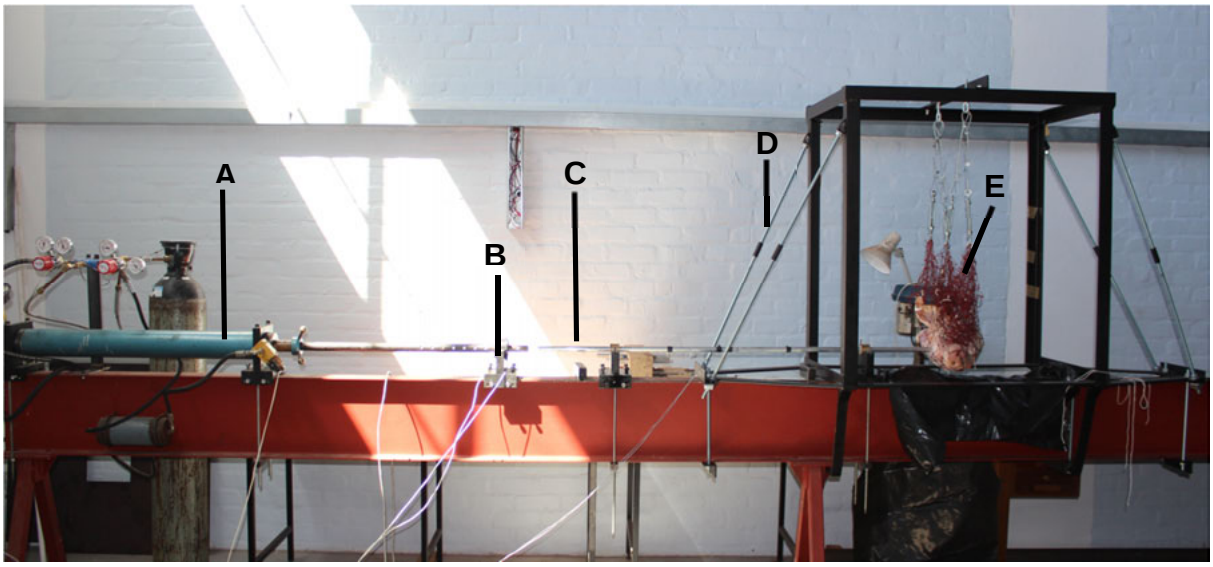

Fig. 5.3 Hopkinson pressure bar configuration. A: Gas gun, B: Speed trap, C: Input bar, D: Suspension rig, E: Specimen.

Hopkinson pressure bar tests

The Hopkinson pressure bar is an apparatus which is most commonly used in material testing to determine the properties of a specific material. It was first described by Bertram Hopkinson in 1914 [37] and has since seen many modifications to the original design utilised. The original theory however, still holds true. The Hopkinson pressure bar utilises one-dimensional stress wave theory to determine the amount of pressure a specimen experiences under impact loading.

The current configuration (fig. 5.3) used a gas gun to propel a striker bar into an input bar which subsequently impacted the specimen suspended by the suspension system. The striker utilised was the same as the one used in the hammer tests. The velocity of the striker was measured using a light based velocity trap. The input bar was made from aluminium and had a length of 1.5m. The diameter of the input bar was the same as the striker bar (20mm). Two strain gauges were mounted diametrically opposite one another at the midpoint of the input bar. The input bar is held in place by bushes which allow for almost frictionless movement of the bar. The

impacts caused by the Hopkinson pressure bar will therefore be similar to the impacts caused by the striker bar alone.

Upon impact between the striker bar and the input bar a stress wave is generated which travels along the input bar and interacts with the specimen. Due to an impedance mismatch between the input bar and the specimen, the stress wave is partially reflected back down the input bar in the opposite direction to the original wave. The strain gauges measure these waves and through the use of one-dimensional stress wave theory it is possible to determine what is occuring to the specimen including the impact velocity, force, displacement and energy.

The Hopkinson bar tests were performed under the same three impact conditions as the hammer tests: Condition A, approximately 10m/s; condition B, approximately 15m/s; and condition C, approximately 25m/s. Each condition was tested five times on specimens with the skin removed. Each specimen was subjected to a single impact resulting in a total of 15 Hopkinson bar experiments.

Following impact any remaining soft tissue was removed by dissection. The specimens were then visually inspected for the presence of any fracture. Fractures were documented and photographed in a similar protocol to the hammer tests.

Parametric and non-parametric data was analysed using one way analysis of variance (ANOVA) and the Kruskal-Wallis test respectively to determine if a significant difference existed between the different test conditions. All data were also analysed using a Spearman rank correlation to determine if any correlation exists between the data and level of trauma seen. All statistical analysis was conducted using STATA 11 (StataCorp, Texas, USA).

Results

Hammer tests

Fifteen specimens were impacted under three different test conditions, resulting in the production of nine fractures. The results of these tests can be seen in table 5.1. Examples of the types of lacerations and fractures seen as a result of impact can be seen in figure 5.4 and figure 5.5. Overall the velocity ($P=0.003$) and energy ($P<0.001$) was found to be significantly different between the conditions. No significant correlation existed between the energy of impact and the level of damage seen ($r=0.48$, $P=0.77$), although there appeared to be a trend emerging between the velocity of impact and the level of damage seen ($r=0.48$, $P=0.07$).

Specimens under condition A were impacted at a mean striker velocity of 10.4m/s (±2.38) which resulted in a mean kinetic energy of 10.76J (±6.04J). One specimen under condition A was removed from the study as the impact was not in the correct position. From the remaining three impacts conducted with the skin intact, one presented with a circular shaped superficial laceration, one presented with a semi-circular shaped superficial laceration, and one presented no damage to the soft tissue. None of these impacts produced any fractures. The impact conducted on the specimen with the skin removed resulted in a crescent shaped linear fracture of approximately 18mm long.

Under condition B, specimens were impacted at a mean striker velocity of 18.38m/s (±0.72m/s) which resulted in a mean kinetic energy of 33.84J (±2.58J). Two of the impacts presented with superficial circular lacerations, one with no corresponding fracture of the skull and the other with three corresponding radiating linear fractures. One impact presented with a deep circular laceration resulting in a depressed

comminuted fracture which was irregular in shape measuring approximately 32mm x 26mm. Another impact presented with a deep L-shaped laceration (10mm x 7mm) which had a corresponding, fine S-shaped linear fracture (13mm). The impact conducted on the specimen with the skin removed presented with a semi-circular depressed fracture (16mm x 6mm).

Under condition C, specimens were impacted at a mean striker velocity of 23.7m/s (±0.41m/s) which resulted in a mean kinetic energy of 56.17J (±1.95J). Two of the impacts presented with semi-circular deep lacerations, one of which presented with a corresponding irregularly shaped depression (15mm x 3mm) and the other a semi-circular depression (16mm x 6mm). One impact presented with a deep linear laceration of approximately 15mm in length with a corresponding linear fracture of approximately 47mm. Another impact presented with an irregular shaped deep laceration measuring approximately 7mm; however, this impact did not result in any visible fracture. The impact conducted with the skin removed presented with a circular depressed comminuted fracture of the same dimensions as the impacting surface of the striker (20mm x 20mm).

Table 5.1 Hammer test results

Specimen No.	Scalp Thickness (mm)	Velocity (m/s)	Kinetic Energy (J)	Laceration Observed	Laceration Size (mm)	Fracture Observed	Fracture Size (mm)
Condition A							
P07-13	5	11.26	12.68	Circular SL	16 x16	None	—
P08-13	7	9.34	8.72	None	—	None	—
P09-13	6	7.75	6.01	Semi-circular SL	18 x 8	None	—
P14-13	No skin	13.25	17.56	—	—	Linear	18
Mean	6	10.4	10.76				
Standard deviation	1	2.38	6.04				
Condition B							
P02-13	6	18.8	35.34	L-shaped DL	10 x 7	Linear	13
P05-13	6	18.01	32.44	Circular SL	17 x 16	None	—
P06-13	4	17.85	31.86	Circular SL	17 x 17	3x radiating	3; 4; 5
P12-13	6	19.41	37.67	Circular DL	20 x 14	Irregular DC	32 x 26
P15-13	No skin	17.85	31.86	—	—	Semi-circular D	16 x 6
Mean	5.5	18.38	33.84				
Standard deviation	1	0.72	2.58				
Condition C							
P03-13	7	23.25	54.06	Linear DL	15	Linear	47
P04-13	5	23.95	57.36	Semi-circular DL	20 x 10	Semi-circular D	16 x 6
P10-13	8	23.95	57.36	Semi-circular DL	20 x 16	Irregular D	15 x 3
P13-13	5	24.09	58.03	Irregular DL	7	None	—
P16-13	No skin	23.25	54.06	—	—	Circular DC	20 x 20
Mean	6.25	23.70	56.17				
Standard deviation	1.5	0.41	1.95				

Lacerations classified as superficial (SL) or deep (DL). Fractures classified as linear, depressed (D), or depressed comminuted (DC)

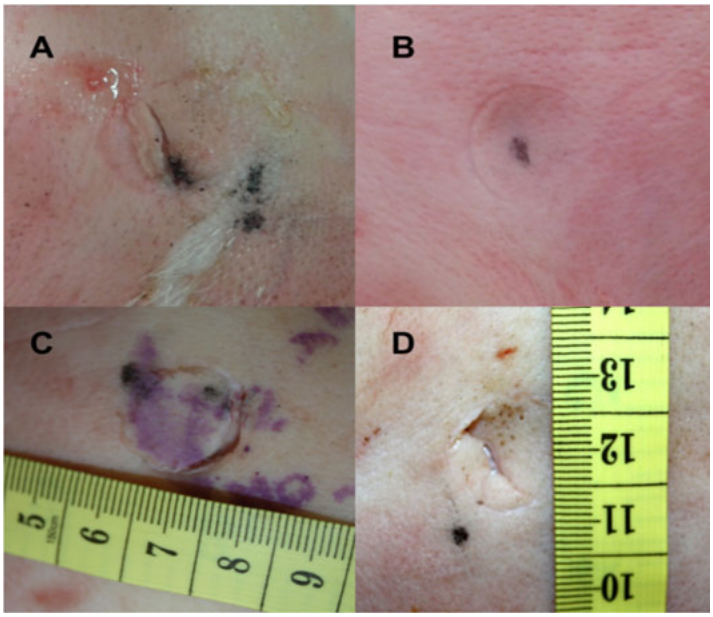

Fig. 5.4 Different types of lacerations observed. A: deep linear laceration (23.25m/s), B: superficial circular laceration (11.26m/s), C: deep circular laceration (23.95m/s), D: deep irregular laceration (24.09m/s).

Hopkinson pressure bar tests

Fifteen specimens were impacted under three different test conditions. The results of the Hopkinson pressure bar tests can be seen in table 5.2. The most common fracture seen in these tests was a semi-circular depressed fracture. Examples of the types of fractures seen can be found in figure 5.5. Of the 15 specimens impacted, nine acquired fractures. The mean impact force resulting in fractures across all the specimens was 7760N (±4150N), with a mean displacement of 3.1mm (±1.1mm). An example of a force-time plot from impacts which produced no fracture and a semi-circular depressed fracture can be found in figure 5.6 and figure 5.7 respectively.

Overall the striker velocity ($P=0.02$), impact velocity ($P=0.02$), peak impact force ($P<0.001$), deformation at peak force ($P=0.015$), and the kinetic energy ($P<0.001$) were found to be significantly different between impact conditions. Although there was no significant difference between the kinetic energy of impact conditions A and B ($P=0.42$). No significant correlation existed between any of the data and the level of damage seen.

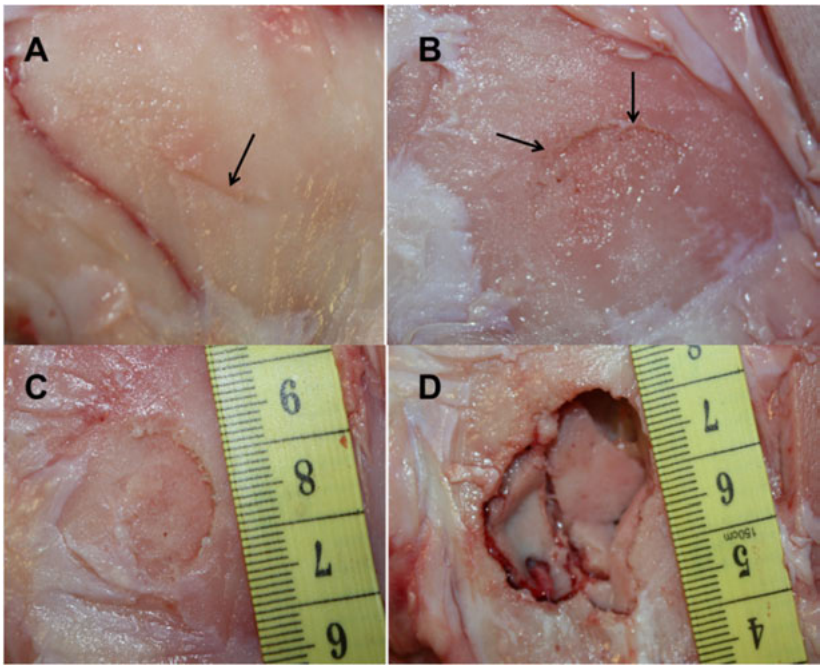

Fig. 5.5 Different types of fractures observed. A: linear (10.8m/s), B: crescent shaped linear (13.25m/s), C: depressed (17.85m/s), D: depressed comminuted (19.41m/s).

Under condition A, specimens were impacted at a mean striker velocity of 11.29m/s (±0.72m/s), which resulted in a mean impact velocity of 8.26m/s (±0.95m/s) and a mean impact energy of 6.56J (±4.07J). The mean peak force of the impacts under condition A was 3024N (±981.55N) with a mean displacement of 2.01mm (±0.72mm). One impact produced a linear fracture of approximately 8mm at a peak force of 1720N and one impact produced a semi-circular depressed fracture measuring 10mm x 5mm at a peak force of 2750N. No other impacts produced fractures.

Under condition B, specimens were impacted at a mean striker velocity of 17.62m/s (±1.77m/s), which resulted in a mean impact velocity of 14.76m/s (±1.95m/s) and a mean impact energy of 17.0J (±10.49J). The mean peak force of the impacts was 7234N (±1937.69N) with a mean displacement of 2.38mm (±1.11mm). Three

impacts resulted in fracture. Two impacts produced semi-circular depressed fractures at peak forces of 6720N and 9110N. Another impact produced an irregular shaped depressed fracture approximately 8mm x 5mm in size at a peak force of 4120N.

Under condition C, specimens were impacted at a mean striker velocity of 23.58m/s (±1.61m/s), which resulted in a mean impact velocity of 20.41m/s (±1.62m/s) and a mean impact energy of 49.16J (±14.34J). The mean peak force of the impacts was 11864N (±1842.79N) with a mean displacement of 4.06mm (±0.68mm). Four of the five impacts under condition C resulted in fractures. These four impacts all produced semi-circular depressed fractures at peak forces of 9080N, 11140N, 12400 and 12800N.

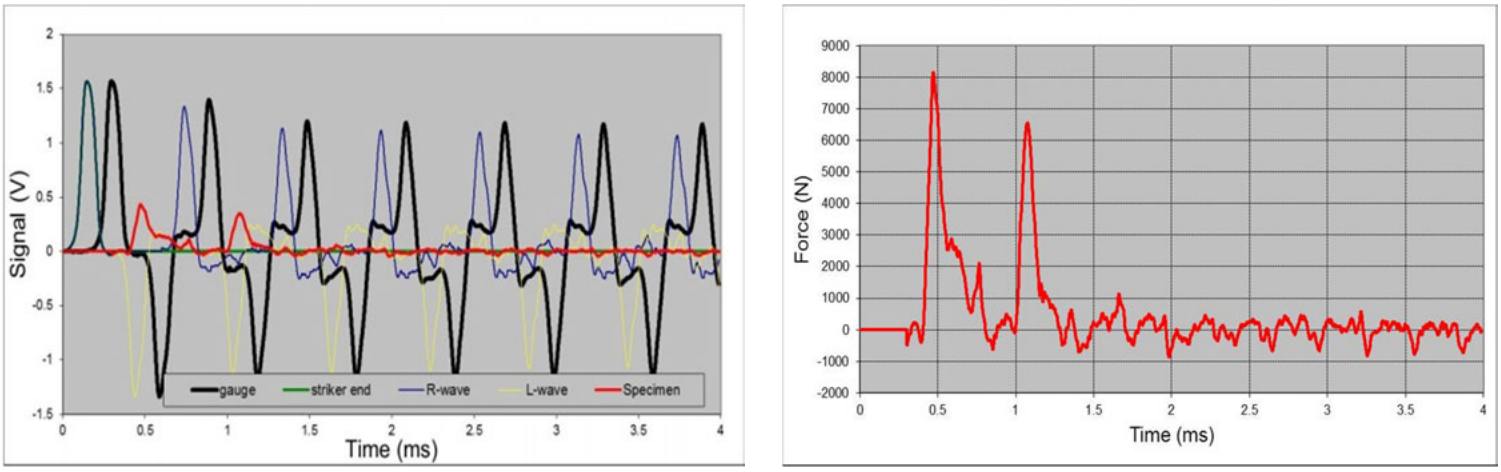

Fig. 5.6 Voltage signals and force-time plot of an impact which produced no visible fracture

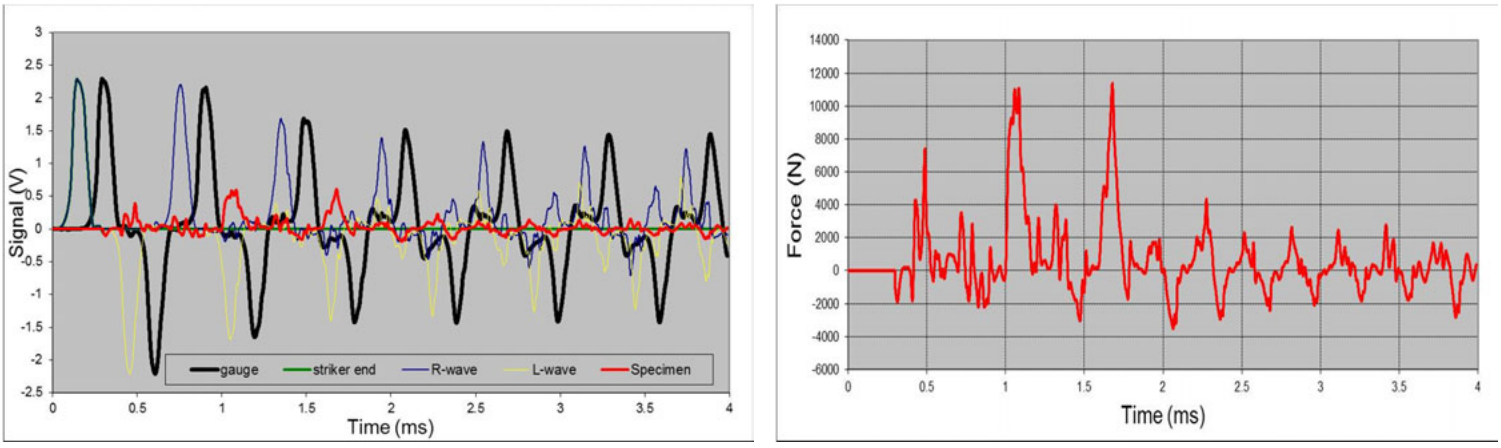

Fig. 5.7 Voltage signals and force-time plot of an impact which produced a depressed fracture

Table 5.2 Hopkinson pressure bar test results

Specimen No.	Striker Velocity (m/s)	Impact Velocity (m/s)	Peak Impact Force (N)	Displacement at peak force (mm)	Impact Energy (J)	Fracture Observed	Fracture Size (mm)
Condition A							
P18-13	10.8	7.68	2760	1.31	3.62	None	—
P19-13	10.8	7.45	1720	1.31	2.25	Linear	8
P20-13	10.71	7.58	2750	1.93	5.31	Semi-circular D	10 x 5
P01-14	11.92	9.14	4340	2.67	11.58	None	—
P03-14	12.23	9.45	3550	2.83	10.05	None	—
Mean	11.29	8.26	3024	2.01	6.56		
Standard deviation	0.72	0.95	981.55	0.72	4.07		
Condition B							
P17-13	15.41	12.3	8150	0.81	6.28	None	—
P21-13	18.75	16.5	9110	3.76	34.25	Semi-circular D	20 x 8
P22-13	17.44	14.8	8070	2.17	17.51	None	—
P23-13	19.91	16.8	6720	2.17	14.58	Semi-circular D	16 x 5
P02-14	16.58	13.38	4120	3.01	12.40	Irregular D	8 x 5
Mean	17.62	14.76	7234	2.38	17.00		
Standard deviation	1.77	1.95	1937.69	1.11	10.49		
Condition C							
P24-13	22	18.9	11140	4.03	44.89	Semi-circular D	15 x 10
P25-13	21.63	18.4	9080	2.89	26.2	Semi-circular D	20 x 10
P04-14	24.72	21.55	12800	4.40	56.32	Semi-circular D	18 x 5
P05-14	24.83	21.66	13900	4.51	62.69	None	—
P06-14	24.72	21.55	12400	4.49	55.68	Semi-circular D	18 x 5
Mean	23.58	20.41	11864	4.06	49.16		
Standard deviation	1.61	1.62	1842.79	0.68	14.34		

Fractures classified as linear, depressed (D), or depressed comminuted (DC)

Discussion

Subjectivity should be eliminated as far as is possible when evaluating evidence. Even though analysis in forensic anthropology is mostly qualitative and therefore by nature often subjective, steps can be taken to improve the objectivity of certain analyses. The current study attempted to determine the forces involved in blunt force trauma to the lateral side of the head using a configuration of the Hopkinson pressure bar. The level of trauma in both soft and hard tissue was also examined to compare with the forces involved.

To the authors' knowledge, the Hopkinson pressure bar has not previously been used to determine forces involved with skull fractures. This configuration provides more accurate data than methods previously utilised as calculations are made directly at the interface of the specimen and impacting implement as opposed to inferring what is occurring at that point. The use of this method also allows for testing to be conducted at a wider range of velocities than are physically capable of attaining through the use of drop tests or free fall tests. Most of the studies previously conducted on lateral impact to the head have used drop tests or free fall tests and as such almost all tests have been conducted at velocities less than 10m/s. To date only Raymond and colleagues have performed blunt impact tests to the lateral side of the head at velocities greater than 10m/s [23, 24].

Determining the forces involved with blunt force trauma to the head will allow quantitative data to be given on the forces associated with certain levels of trauma. Attaching a value to this information will allow a better understanding of an assailant's level of intent to do harm or could give insight into the strength of an assailant, providing more information towards a suspect profile.

The hammer tests were used to determine the level of trauma according to the velocity of impact. In terms of laceration morphology, the most common form of laceration was circular in shape and resembled the size of the striker. As the velocity increased the lacerations tended to become deeper, however the size of the lacerations remained fairly consistent. Interestingly, the dimensions of the lacerations never exceeded the dimensions of the striker surface. These results demonstrate that if circular lacerations are found on a victim's head, the inflicting weapon more

than likely has a circular striking surface of dimensions at least the size of the largest laceration. The presence of linear or irregular lacerations however, does not exclude a weapon with a circular striking surface. It has previously been demonstrated that the size and shape of lacerations and abrasions may be useful in determining the weapon used in an assault, provided the limitations such as the distortion of skin during impact are understood [26, 27, 29–31].

In bone it is more difficult to determine what implement caused a fracture, it has therefore been suggested that trauma analysis should concentrate on other aspects such as the direction and orientation of the blow [39]. However, depressed fractures may resemble the shape of the impacting implement [26, 28, 40]. The most common fractures which occurred in the current study were depressed fractures which resembled the shape of the striker. As the velocity and force of the impacts increased the depressions became more pronounced, as would be expected. However, the depressions which occurred on the porcine skull were atypical. Of the 13 depressed fractures which occurred, none had any form of radiating fracture associated with it and only two had comminuted fractures associated with the depression. The vast majority of the depressed fractures were merely a circular plug of bone which had been depressed. This is possibly as a result of the density and shape of porcine cranial bones. Unlike the smooth, gracile shape of the human skull, the porcine skull is robust and angulated. The parietal region of the porcine skull has a greater density if compared with that in humans. These factors may inhibit the propagation of radiating fractures.

The peak impact forces measured in this study compare well with those measured in other studies conducted on human and porcine specimens (figure 5.8). Sharkey and colleagues [3] conducted impact tests similar to those conducted in the current study. They performed drop tests onto the fronto-parietal region of whole porcine heads. One of the implements used was a hammer which generated fracture forces in the range of 4149N to 8137N (mean: 6076N). The striker utilised in the current study resembled the shape and weight of a common household hammer. Although the range of forces created by this striker were greater than those seen in the Sharkey et al. study, the mean fracture force of 7760N is similar.

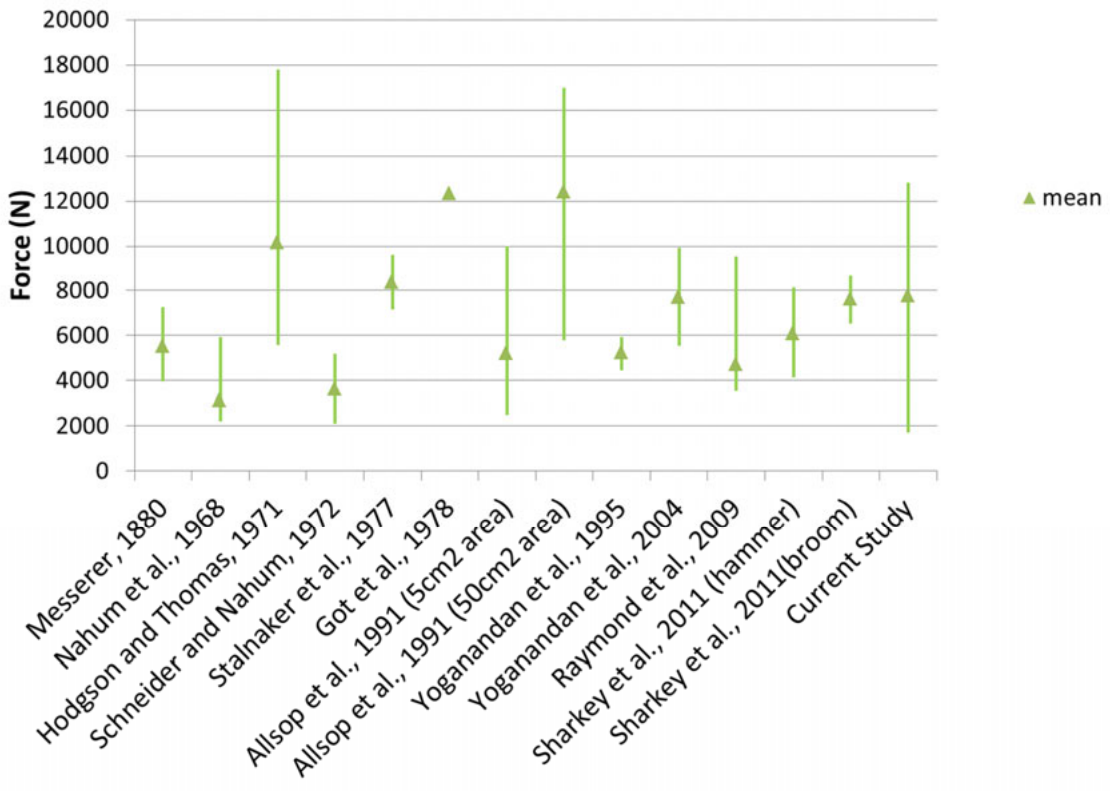

Fig. 5.8 Comparison of peak fracture force of lateral part of skull between studies

The types of fracture observed, however, differ between the studies. Sharkey and colleagues [3] mostly observed fractures in the form of suture separation, While the current study mostly observed depressed fractures. This difference may be attributed to the differences in method of impact. Using heavy weights and a drop rig to impart a blow, produces an impact which is more akin to a crushing force. In the current study the specimen was suspended from a specifically designed suspension rig which allowed free movement of the head after impact. In real life, a head does not remain rigid during an impact. The neck allows some movement of the head. Although the suspension system utilised allows far greater movement of the head than in real life, the authors believe the impacts produced using this system more closely resemble impacts produced in real life than impacts produced by drop tests do. The use of the suspension rig also ensures that any fractures noted on the specimen are due to the impact.

Conclusion

The production of lacerations or fractures is influenced by a wide range of factors. Attempting to determine the forces involved with a particular level of damage appears to be problematic as no clear trend existed between level of damage and peak impact force, although with a larger sample size a trend may emerge. The main inhibiting factor is natural variation as some skulls fracture at a low force while others are able to withstand a far greater force without fracturing.

The procurement of human material for research is becoming increasingly difficult. Therefore the use of animal models in research is becoming ever more important. An ideal animal model should be inexpensive, easy to acquire and provide results which are similar to those seen in humans. The domestic pig has been used in numerous studies due to its similarities with humans. The long bones and particularly the skin of pigs have been shown to have similar characteristics to that of humans [38]. The pig skull is also similar to humans in that it is made up of three layers, although the pig skull is more robust and angulated than in humans.

The current study produced fracture forces in porcine skulls which are similar to those found in studies conducted on human specimens; however the types of fracture differ greatly from those seen in humans. Unfortunately the pig skull does not appear to be a good model for determining the types of damage which may occur during blunt impact.

Future research should focus on determining if other animal models may be better suited to this type of research.

Acknowledgements

The authors thank Mr Rudi Harmse (Winelands Pork) for supplying the porcine specimens used in this study and the University of Cape Town Postgraduate Office for funding.

Ethical Standards

The current study complies with all the ethical standards of the university and the ethical laws of the Republic of South Africa.

References

1. Ambade VN, Godbole HV (2006) Comparison of wound patterns in homicide by sharp and blunt force. Forensic Sci Int 156:166 – 70.

2. Henderson JP, Morgan SE, Patel F, Tiplady ME (2005) Patterns of non-firearm homicide. J Clin Forensic Med 12:128 – 132.

3. Sharkey E, Cassidy M, Brady J, Gilchrist M, NicDaeid N (2011) Investigation of the force associated with the formation of lacerations and skull fractures. Int J Leg Med 126:835 – 834.

4. Gilbert L (1996) Urban violence and health - South Africa 1995. Soc Sci Med 43:873 – 886.

5. Groenewald P, Bradshaw D, Daniels J, Matzopoulos R, Bourne D, Blease D, Zinyakatira N, Naledi NT (2008) Cause of death and premature mortality in Cape Town, 2001 - 2006. South African Medical Research Council, Cape Town.

6. Lerer LB, Matzopoulos RG, Phillips R (1997) Violence and injury mortality in the Cape Town metropole. S Afr Med J 87:298 – 301.

7. Yoganandan NA, Pintar FA (2004) Biomechanics of temporo-parietal skull fracture. Clin Biomech 19:225 – 239.

8. Kremer C, Racette S, Dionne C, Sauvageau A (2008) Discrimination of falls and blows in blunt head trauma: Systematic study of the hat brim line rule in relation to skull fractures. J Forensic Sci 53:716 – 719.

9. Kremer C, Sauvageau A (2009) Discrimination of falls and blows in blunt head trauma: Assessment of predictability through combined criteria. J Forensic Sci 54:923 – 926.

10. Guyomarc'h P, Campagna-vaillancourt M, Kremer C, Sauvageau A (2010) Discrimination of falls and blows in blunt head trauma: A multi-criteria approach. J Forensic Sci 55:423 – 427.

11. Messerer O (1880) Über Elasticität and Festigkeit der menschlichen Knochen. J G Cottaschen Buchhandling, Stuttgart.

12. Nahum AM, Gatts JD, Gadd CW, Danforth J (1968) Impact tolerance of the skull and face. Proc Stapp Car Crash Conf 12:302 – 316.

13. Schneider DC, Nahum AM (1972) Impact studies of facial bones and skulls. Proc Stapp Car Crash Conf 16:186 – 203.

14. Allsop D, Perl TR, Warner CY (1991) Force/deflection and fracture characteristics of the temporo-parietal region of the human head. Proc Stapp Car Crash Conf 35:269 – 278.

15. Baumer TG, Passalacqua N V, Powell BJ, Newberry WN, Fenton TW, Haut RC (2010) Age dependent fracture characteristics of rigid and compliant surface impacts on the infant skull—A porcine model. J Forensic Sci 55:993 – 997.

16. Powell BJ, Passalacqua N V, Baumer TG, Fenton TW, Haut RC (2012) Fracture patterns on the infant porcine skull following severe blunt impact. J Forensic Sci 57:312 – 317.

17. Powell B, Passalacqua N, Fenton T, Haut R (2013) Fracture characteristics of entrapped head impacts versus controlled head drops in infant porcine specimens. J Forensic Sci 58:678 – 683.

18. Hodgson VR, Thomas LM (1971) Breaking strength of the human skull vs. impact surface curvature. DOT HS–800–583.

19. Got C, Patel A, Fayon A, Tarriere C, Walfisch G (1978) Results of experimental head impacts on cadavers: The various data obtained and their relations to some measured physical parameters. Proc Stapp Car Crash Conf 22:57 – 97.

20. Yoganandan N, Zhang J, Pintar F (2004) Force and Acceleration Corridors from Lateral Head Impact. Traffic Inj Prev 5:368 – 373.

21. Stalnaker R, Melvin J, Nuscholtz G, Alem N, Benson J (1977) Head impact response. Proc Stapp Car Crash Conf 21:305 – 335.

22. Yoganandan NA, Pintar FA, Sances A, Walch PR, Ewing CL, Thomas DJ, Snyder RG (1995) Biomechanics of skull fracture. J Neurotrauma 12:659 – 668.

23. Raymond D, Van Ee C, Crawford G, Bir C (2009) Tolerance of the skull to blunt ballistic temporo-parietal impact. J Biomech 42:2479 – 2485.

24. Raymond D, Crawford G, Van Ee C, Bir C (2009) Development of biomechanical response corridors of the head to blunt ballistic temporo-parietal impact. J Biomech Eng. doi: 10.1115/1.3194751.

25. Verschueren P, Delye H, Depreitere B, Van Lierde C, Haex B, Berckmans D, Verpoest I, Goffin J, Vander Sloten J, Van der Perre G (2007) A new test set-up for skull fracture characterisation. J Biomech 40:3389 – 3396.

26. Clark EG, Sperry KL (1992) Distinctive blunt force injuries caused by a crescent wrench. J Forensic Sci 37:1172 – 1178.

27. Thali MJ, Braun M, Brueschweiler W, Dirnhofer R (2003) “Morphological imprint”: Determination of the injury-causing weapon from the wound morphology using forensic 3D/CAD-supported photogrammetry. Forensic Sci Int 132:177 – 181.

28. Grassberger M, Gehl A, Püschel K, Turk EE (2011) 3D reconstruction of emergency cranial computed tomography scans as a tool in clinical forensic radiology after survived blunt head trauma - Report of two cases. Forensic Sci Int 207:e19 – 23.

29. Zugibe FT, Costello JT (1985) Identification of a murder weapon by a peculiar blunt force injury pattern and histochemical analysis. J Forensic Sci 30:239 – 242.

30. Zugibe FT, Costello JT (1986) Identification of the murder weapon by intricate patterned injury measurements. J Forensic Sci 31:773 – 777.

31. Rao VJ (1986) Patterned injury and its evidentiary value. J Forensic Sci 31:768 – 772.

32. Bolliger SA, Ross S, Oesterhelweg L, Thali MJ, Kneubuehl BP (2009) Are full or empty beer bottles sturdier and does their fracture-threshold suffice to break the human skull? J Forensic Leg Med 16:138 – 142.

33. Gläser N, Kneubuehl BP, Zuber S, Axmann S, Ketterer T, Thali MJ, Bolliger SA (2011) Biomechanical examination of blunt trauma due to baseball bat blows to the head. J Forensic Biomech 2:1 – 5.

34. Calce SE, Rogers TL (2007) Taphonomic changes to blunt force trauma: A preliminary study. J Forensic Sci 52:519 – 527.

35. Jordana F, Colat-Parros J, Bénézech M (2013) Diagnosis of skull fractures according to postmortem interval: An experimental approach in a porcine model. J Forensic Leg Med 58:156 – 162.

36. Kroman A, Kress T, Porta D (2011) Fracture propagation in the human cranium : A re-testing of popular theories. Clin Anat 24:309 – 318.

37. Hopkinson B (1914) A method of measuring the pressure produced in the detonation of high explosives or by the impact of bullets. Proc R Soc Lond, A 213:437 – 456.

38. Passalacqua N, Fenton T (2012) Developments in skeletal trauma : Blunt-force trauma. In: Dirkmaat DC (ed) A Companion to Forensic Anthropology. Blackwell, Oxford, pp 400 – 411.

39. Dirkmaat DC, Cabo LL, Ousley SD, Symes SA (2008) New perspectives in forensic anthropology. Yearb Phys Anthr 51:33 – 52.

40. Delannoy Y, Becart A, Colard T, Delille R (2012) Skull wounds linked with blunt trauma (hammer example). A report of two depressed skull fractures–Elements of biomechanical explanation. Leg Med 14:258 – 262.

Appendix A
Design Drawings

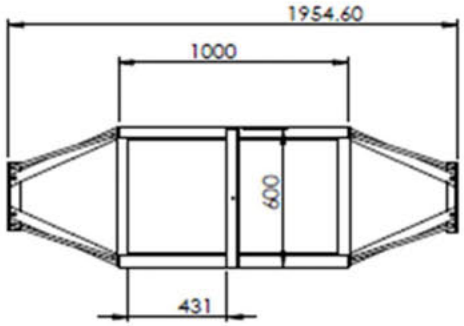

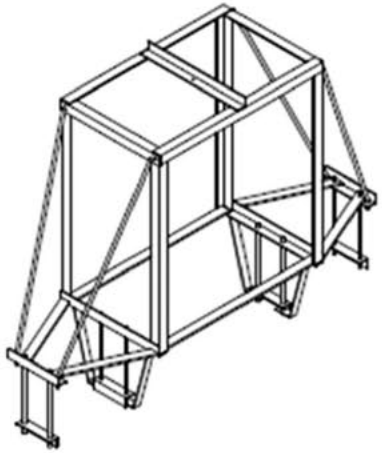

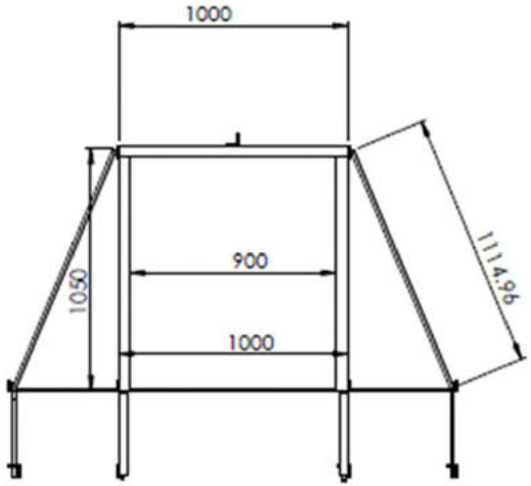

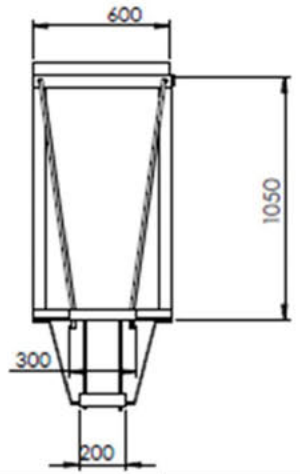

UNLESS OTHERWISE SPECIFIED: DIMENSIONS ARE IN MILLIMETRES SURFACE FINISH: TOLERANCES: LINEAR: ANGULAR:						DRAW AND BREAK SHARP EDGES	DO NOT SCALE DRAWING	REVISION
	NAME	SIGNATURE	DATE				TITLE:
DRAWN							
CHK'D							
APP'VD							
MFG							
QA				MATERIAL:			DWG NO. Assembly A3
				WEIGHT:			SCALE:1:50 SHEET 1 OF 1

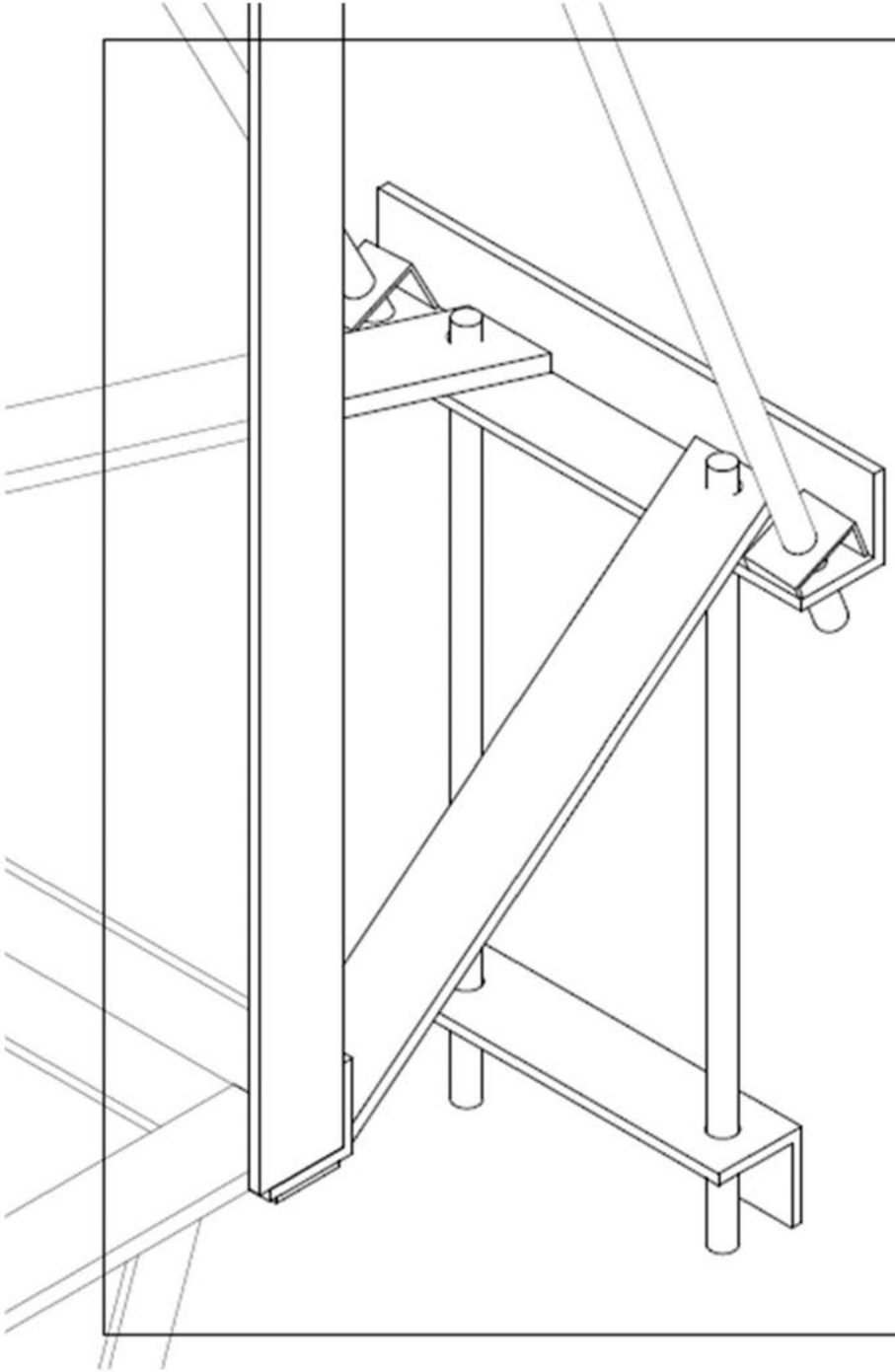

UNLESS OTHERWISE SPECIFIED: DIMENSIONS ARE IN MILLIMETERS SURFACE FINISH: TOLERANCES: LINEAR: ANGULAR:						DEBUR AND BREAK SHARP EDGES	DO NOT SCALE DRAWING	REVISION
	NAME	SIGNATURE	DATE				TITLE: Assembly zoom front	
DRAWN								
CHK'D								
APPV'D								
MFG								
Q.A				MATERIAL:			DWG NO.	3
				WEIGHT:			SCALE:1.00	SHEET 1 OF 1

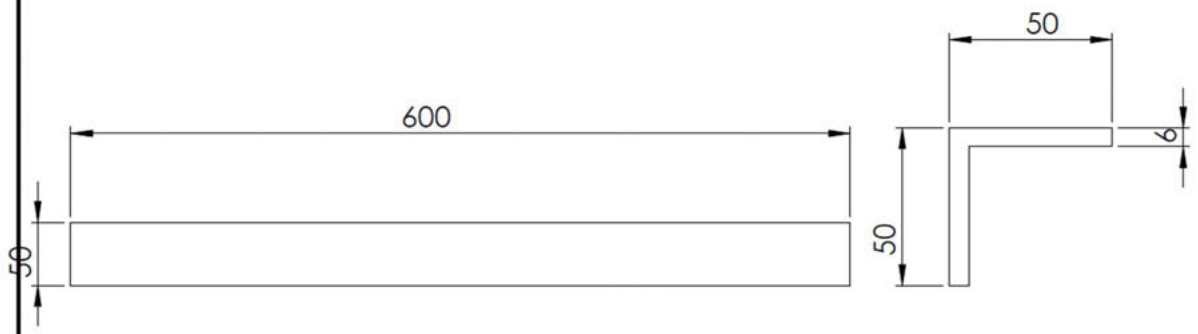

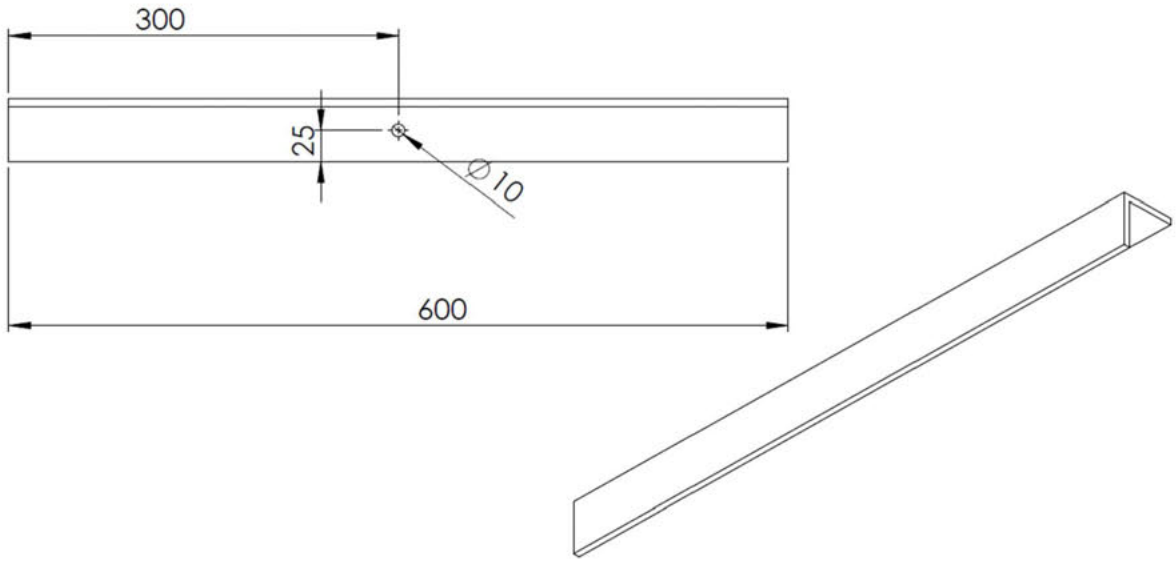

UNLESS OTHERWISE SPECIFIED: DIMENSIONS ARE IN MILLIMETERS SURFACE FINISH: TOLERANCES: LINEAR: ANGULAR:		FINISH:			DEBUR AND BREAK SHARP EDGES	DO NOT SCALE DRAWING	REVISION
	NAME	SIGNATURE	DATE			TITLE:	
DRAWN							
CHK'D							
APPV'D							
MFG							
Q.A				MATERIAL:		DWG NO. Top bar Angleiron	A4
				WEIGHT:		SCALE:1:10	SHEET 1 OF 1

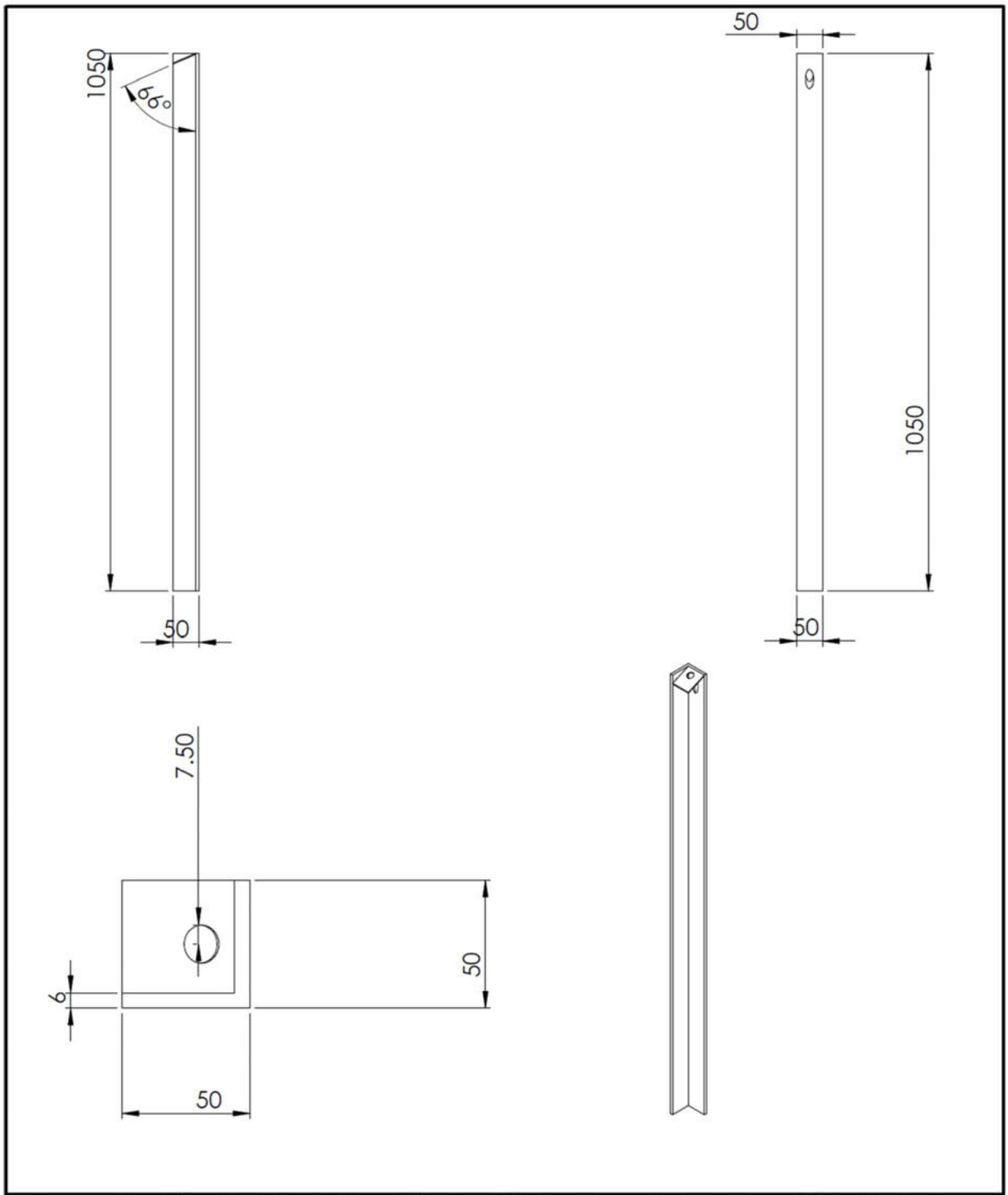

UNLESS OTHERWISE SPECIFIED: DIMENSIONS ARE IN MILLIMETERS SURFACE FINISH: TOLERANCES: LINEAR: ANGULAR:	FINISH:		DEBUR AND BREAK SHARP EDGES			DO NOT SCALE DRAWING	REVISION
	NAME	SIGNATURE	DATE			TITLE:	
DRAWN							
CHK'D							
APPV'D							
MFG							
Q.A				MATERIAL: Material <not specified>		DWG NO. Upright	A4
				WEIGHT:		SCALE:1:10	SHEET 1 OF 1

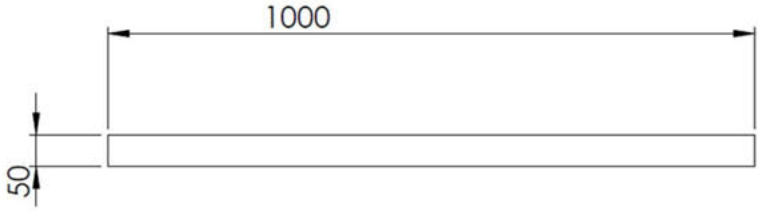

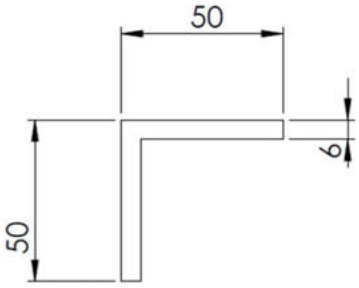

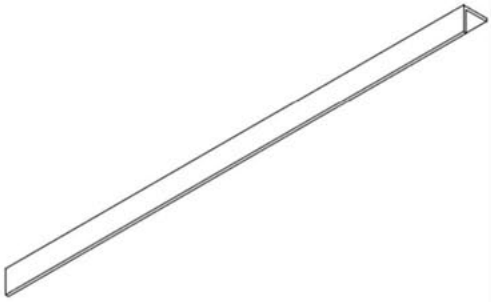

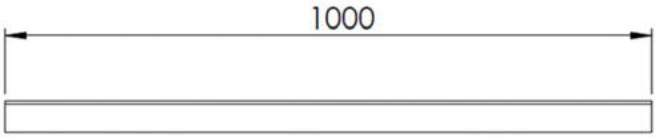

UNLESS OTHERWISE SPECIFIED: DIMENSIONS ARE IN MILLIMETERS SURFACE FINISH: TOLERANCES: LINEAR: ANGULAR:	FINISH:		DEBUR AND BREAK SHARP EDGES			DO NOT SCALE DRAWING	REVISION
	NAME	SIGNATURE	DATE			TITLE:	
DRAWN							
CHK'D							
APPV'D							
MFG							
Q.A				MATERIAL: Material <not specified>		DWG NO. top angle iron side	A4
				WEIGHT:		SCALE:1:10	SHEET 1 OF 1

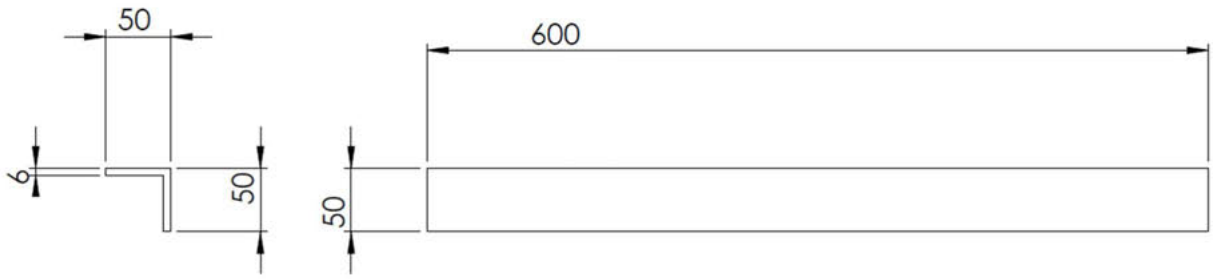

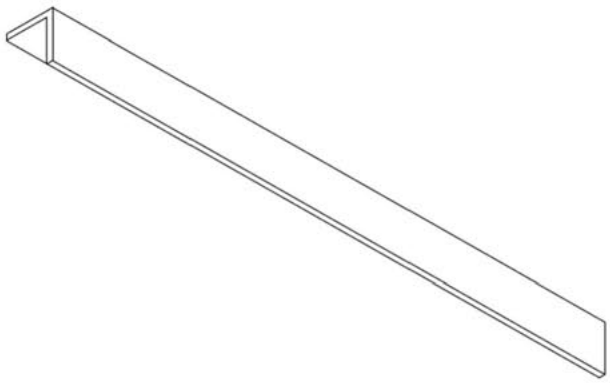

UNLESS OTHERWISE SPECIFIED: DIMENSIONS ARE IN MILLIMETERS SURFACE FINISH: TOLERANCES: LINEAR: ANGULAR:		FINISH:				DEBUR AND BREAK SHARP EDGES	DO NOT SCALE DRAWING / REVISION
	NAME	SIGNATURE	DATE				TITLE:
DRAWN							
CHK'D							
APPV'D							
MFG							
Q.A				MATERIAL: Material <not specified>			DWG NO. top angle iron front / A4
				WEIGHT:		SCALE:1:10	SHEET 1 OF 1

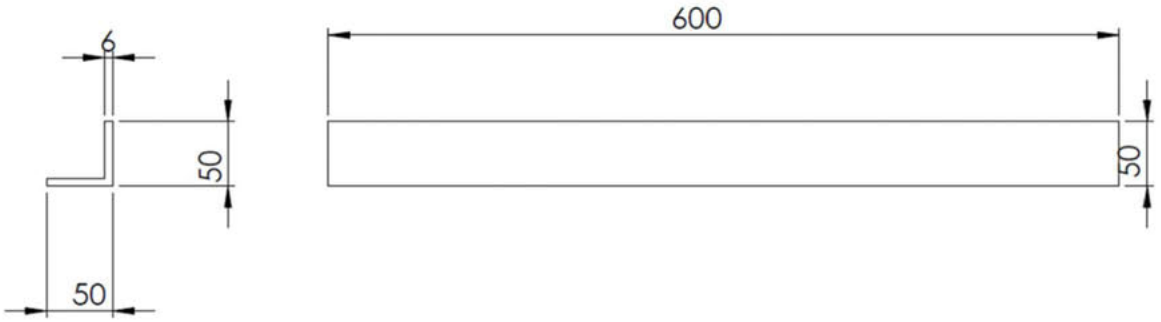

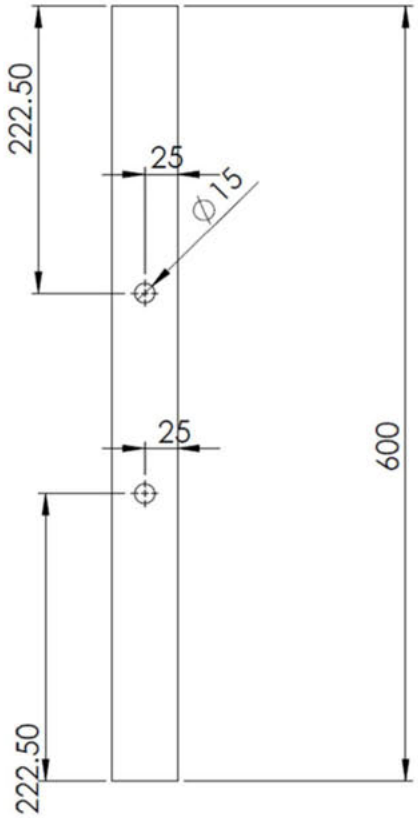

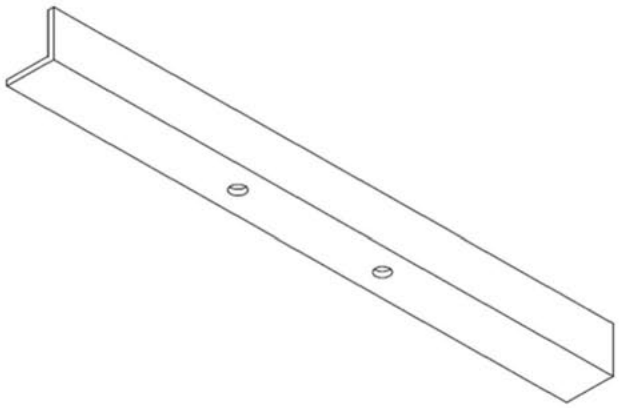

UNLESS OTHERWISE SPECIFIED: DIMENSIONS ARE IN MILLIMETERS SURFACE FINISH: TOLERANCES: LINEAR: ANGULAR:		FINISH:			DEBUR AND BREAK SHARP EDGES	DO NOT SCALE DRAWING	REVISION
	NAME	SIGNATURE	DATE			TITLE:	
DRAWN							
CHK'D							
APPV'D							
MFG							
Q.A				MATERIAL:		DWG NO. Bottom middle angle iron	A4
				WEIGHT:		SCALE:1:10	SHEET 1 OF 1

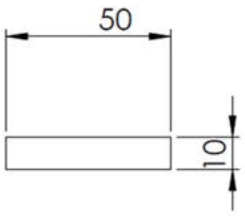

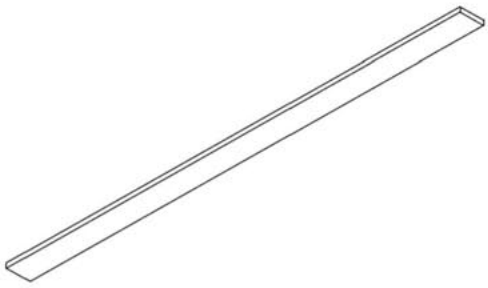

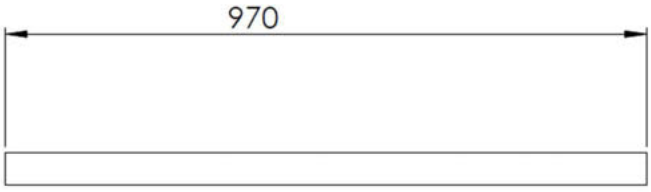

UNLESS OTHERWISE SPECIFIED: DIMENSIONS ARE IN MILLIMETERS SURFACE FINISH: TOLERANCES: LINEAR: ANGULAR:		FINISH:				DEBUR AND BREAK SHARP EDGES	DO NOT SCALE DRAWING	REVISION
	NAME	SIGNATURE	DATE				TITLE:	
DRAWN								
CHK'D								
APPV'D								
MFG								
Q.A				MATERIAL: Material <not specified>			DWG NO. bottom side	A4
				WEIGHT:			SCALE:1:10	SHEET 1 OF 1

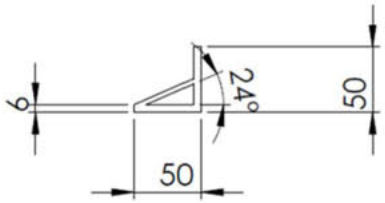

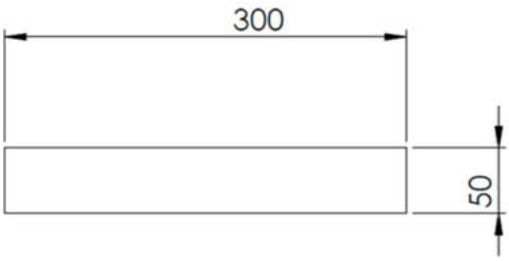

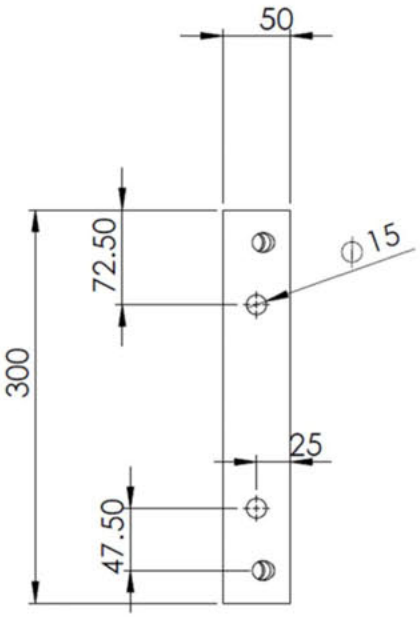

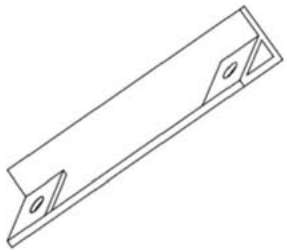

UNLESS OTHERWISE SPECIFIED: DIMENSIONS ARE IN MILLIMETERS SURFACE FINISH: TOLERANCES: LINEAR: ANGULAR:		FINISH:			DEBUR AND BREAK SHARP EDGES	DO NOT SCALE DRAWING	REVISION
	NAME	SIGNATURE	DATE			TITLE:	
DRAWN							
CHK'D							
APPV'D							
MFG							
Q.A				MATERIAL:		DWG	Bottom front angle iron
				WEIGHT:		SCALE:1:5	SHEET 1 OF 1

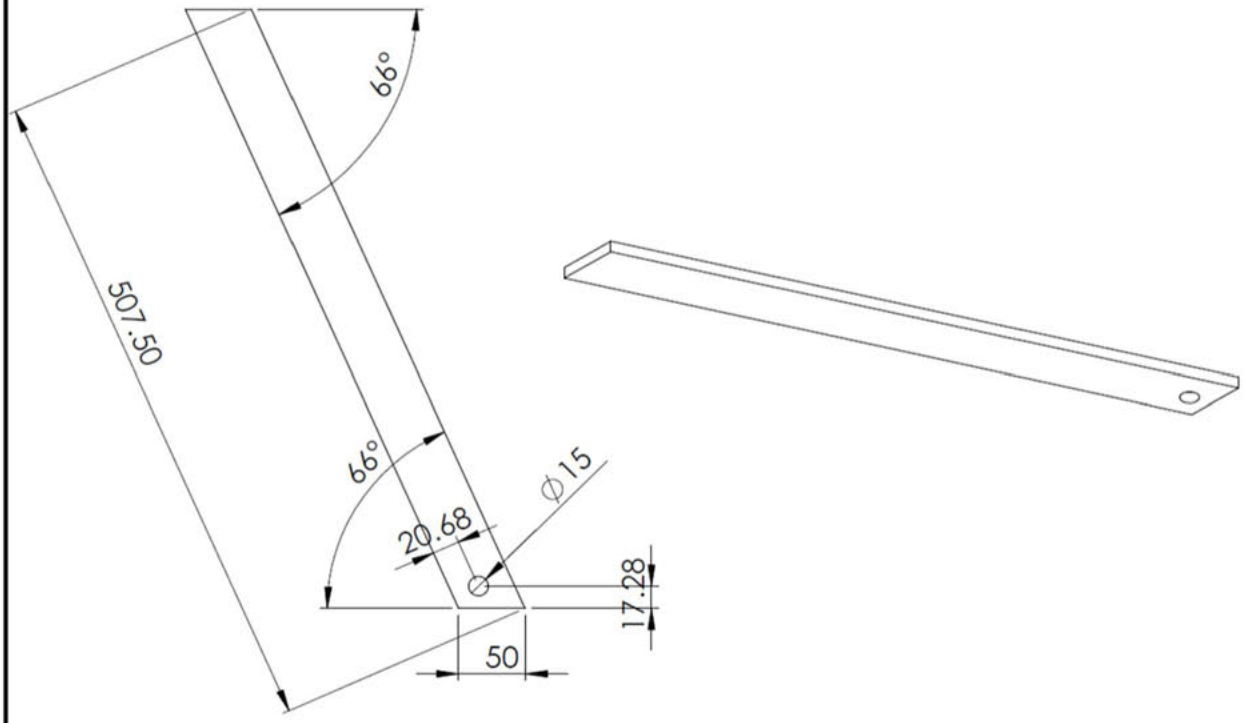

UNLESS OTHERWISE SPECIFIED: DIMENSIONS ARE IN MILLIMETERS SURFACE FINISH: TOLERANCES: LINEAR: ANGULAR:		FINISH:			DEBUR AND BREAK SHARP EDGES	DO NOT SCALE DRAWING	REVISION
	NAME	SIGNATURE	DATE			TITLE:	
DRAWN							
CHK'D							
APPV'D							
MFG							
Q.A				MATERIAL: Material <not specified>		DWG NO. bottom front side	A4
				WEIGHT:		SCALE:1:10	SHEET 1 OF 1

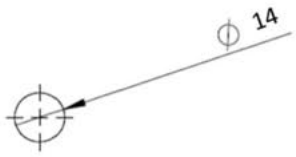

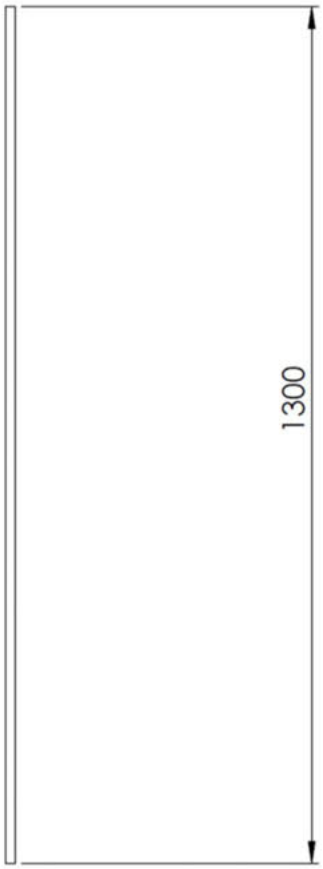

UNLESS OTHERWISE SPECIFIED: DIMENSIONS ARE IN MILLIMETERS SURFACE FINISH: TOLERANCES: LINEAR: ANGULAR:	FINISH:			DEBUR AND BREAK SHARP EDGES	DO NOT SCALE DRAWING	REVISION	
	NAME	SIGNATURE	DATE			TITLE:	
DRAWN							
CHK'D							
APPV'D							
MFG							
Q.A				MATERIAL:		DWG NO. front bar	A4
				WEIGHT:		SCALE:1:10	SHEET 1 OF 1

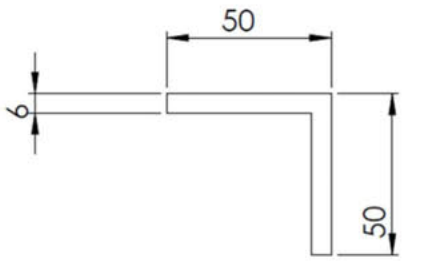

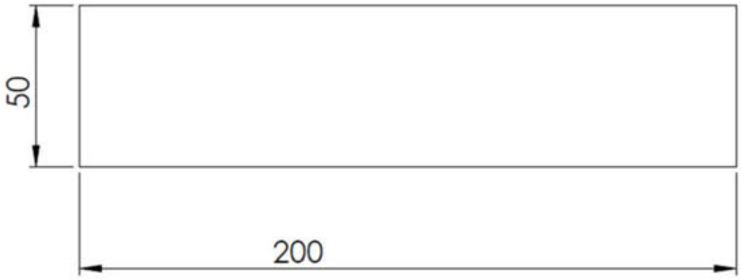

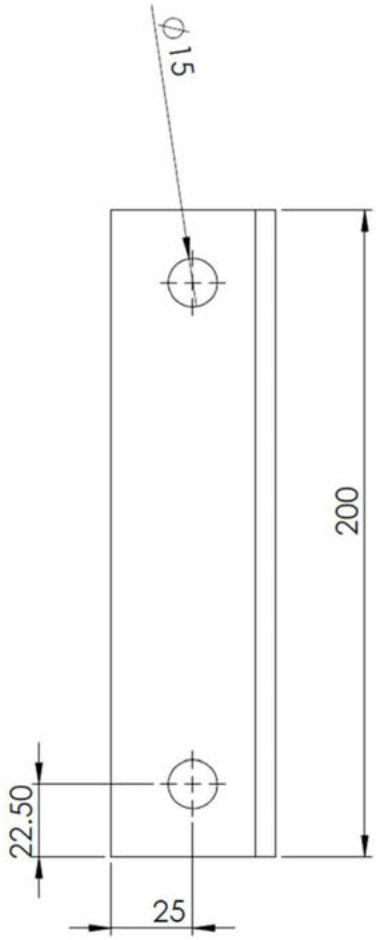

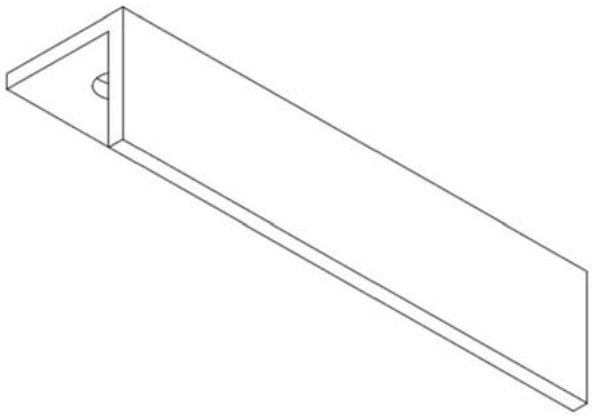

UNLESS OTHERWISE SPECIFIED: DIMENSIONS ARE IN MILLIMETERS SURFACE FINISH: TOLERANCES: LINEAR: ANGULAR:	FINISH:		DEBUR AND BREAK SHARP EDGES	DO NOT SCALE DRAWING		REVISION
	NAME	SIGNATURE	DATE			TITLE:
DRAWN						
CHK'D						
APPV'D						
MFG						
Q.A				MATERIAL:		Bottom base angle iron
				WEIGHT:	SCALE:1:5	SHEET 1 OF 1

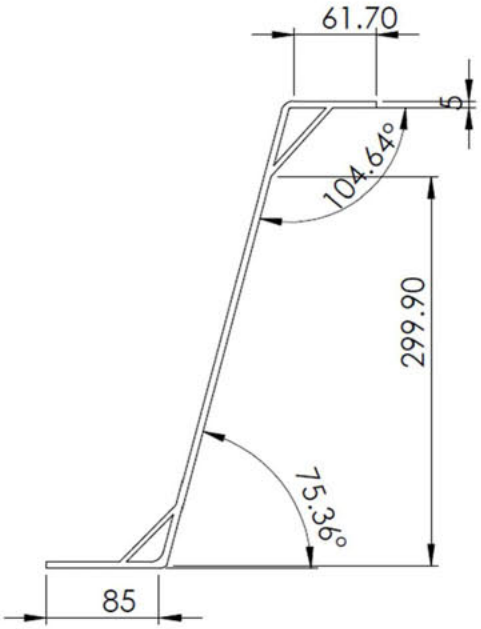

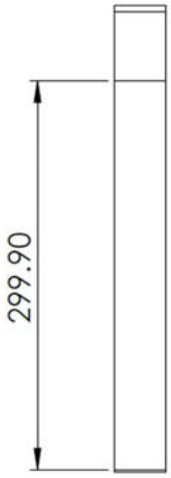

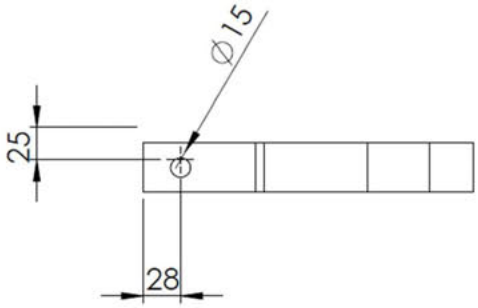

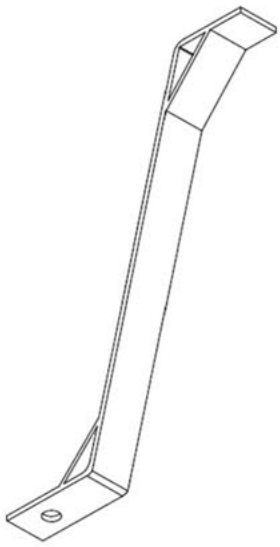

UNLESS OTHERWISE SPECIFIED: DIMENSIONS ARE IN MILLIMETERS SURFACE FINISH: TOLERANCES: LINEAR: ANGULAR:		FINISH:			DEBUR AND BREAK SHARP EDGES	DO NOT SCALE DRAWING	REVISION
	NAME	SIGNATURE	DATE			TITLE:	
DRAWN							
CHK'D							
APPV'D							
MFG							
Q.A				MATERIAL:		DWG NO. bottom strut	A4
				WEIGHT:		SCALE:1:5	SHEET 1 OF 1

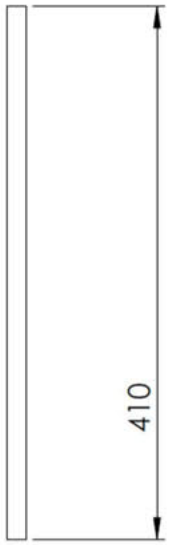

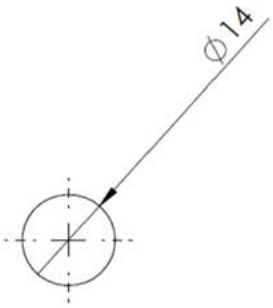

UNLESS OTHERWISE SPECIFIED: DIMENSIONS ARE IN MILLIMETERS SURFACE FINISH: TOLERANCES: LINEAR: ANGULAR:	FINISH:				DEBUR AND BREAK SHARP EDGES	DO NOT SCALE DRAWING / REVISION
	NAME	SIGNATURE	DATE			TITLE:
DRAWN						
CHK'D						
APPV'D						
MFG						
Q.A				MATERIAL:		DWG NO. threaded bar / A4
				WEIGHT:		SCALE:1:5 / SHEET 1 OF 1

Appendix B
Design Calculations

B1. Determination of apparatus size

The apparatus utilised in this study was designed to be secured to an I-beam of standard dimensions. In general, apart from the mounting brackets, the size of the apparatus is not an issue. The only issue being to provide enough space for the pendulum system to swing unobstructed. In the setting of this study enough width needed to be provided to accommodate a porcine head and a great enough length to accommodate the greatest distance attained by the pendulum's arc under test conditions.

Calculating this distance essentially involves the answering of the question, "How much will the porcine head move after impact?" This can be accomplished by transforming the pendulum motion of the porcine head after impact into a triangle (fig. B.1) and solving for the unknown dimensions using trigonometric functions and general physics equations.

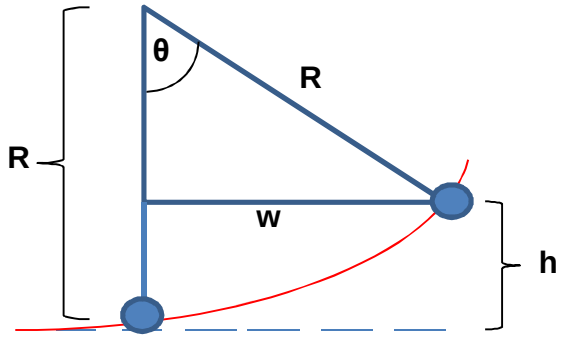

Fig. B.1 Motion of a pendulum. R: radius of pendulum arc. θ: angle of swing. w: longitudinal distance of swing. h: height of swing.

The results of these calculations can be found in table B.1. First the velocity of the porcine head after impact needs to be calculated.

$$V_0 = \frac{mV_p}{M + m}$$

Where: V_0 is the velocity of the pigs head after impact, V_p is the velocity of the projectile, m is the mass of the projectile, and M is the mass of the porcine head.

Following this the height attained by the pendulum (h) can be calculated

$$KE = \frac{1}{2}(M + m){V_0}^2 = (M + m)gh$$

$$\therefore h = \frac{{V_0}^2}{2g}$$

Where KE is kinetic energy, g is gravitational acceleration (9.8m/s^2), and h is the height attained by the pendulum.

Following this the angle of the swing (θ) can be calculated:

$$\theta = cos^{-1}[1 - \frac{h}{R}]$$

And finally the longitudinal distance (w) of the swing can be calculated:

$$w = R \sin \theta$$

The length of "R" in our tests was chosen to be 1 000mm. Using these equations it was determined that the greatest longitudinal distance the pendulum swing would attain under test conditions would be 444mm. This would occur at an impact velocity of 30m/s with a 0.2kg projectile if the porcine head weighs 4Kg. Thus the apparatus was designed to accommodate a pendulum swing of at least this magnitude.

Table B.1 Results of pendulum motion calculations

R	M	m	V_p	V_0	h	θ	w	
(m)	(Kg)	(Kg)	(m/s)	(m/s)	(m)	(deg)	(m)	(mm)
1	5	0.1	10	0.196	0.00196	3.59	0.0626	**62.6**
1	5	0.1	20	0.392	0.00784	7.18	0.125	**125**
1	5	0.1	30	0.588	0.01765	10.78	0.187	**187.1**
1	5	0.2	10	0.384	0.00754	7.04	0.1226	**122.6**
1	5	0.2	20	0.769	0.03019	14.11	0.2438	**243.9**
1	5	0.2	30	1.153	0.06792	21.24	0.3626	**362.3**
1	4	0.1	10	0.243	0.00303	4.47	0.0778	**77.9**
1	4	0.1	20	0.488	0.01214	8.94	0.1553	**155.3**
1	4	0.1	30	0.732	0.02731	13.42	0.2321	**232.1**
1	4	0.2	10	0.476	0.01156	8.72	0.1516	**151.7**
1	4	0.2	20	0.952	0.04627	17.5	0.3006	**300.7**
1	4	0.2	30	1.428	0.10412	26.38	0.4443	**444.3**

B2. Deflection calculations

The overall structure of the apparatus needs to be as stable as possible and the beams which support the weight of the specimen should bend or deflect as little as possible. Steel angle iron was chosen as the major material in the assembly of the apparatus. Because of its design, angle iron is far stronger and more resistant to bending than steel flat plate. It is still necessary however to determine if the dimensions of the chosen angle iron are great enough to resist as much bending as possible.

Before the maximum deflection can be calculated it is first necessary to calculate the second moment area (I) of the angle iron (50mm x 50mm x 6mm). The second moment area is a geometric property of an area reflecting where its points lie in relation to an arbitrary axis. The second moment area of an angle iron may be calculated by dividing it up into rectangles about the neutral axis as seen in figure B.2 and calculating the second moment area of each rectangle. The equation to determine the second moment area of a rectangle about an axis through its side is:

$$\boldsymbol{I = \frac{bh^3}{3}}$$

Where b is the length of the base and h is the height of the rectangle. The second moment area of the angle iron as seen in figure B.2 therefore becomes:

$$\boldsymbol{I_{angle\ iron} = I_{bottom\ rectangle} - I_{shaded} + I_{vertical\ rectangle}}$$

$$\boldsymbol{I = \frac{1}{3}[bd^3 - (b-c)(d-c)^3 + c(a-d)^3]}$$

If a=0.05m, b=0.05m, c=0.006m and d=0.0147m then the second moment area of an angle iron with dimensions 50mm x 50mm x 6mm is 1.312 x 10^{-7} m^4.

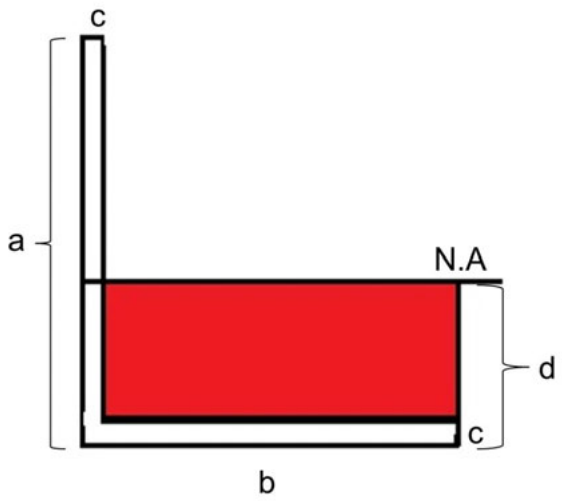

Fig. B.2 Angle iron for calculations. N.A – Neutral Axis

We wish to calculate the maximum deflection of the top side angle irons and the top bar angle iron. These components may be modelled as simply supported beams with a concentrated load at the centre. The equation to determine the maximum deflection of such beams is:

$$\Delta = \frac{\boldsymbol{WL^3}}{\boldsymbol{48E_yI}}$$

Where Δ is the deflection, W is the weight of the load (mass of the porcine head multiplied by gravitational acceleration), L is the length of the beam, E_y is the Young's modulus of the material, and I is the second moment area of the beam. The results of these calculations can be found in table B.2. The deflection in all these beams is less than 0.5mm. Therefore the use of angle iron of dimension 50mm x 50mm x 6mm is sufficient for these parts of the assembly.

Table B.2 Results of deflection calculations

Part	M	W	L	E_y	I	Δ	
	(Kg)	(N)	(m)	(N/m^2)	(m^4)	(m)	(mm)
Top bar	5	49	0.6	2×10^{11}	1.312×10^{-7}	8.399×10^{-6}	**0.008**
Top bar	4	39.2	0.6	2×10^{11}	1.312×10^{-7}	6.719×10^{-6}	**0.007**
Top side	5	49	1	2×10^{11}	1.312×10^{-7}	3.88×10^{-5}	**0.039**
Top side	4	39.2	1	2×10^{11}	1.312×10^{-7}	3.11×10^{-5}	**0.031**

B3. Vibrational analysis

When a force is applied to a solid it often causes the solid to vibrate. Such vibrations are termed forced vibrations. In the current context, impacting the porcine head will cause the entire suspension rig to vibrate. Of particular importance are the vibrations of the top bar and top side angle irons, as the vibrations of these elements may interfere with the pendulum motion of the head after impact and thus may affect any subsequent calculations based on smooth pendulum motion. A high vibrational frequency will have a small effect on the pendulum motion while a low vibrational frequency will have a far greater effect on the pendulum motion.

The following equation may be used to calculate the vibrational frequency of a bar:

$$f = \frac{1}{2\pi}\sqrt{\frac{48E_yI}{ML^3}}$$

This may be simplified because we know from the deflection calculations:

$$\Delta = \frac{WL^3}{48E_yI}$$

$$\therefore f = \frac{1}{2\pi}\sqrt{\frac{g}{\Delta}}$$

Where f is the frequency, g is gravitational acceleration (9.8m/s^2), and Δ is the maximum deflection of the beam.

The period of oscillation is the inverse of the frequency.

$$T = \frac{1}{f}$$

The results of these calculations can be found in table B.3.

Table B.3 Results of vibrational analysis

Part	g	Δ	f	T
	(m/s^2)	(m)	(Hz)	(sec)
Top bar	9.8	8.399 x10^{-6}	**171.91**	**0.0058**
Top bar	9.8	6.719 x10^{-6}	**192.2**	**0.0052**
Top side	9.8	3.88 x10^{-5}	**79.9**	**0.0125**
Top side	9.8	3.11 x10^{-5}	**89.32**	**0.0112**

B4. Velocity of impact

This study examined impacts at velocities of approximately 10m/s, 15m/s and 25m/s. These impact velocities were chosen to represent impacts of low, medium and high velocities respectively which may be attained by an assailant wielding a hammer. Very little data exists on the impact velocities of non-ballistic weapons. As such it was necessary to determine the possible upper limit impact velocity which may be attained by a blow with a hammer.

This study attempted to replicate impacts by a household hammer of 0.2Kg. In order to determine what impact velocities a person is capable of achieving, it is sometimes easier to think in terms of everyday activities. For instance: Is a normal person capable of throwing a 0.2Kg hammer across the width of a sports field? The answer to this

question is, “Yes”. Most people would be able to throw a 0.2Kg hammer across the width of a field. Very few people however, would be able to throw much further than this.

In keeping with the sports field analogy, what then would the velocity of the hammer be once it is released from the hand? This can be calculated by using one of the equations for projectile motion.

$$s = \frac{V_0^{\,2} \sin 2\theta}{g}$$

Where s is the horizontal distance travelled, V_0 is the initial velocity, θ is the release angle, and g is gravitational acceleration (9.8m/s^2).

Solving for V_0 this becomes:

$$V_0 = \sqrt{\frac{sg}{\sin 2\theta}}$$

The width of a rugby field is 50m and the angle for optimum launch is 45 degrees. Therefore in order to throw the hammer across the width of a rugby field the velocity of the hammer at release would have to be 22.14m/s.

The motion used to throw a hammer is similar to the motion of using it as a blunt instrument. Looking at this calculation it is therefore a reasonable assumption that most people would be able to attain an impact velocity of at least 20m/s with a hammer. Therefore in this study an upper limit impact velocity of 25m/s was chosen.

B5. Pressure calculations

A gas gun utilises shop air to fire a projectile. The velocity of the projectile is determined by the pressure generated by the gas gun. The velocities produced in this study were 10m/s, 15m/s and 25m/s. The pressure required to attain these velocities can be calculated as follows:

$$KE = \frac{1}{2}MV^2 = PAL$$

$$\therefore P = \frac{MV^2}{2AL}$$

Where KE is kinetic energy, M is the mass of the projectile, V is the velocity of the projectile, P is pressure, A is the surface area of the back of the projectile, and L is the length of the barrel.

The results of these calculations can be found in table B.4.

Table B.4 Results of pressure calculations

M	**V**	**A**	**L**	**P**		
(Kg)	(m/s)	(m^2)	(m)	(Pa)	(KPa)	(Bar)
0.1	10	3.1×10^{-4}	1	15915.49	15.915	**0.15**
0.1	15	3.1×10^{-4}	1	36290.32	36.290	**0.36**
0.1	25	3.1×10^{-4}	1	100806.4	100.81	**1.01**
0.2	10	3.1×10^{-4}	1	31830.99	31.8	**0.32**
0.2	15	3.1×10^{-4}	1	72580.64	72.58	**0.73**
0.2	25	3.1×10^{-4}	1	201612.9	201.61	**2.02**

Appendix C
Test results

C1. Hammer tests

Specimen No.	Scalp thickness	Implement weight	Gas gun pressure	Striker velocity	Kinetic energy	Presence of fracture	Soft tissue damage	Hard tissue damage
P02-13	6mm	200g	160KPa	18.8m/s	35.34J	Yes	 L-shaped deep laceration (10mm x 7mm)	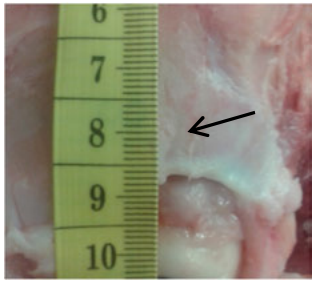 Small S-shaped linear fracture (13mm) on orbital ridge
P03-13	7mm	200g	240KPa	23.25m/s	54.06J	Yes	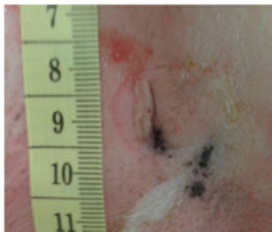 Semi-circular abrasion (19mm x 12mm) with straight deep laceration (15mm) through centre	 Small linear fracture (47mm)

Specimen No.	Scalp thickness	Implement weight	Gas gun pressure	Striker velocity	Kinetic energy	Presence of fracture	Soft tissue damage	Hard tissue damage
P04-13	5mm	200g	240KPa	23.95m/s	57.3J	Yes	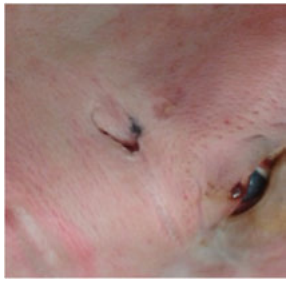 Semi-circular (20mm x 10mm) deep laceration	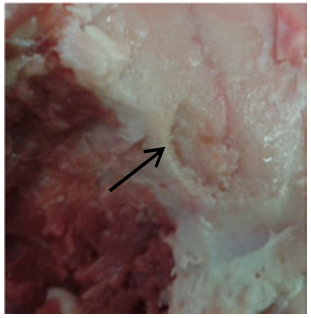 Semi-circular (16x6mm) depressed fracture (1mm deep
P05-13	6mm	200g	160KPa	18.01m/s	32.44J	No	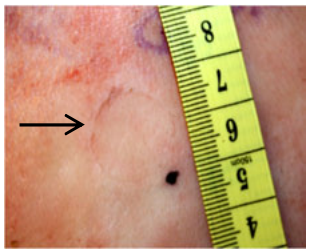 Superficial circular laceration (17mm x 16mm)	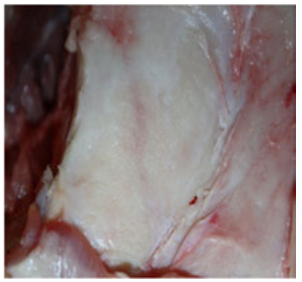 No damage

Specimen No.	Scalp thickness	Implement weight	Gas gun pressure	Striker velocity	Kinetic energy	Presence of fracture	Soft tissue damage	Hard tissue damage
P06-13	4mm	200g	140 KPa	17.85m/s	31.86J	Yes	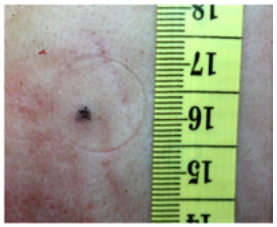 Superficial circular laceration (17mm x 17mm)	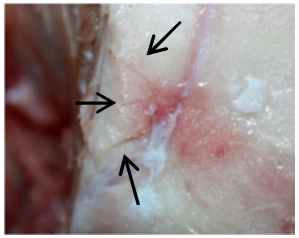 3 small radiating fractures. Sup. 5mm, mid. 3mm, inf. 4mm.
P07-13	5mm	200g	120 KPa Half Barrel	11.26m/s	12.67J	No	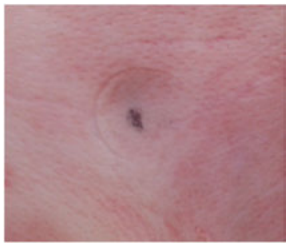 Superficial circular laceration (16mm x 16mm). Circular defect to fascia sup. to periosteum (20mm x 10mm)	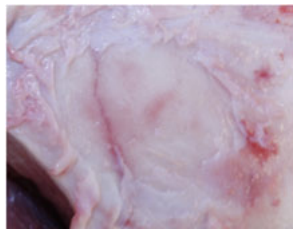 No damage

Specimen No.	Scalp thickness	Implement weight	Gas gun pressure	Striker velocity	Kinetic energy	Presence of fracture	Soft tissue damage	Hard tissue damage
P08-13	7mm	200g	80 KPa Half Barrel	9.34m/s	8.72J	No	No damage	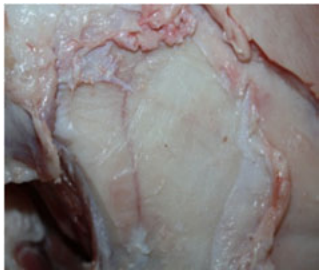 No damage
P09-13	6mm	200g	80 KPa Half Barrel	7.75m/s	6.01J	No	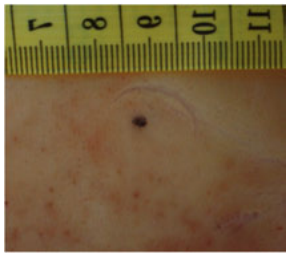 Superficial semi-circular abrasion (18mm x 8mm)	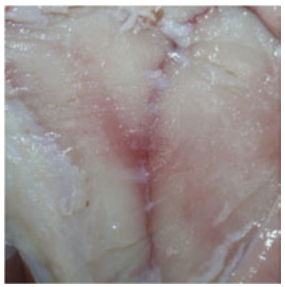 No damage

Specimen No.	Scalp thickness	Implement weight	Gas gun pressure	Striker velocity	Kinetic energy	Presence of fracture	Soft tissue damage	Hard tissue damage
P10-13	8mm	200g	240 KPa	23.95m/s	57.36J	Yes	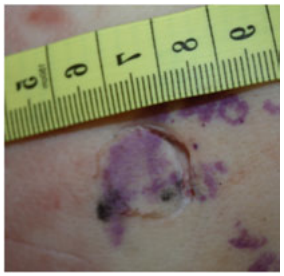 Semi-circular deep laceration (20mm x 16mm)	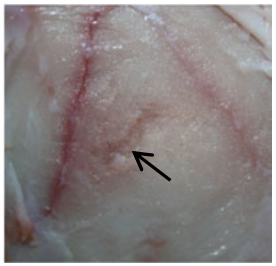 Irregular shaped depression (15mm x 3mm)
P11-13 Test discarded because impact was not in correct position	4mm	200g	80 KPa Half Barrel	13.38m/s	17.9J	Yes	 Superficial circular laceration (18mm x 16mm)	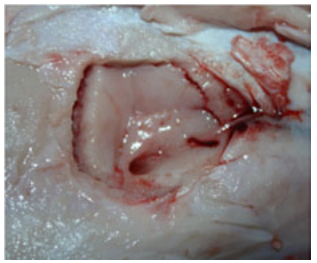 Depressed fracture (20mm x 20mm)

Specimen No.	Scalp thickness	Implement weight	Gas gun pressure	Striker velocity	Kinetic energy	Presence of fracture	Soft tissue damage	Hard tissue damage
P12-13	6mm	200g	160 KPa	19.41m/s	37.67J	Yes	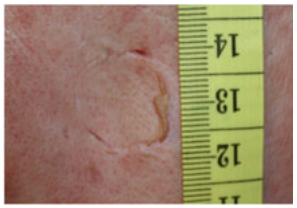 Deep circular laceration (20mm x 14mm)	 Deep comminuted circular depression (32mm x 26mm)
P13-13	5mm	200g	240KPa	24.09m/s	58.03J	No	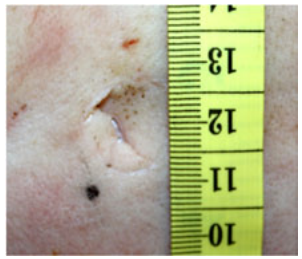 Irregular Y-shaped laceration (7mm)	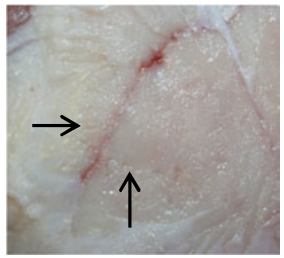 Faint semi-circular impression

Specimen No.	Scalp thickness	Implement weight	Gas gun pressure	Striker velocity	Kinetic energy	Presence of fracture	Soft tissue damage	Hard tissue damage
P14-13	No skin	200g	80 KPa Half Barrel	13.25m/s	17.56J	Yes	No skin	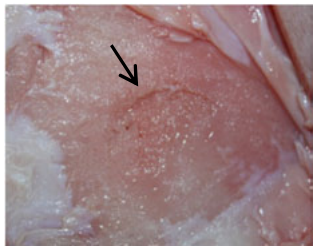 Crescent shaped linear fracture (18mm)
P15-13	No skin	200g	140 KPa	17.85m/s	31.86	Yes	No skin	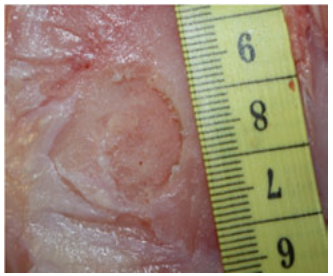 Semi-circular depressed fracture (16mm x 6mm)

Specimen No.	Scalp thickness	Implement weight	Gas gun pressure	Striker velocity	Kinetic energy	Presence of fracture	Soft tissue damage	Hard tissue damage
P16-13	No skin	200g	240 KPa	23.25m/s	54.06	Yes	No skin	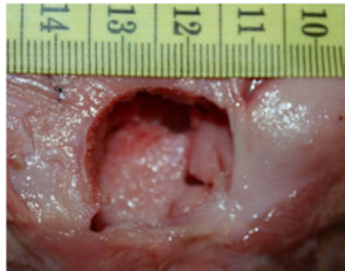 Deep comminuted circular depression (20mm x 20mm)

C2. Hopkinson pressure bar tests

Specimen No.	Scalp thickness	Implement weight	Gas gun pressure	Striker velocity	Impact energy	Peak force	Presence of fracture	Hard tissue damage
P17-13	No skin	200g	200KPa	15.41m/s	6.28J	8150N	No	 No damage

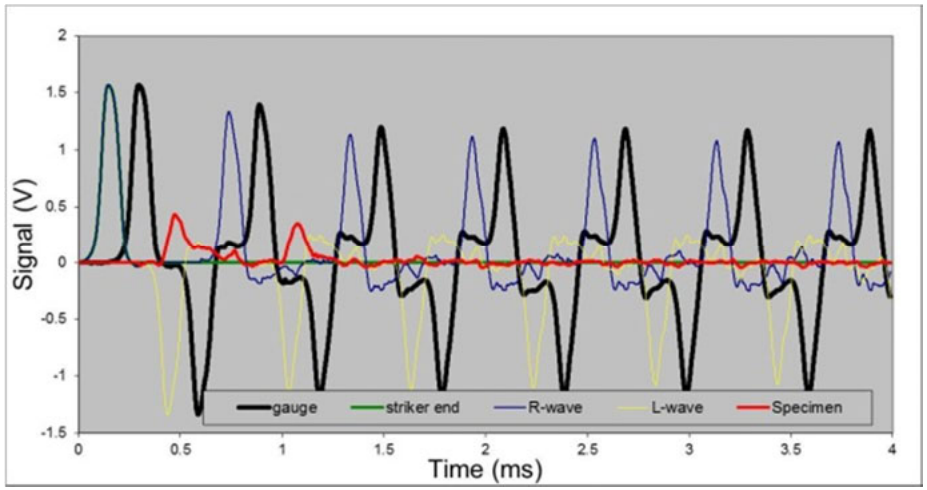

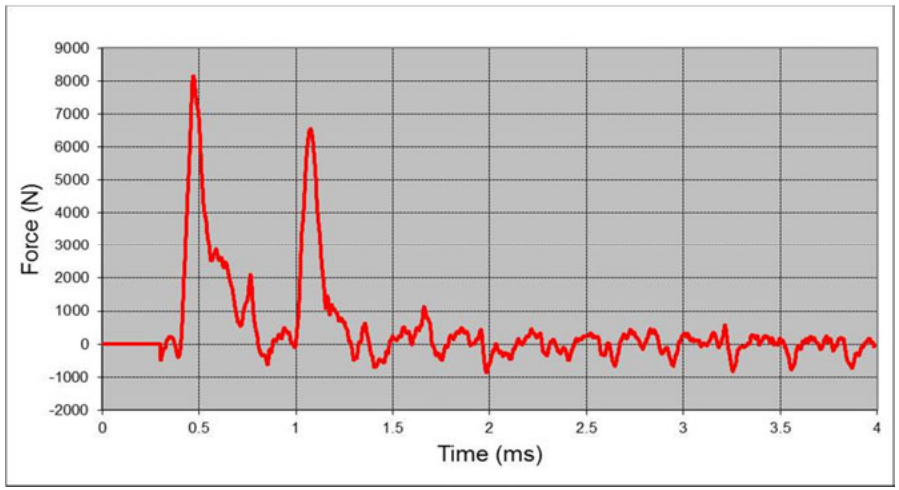

Specimen No.	Scalp thickness	Implement weight	Gas gun pressure	Striker velocity	Impact energy	Peak force	Presence of fracture	Hard tissue damage
P18-13	No skin	200g	100KPa	10.8m/s	3.62J	2760N	No	 No damage

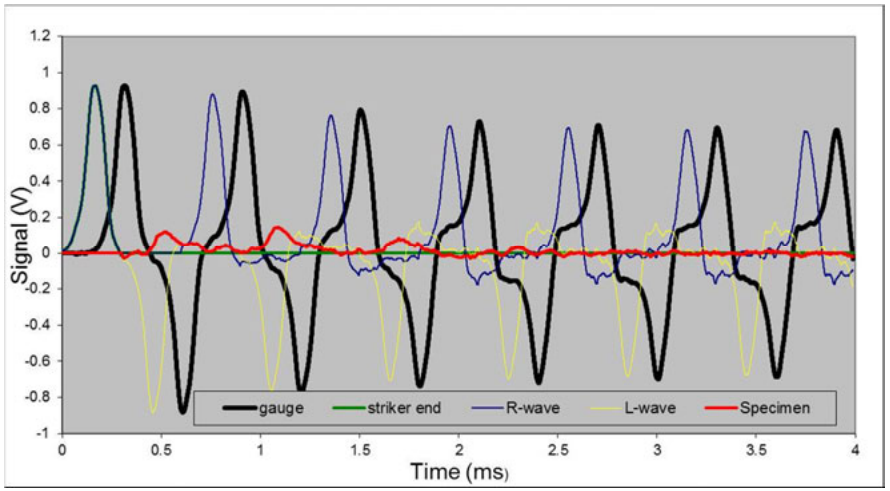

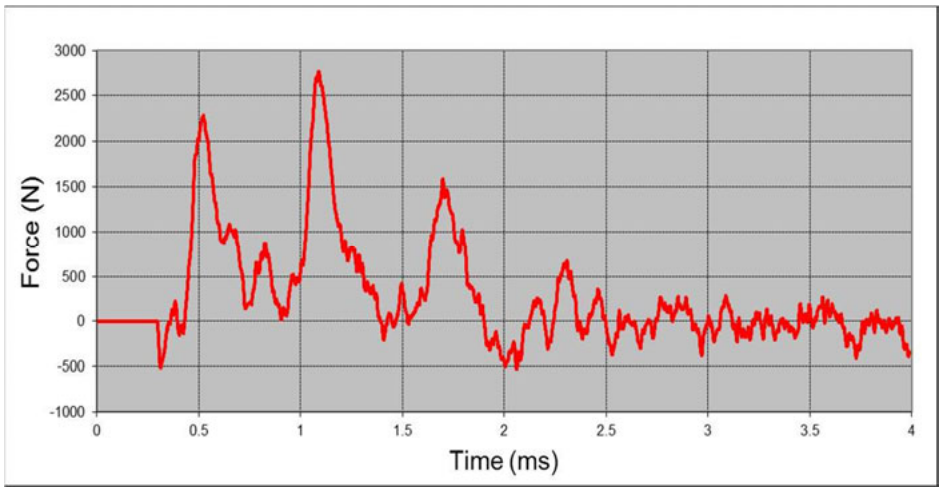

Specimen No.	Scalp thickness	Implement weight	Gas gun pressure	Striker velocity	Impact energy	Peak force	Presence of fracture	Hard tissue damage
P19-13	No skin	200g	80KPa	10.8m/s	2.25J	1720N	Yes	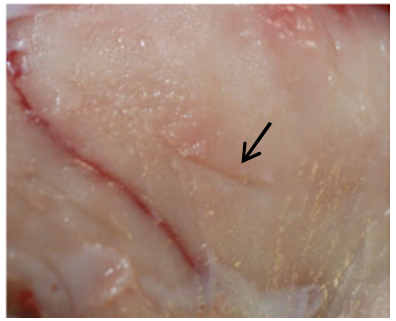 Linear fracture (8mm)

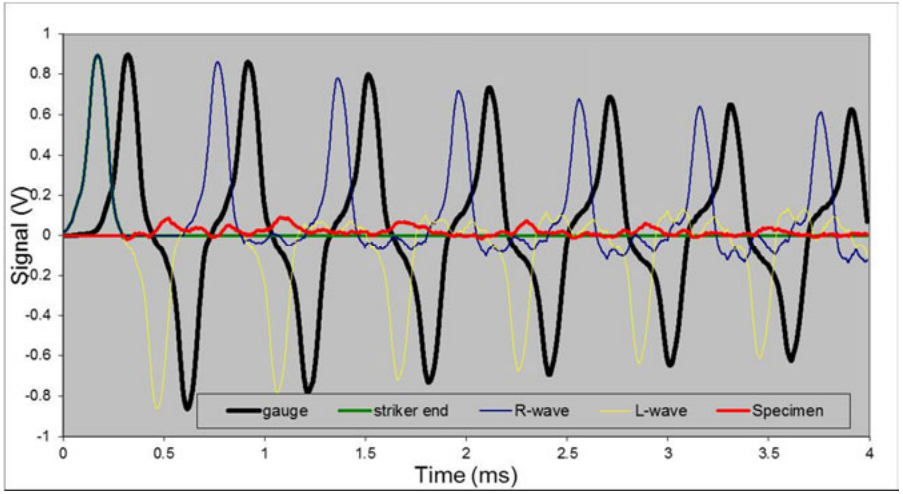

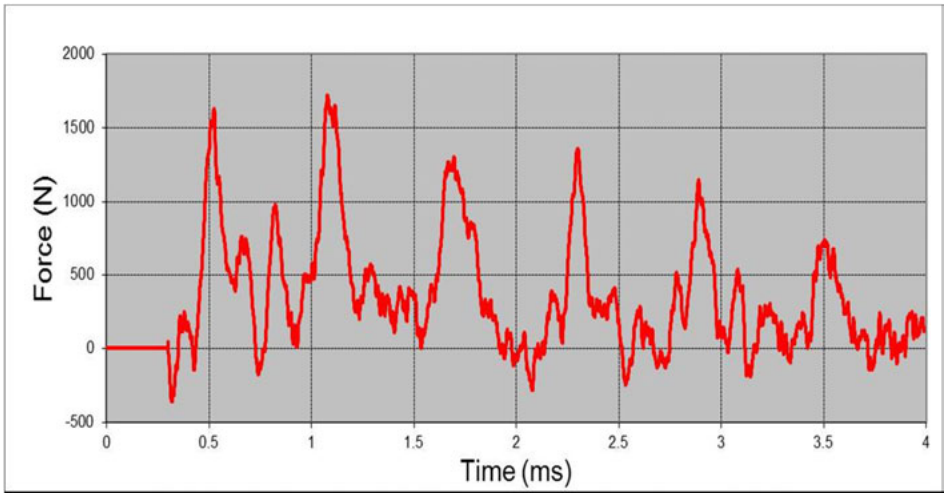

Specimen No.	Scalp thickness	Implement weight	Gas gun pressure	Striker velocity	Impact energy	Peak force	Presence of fracture	Hard tissue damage
P20-13	No skin	200g	80KPa	10.71m/s	5.31J	2750N	Yes	 Slight semi-circular depression (±10mm)

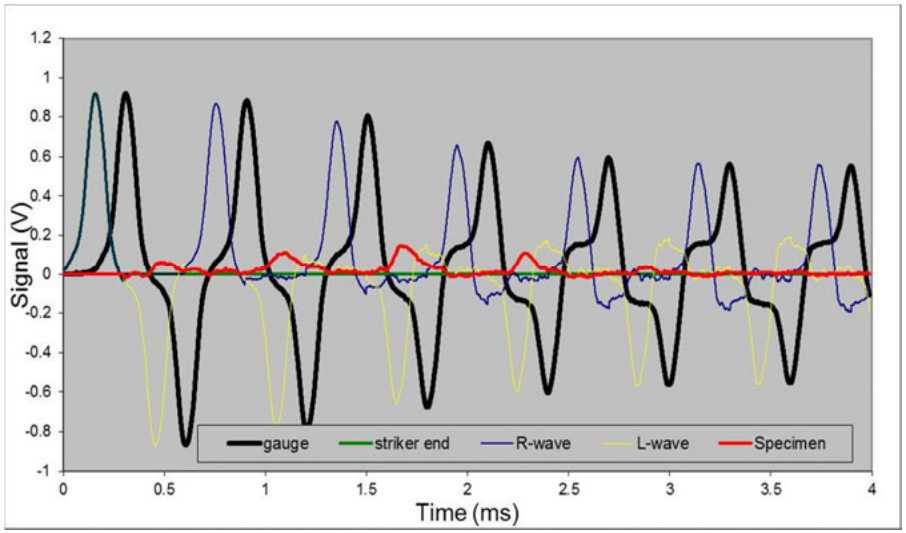

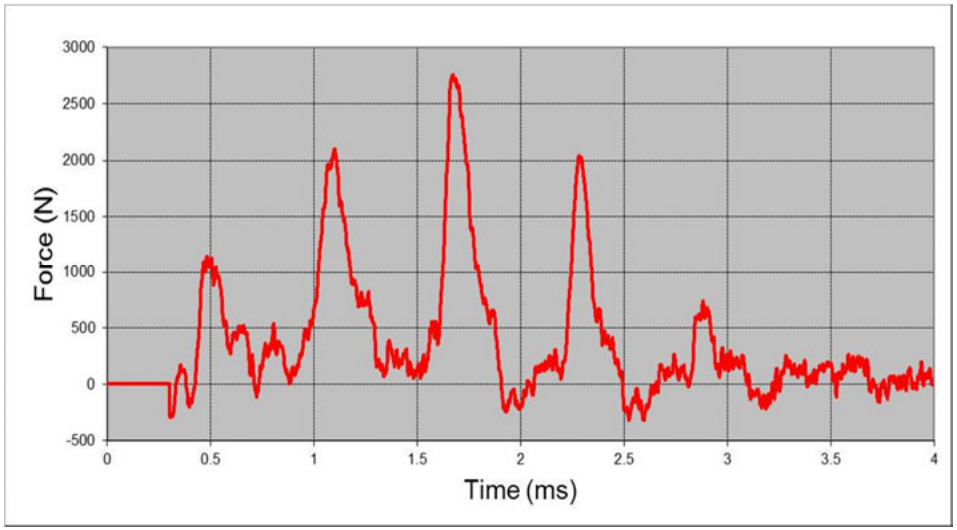

Specimen No.	Scalp thickness	Implement weight	Gas gun pressure	Striker velocity	Impact energy	Peak force	Presence of fracture	Hard tissue damage
P21-13	No skin	200g	140KPa	18.75m/s	34.25J	9110N	Yes	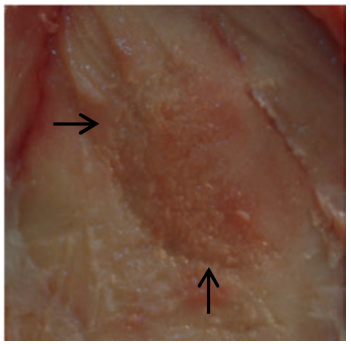 Slight semi-circular depression (20mm x 8mm)

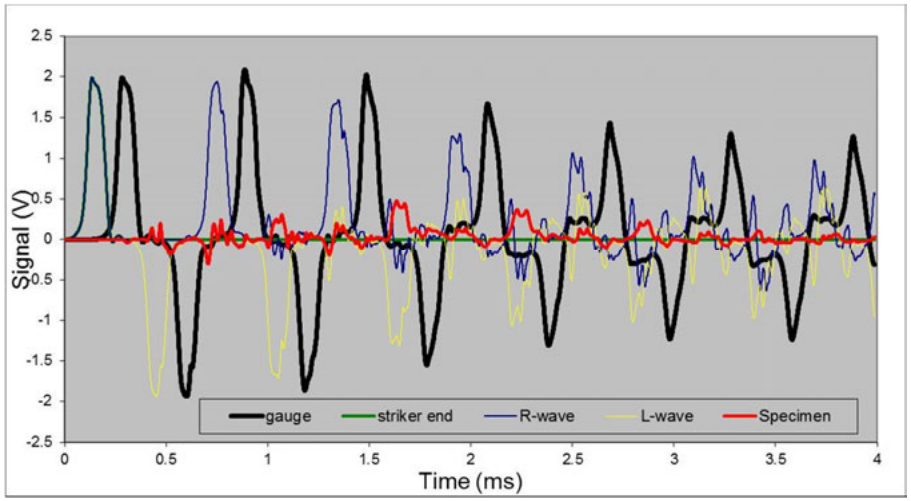

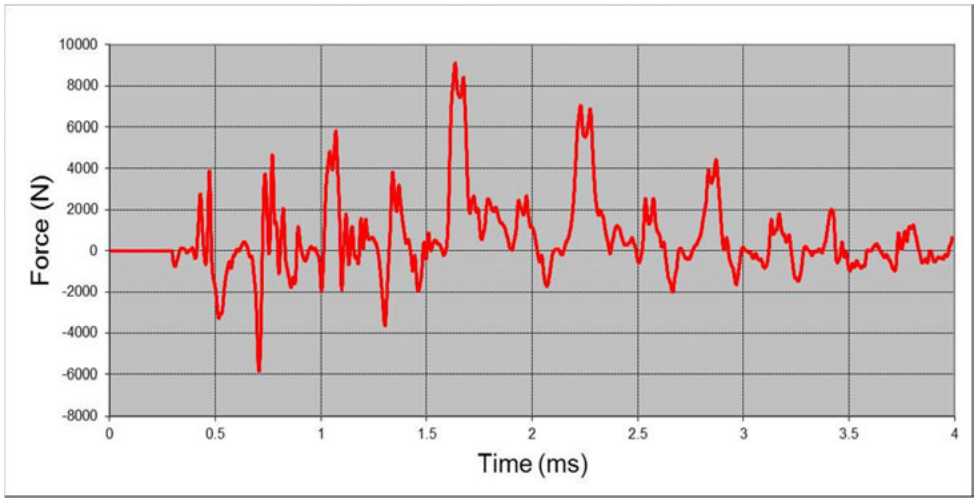

Specimen No.	Scalp thickness	Implement weight	Gas gun pressure	Striker velocity	Impact energy	Peak force	Presence of fracture	Hard tissue damage
P22-13	No skin	200g	140KPa	17.44m/s	17.51J	8070N	No	 No damage

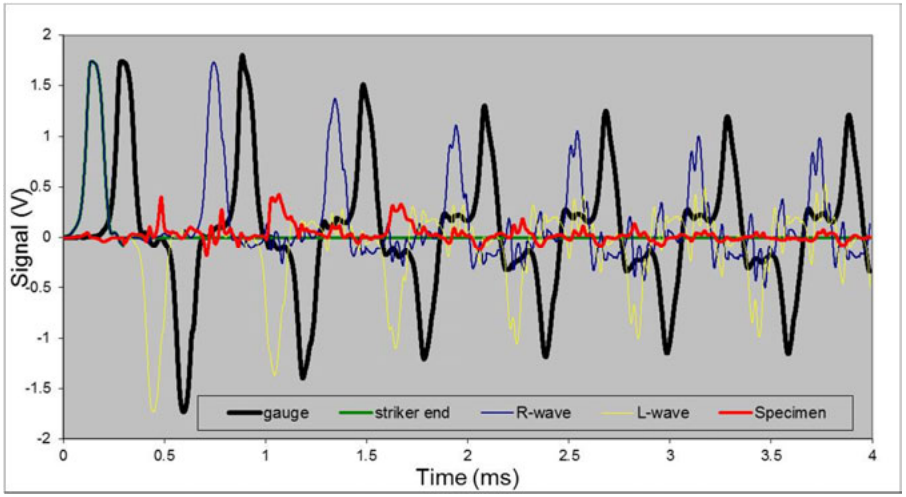

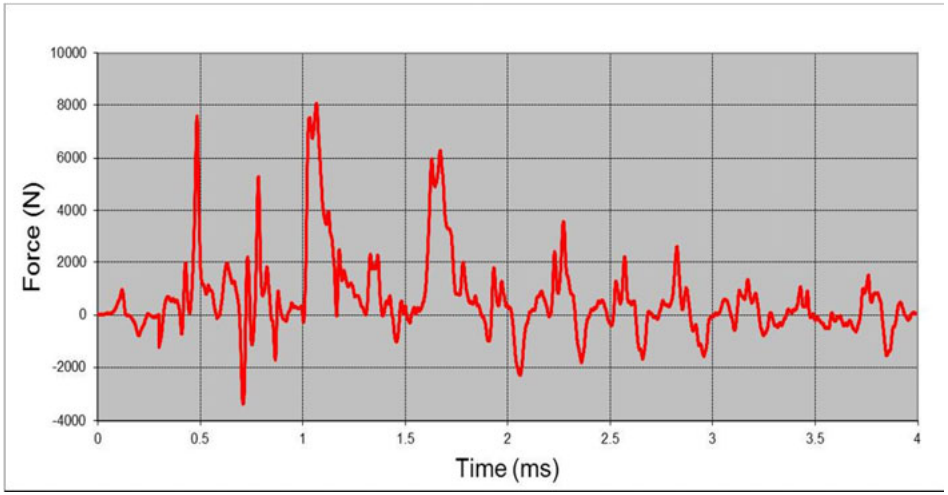

Specimen No.	Scalp thickness	Implement weight	Gas gun pressure	Striker velocity	Impact energy	Peak force	Presence of fracture	Hard tissue damage
P23-13	No skin	200g	200KPa	19.91	14.58J	6720N	Yes	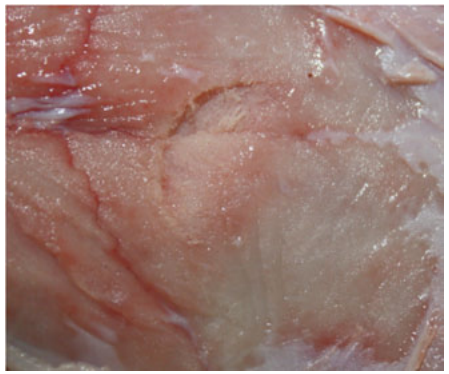 Semi-circular depressed fracture (16mm x 5mm)

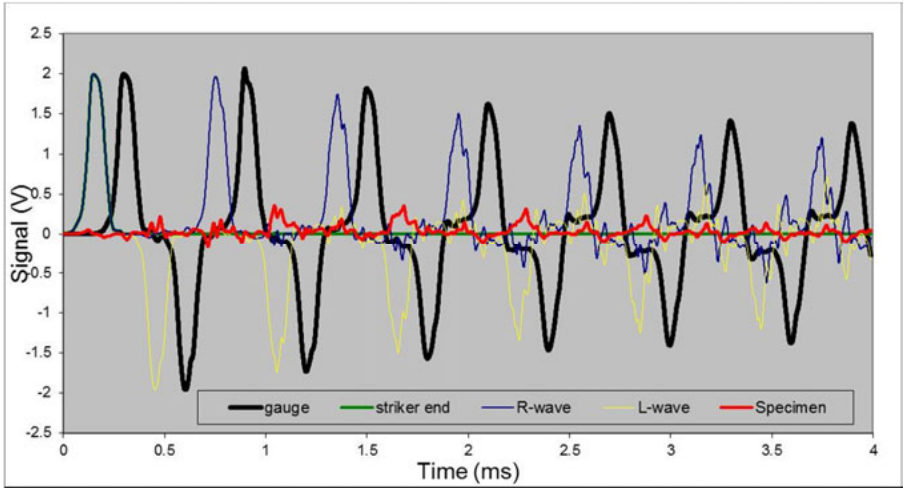

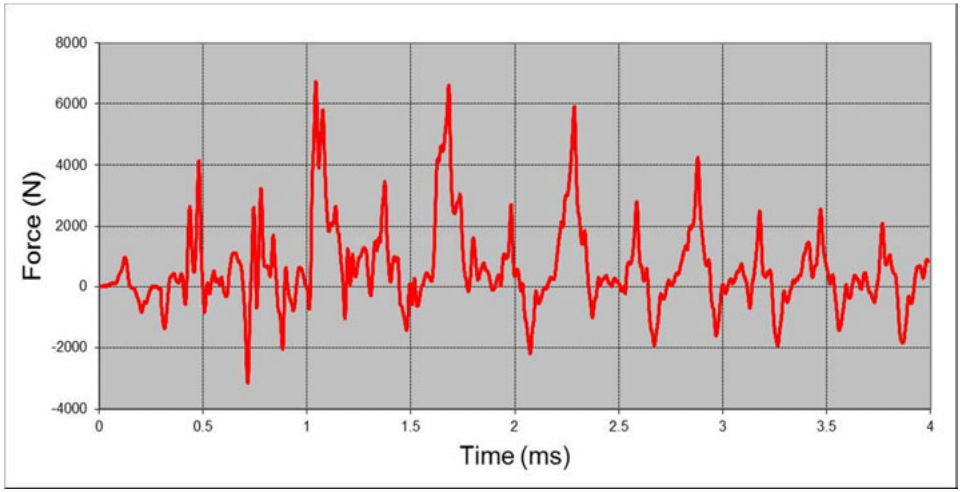

Specimen No.	Scalp thickness	Implement weight	Gas gun pressure	Striker velocity	Impact energy	Peak force	Presence of fracture	Hard tissue damage
P24-13	No skin	200g	240KPa	22m/s	44.89J	11140N	Yes	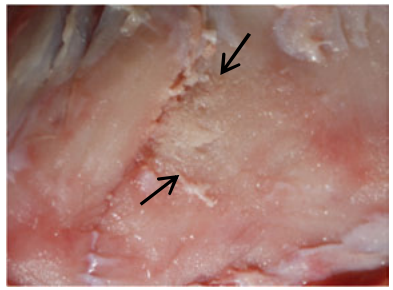 Slight semi-circular depression (15mm x 10mm)

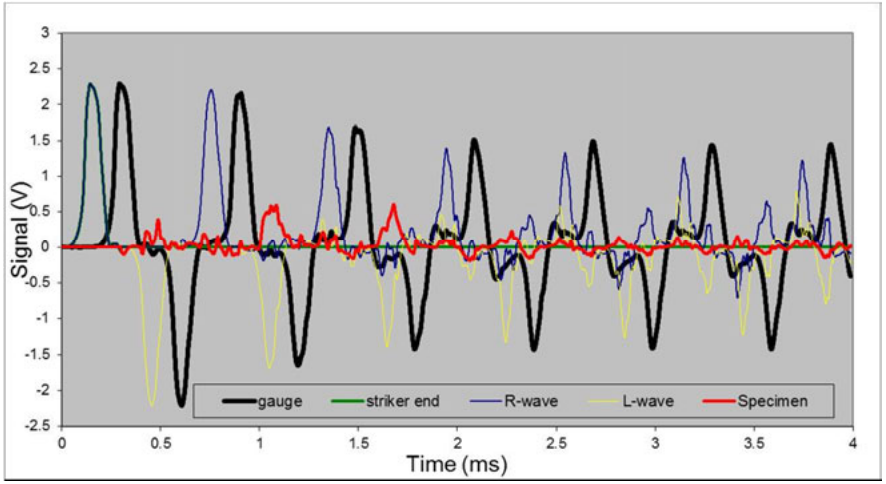

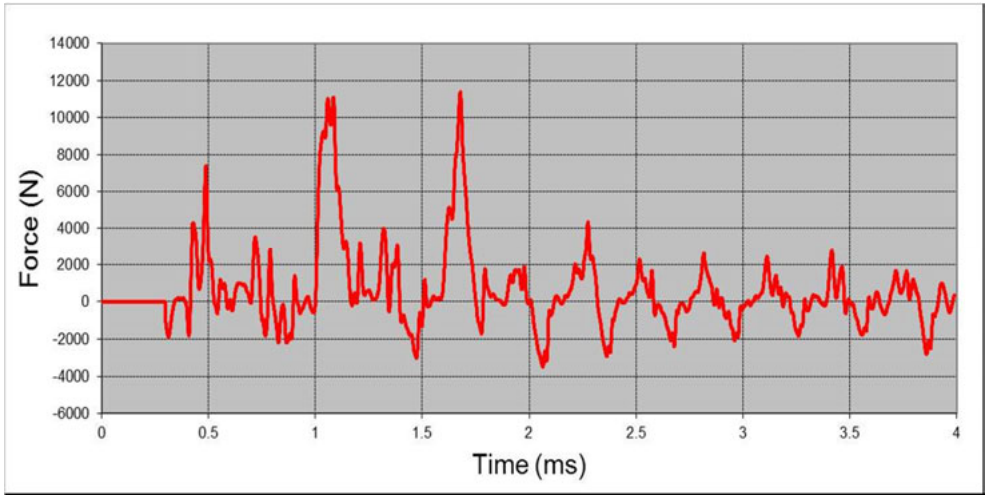

Specimen No.	Scalp thickness	Implement weight	Gas gun pressure	Striker velocity	Impact energy	Peak force	Presence of fracture	Hard tissue damage
P25-13	No skin	200g	240KPa	21.63m/s	26.2J	9080N	Yes	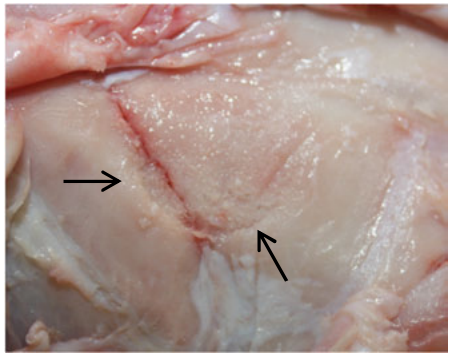 Semi-circular depressed fracture (20mm x 10mm)

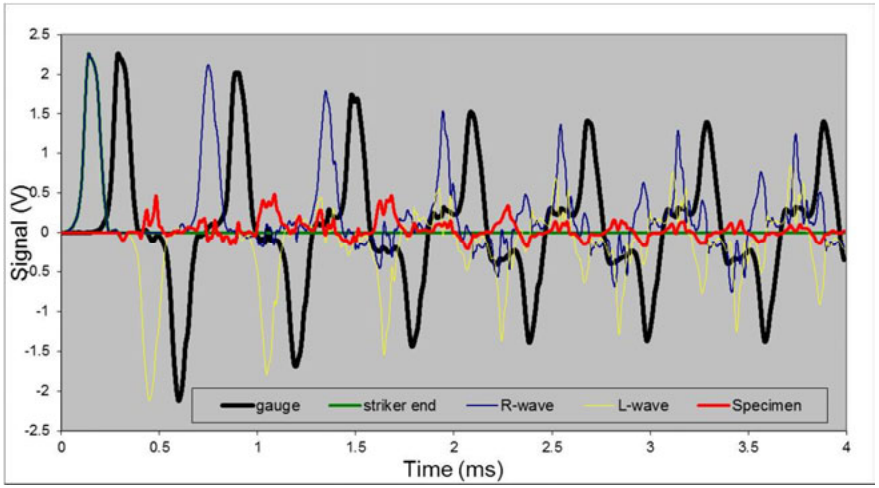

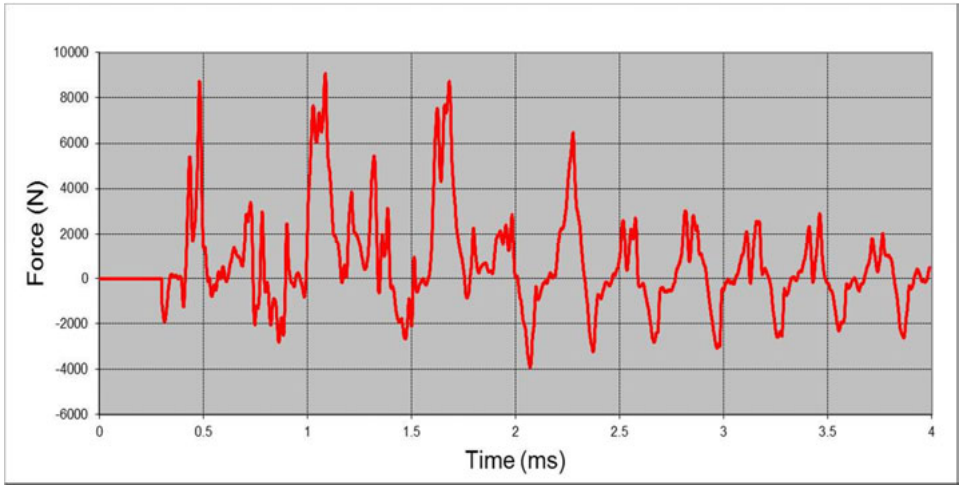

Specimen No.	Scalp thickness	Implement weight	Gas gun pressure	Striker velocity	Impact energy	Peak force	Presence of fracture	Hard tissue damage
P01-14	No skin	200g	80KPa Half Barrel	11.92m/s	11.58J	4340N	No	 No Damage

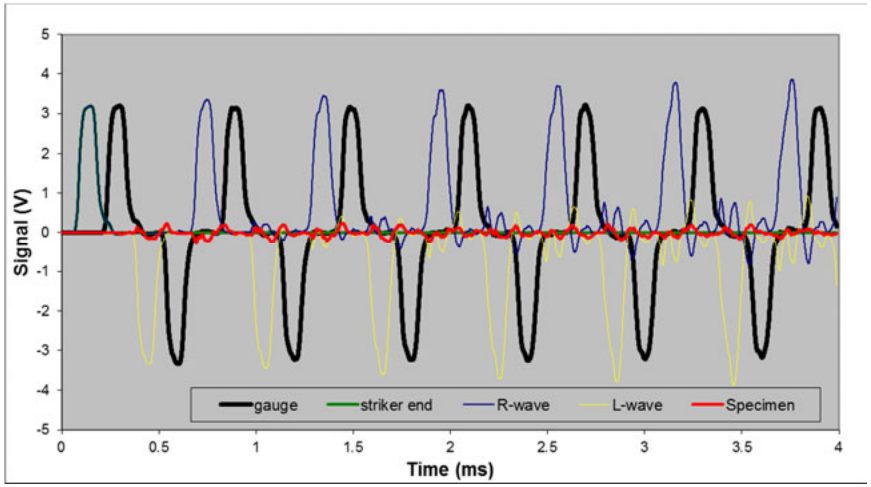

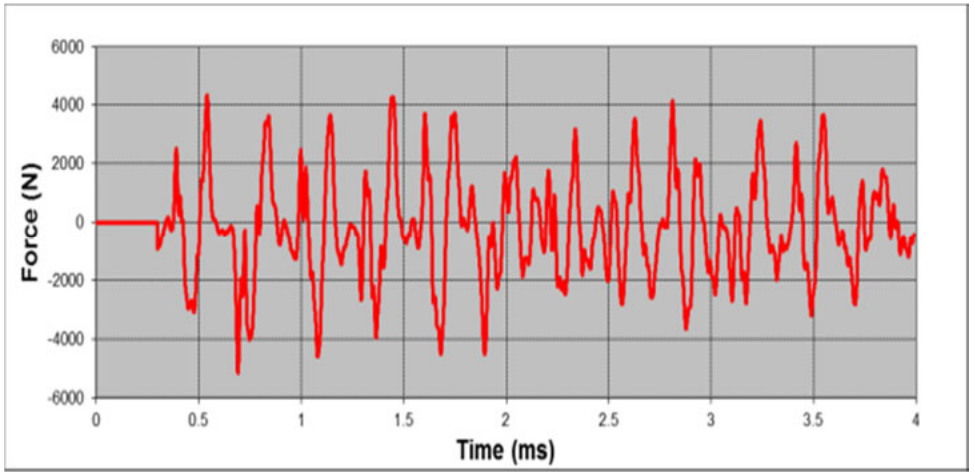

Specimen No.	Scalp thickness	Implement weight	Gas gun pressure	Striker velocity	Impact energy	Peak force	Presence of fracture	Hard tissue damage
P02-14	No skin	200g	140KPa	16.58m/s	12.4J	4120N	Yes	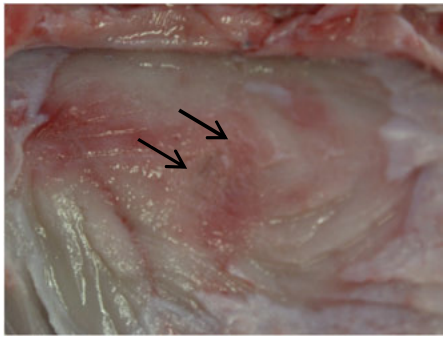 Irregular shaped depressed fracture (8mm x 5mm)

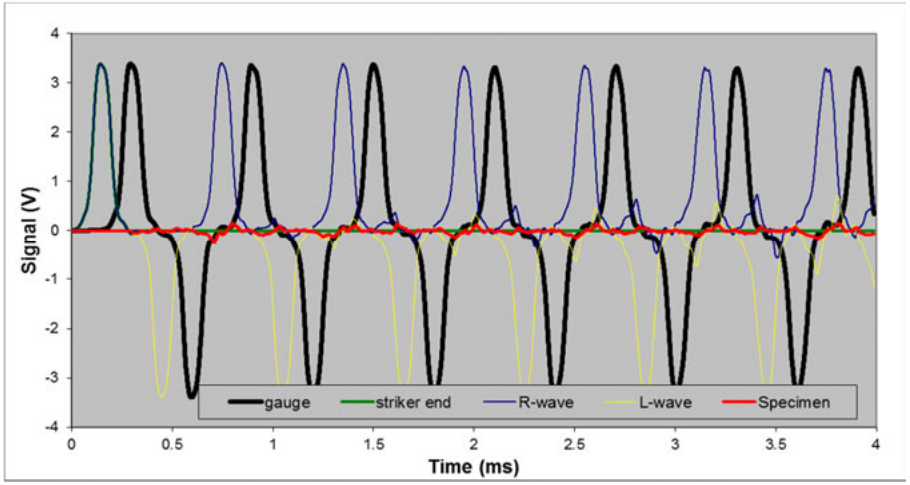

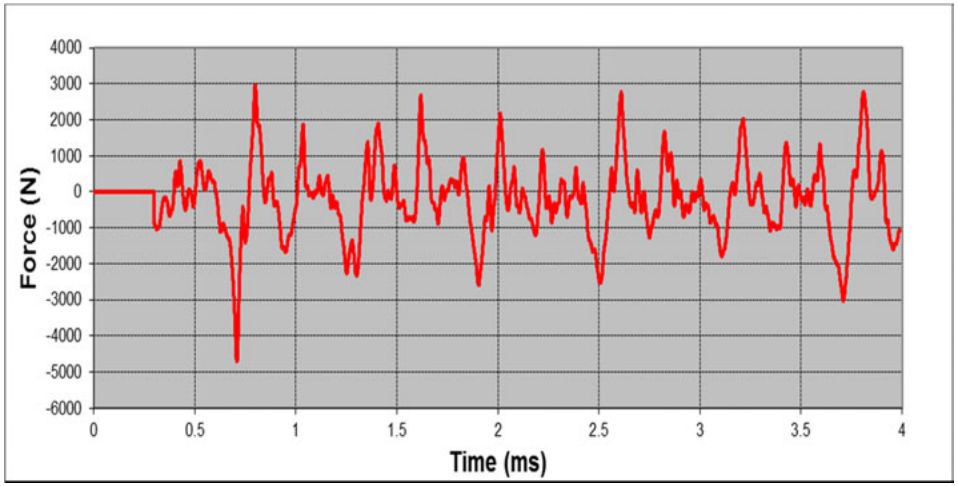

Specimen No.	Scalp thickness	Implement weight	Gas gun pressure	Striker velocity	Impact energy	Peak force	Presence of fracture	Hard tissue damage
P03-14	No skin	200g	80KPa Half Barrel	12.23m/s	10.05J	3550N	No	 No Damage

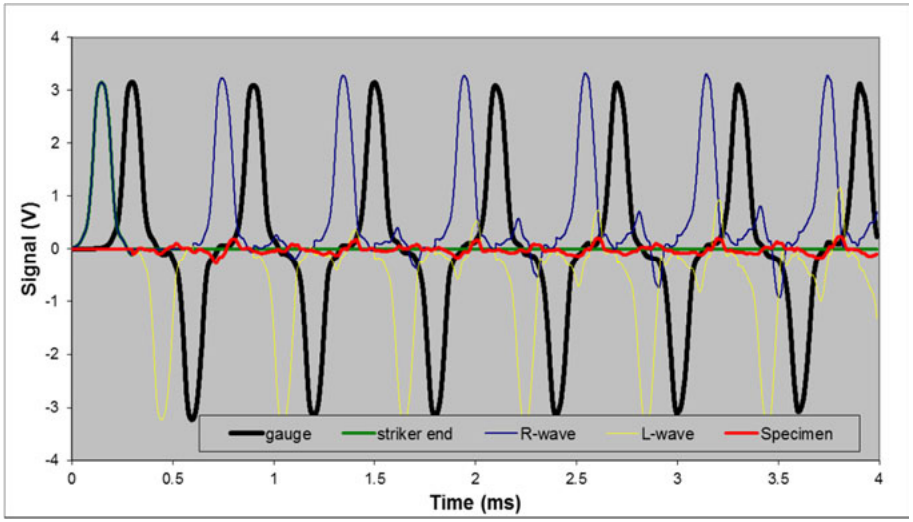

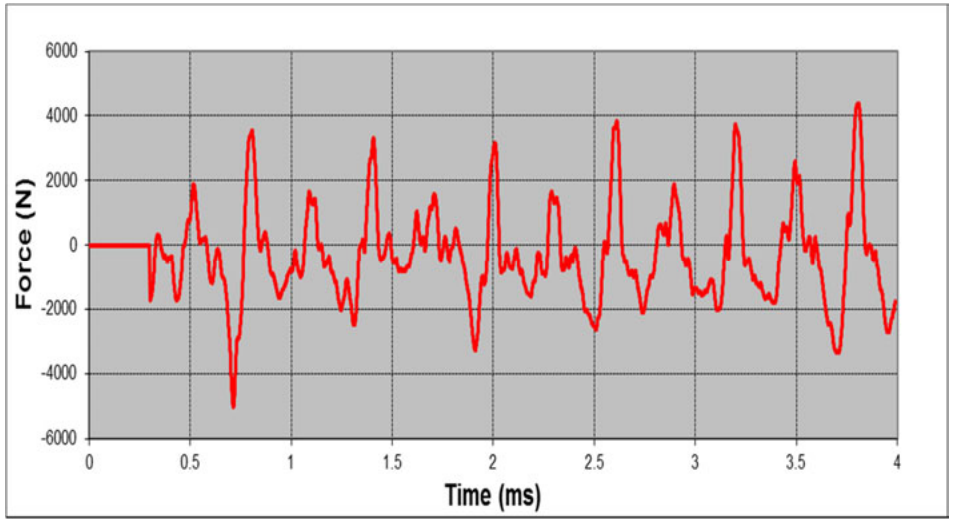

Specimen No.	Scalp thickness	Implement weight	Gas gun pressure	Striker velocity	Impact energy	Peak force	Presence of fracture	Hard tissue damage
P04-14	No skin	200g	240KPa	24.72m/s	56.32J	12800N	Yes	 Semi-circular depressed fracture (18mm x 5mm)

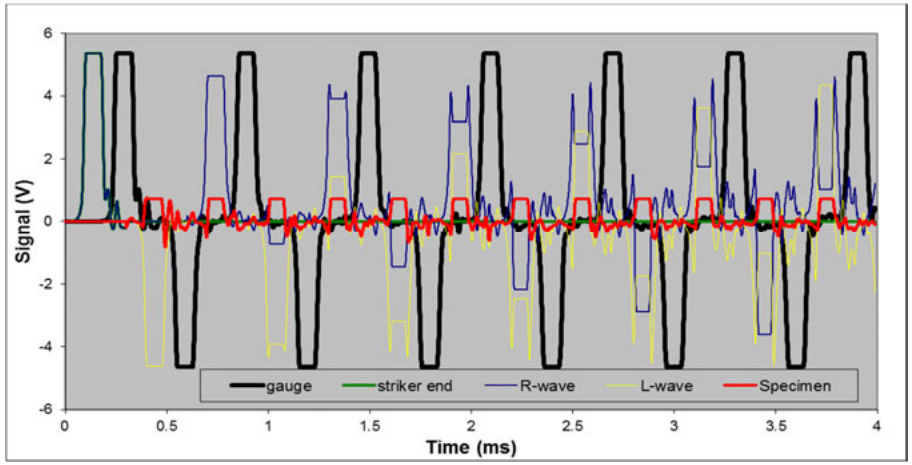

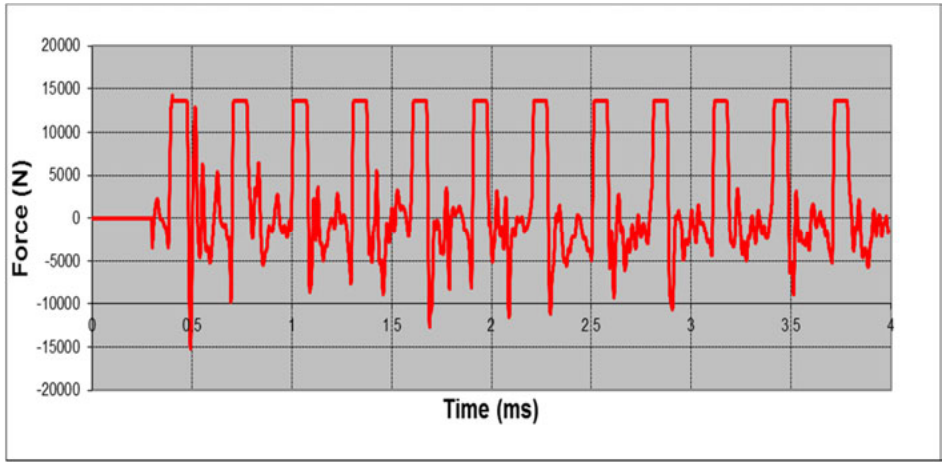

*Data from specimens P04-14, P05-14 and P06-14 produced square spikes which are artefacts. The true peak force can still be seen on the force-time plot as a natural spike.

Specimen No.	Scalp thickness	Implement weight	Gas gun pressure	Striker velocity	Impact energy	Peak force	Presence of fracture	Hard tissue damage
P05-14	No skin	200g	240KPa	24.83m/s	62.69J	13900N	No	 No Damage

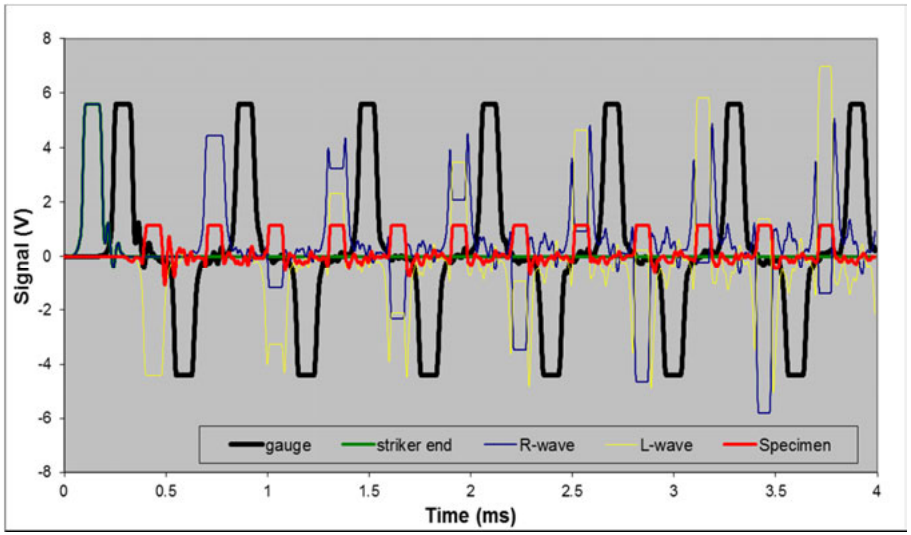

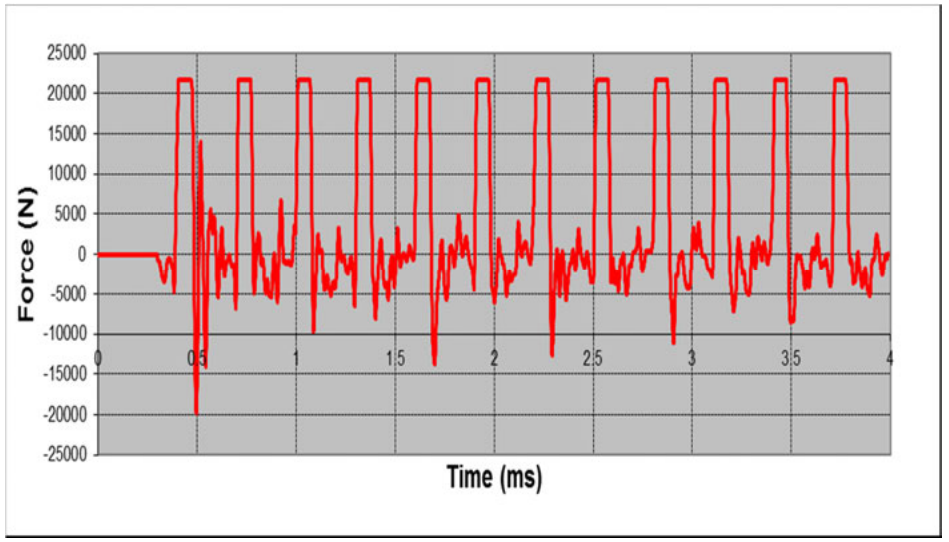

Specimen No.	Scalp thickness	Implement weight	Gas gun pressure	Striker velocity	Impact energy	Peak force	Presence of fracture	Hard tissue damage
P06-14	No skin	200g	240KPa	24.72m/s	55.68J	12400N	Yes	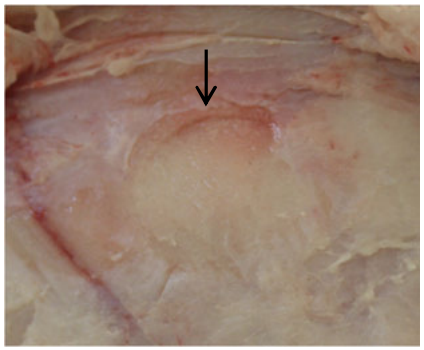 Slight semi-circular depressed fracture (18mm x 5mm)

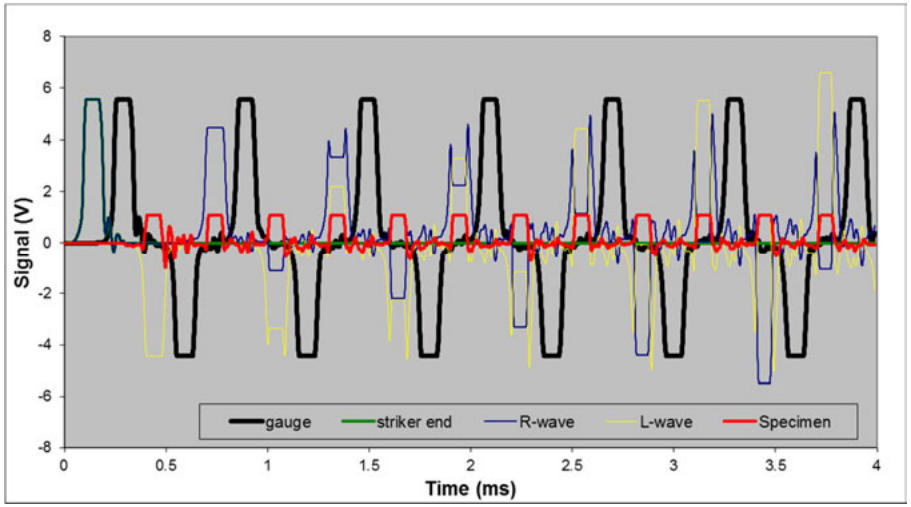

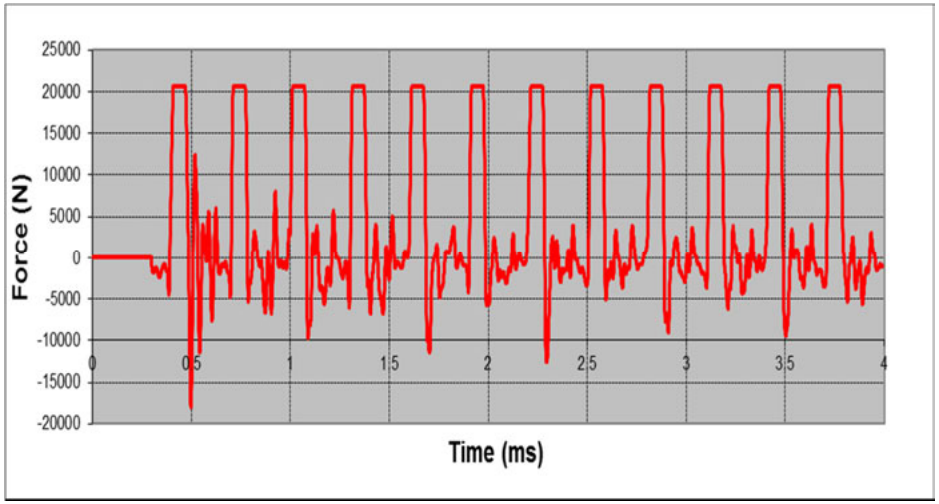

Appendix D
Author Guidelines
International Journal of Legal Medicine

International Journal of Legal Medicine

Editors in chief: H. Pfeiffer, Th. Bajanowski

ISSN: 0937-9827 (print version)

ISSN: 1437-1596 (electronic version)

Journal no. 414

IF: 2.686 (2012)

Instructions for authors

Manuscript Submission

Submission of a manuscript implies: that the work described has not been published before; that it is not under consideration for publication anywhere else; that its publication has been approved by all authors, if any, as well as by the responsible authorities – tacitly or explicitly – at the institute where the work has been carried out. The publishers will not be held legally responsible should there be any claims for compensation.

Permissions

Authors wishing to include figures, tables, or text passages that have already been published elsewhere are required to obtain permission from the copyright owner(s) for both the print and online format and to include evidence that such permission has been granted when submitting their papers. Any material received without such evidence will be assumed to originate from the authors.

Online submissions

Authors should submit their manuscripts online. Electronic submissions substantially reduce the editorial processing and reviewing times and shortens the overall publication times.

Title page

The title page should include:

- The name(s) of the author(s)
- A concise and informative title
- The affiliation(s) and address(es) of the author(s)
- The email address, telephone and fax numbers of the corresponding author

Abstract

Please provide an abstract of 150 to 250 words. The abstract should not contain any unidentified abbreviations or unspecified references

Keywords

Please [provide 4 to 6 keywords which can be used for indexing purposes.

Text formatting

Manuscripts should be submitted in Word.

- Use normal, plain font (e.g., 12 point Times Roman) for text
- Use italics for emphasis
- Use the automatic page numbering function to number the pages
- Do not use field functions
- Use tab stops or other commands for indents, not the space bar
- Use the table function, not spreadsheets, to make tables
- Use the equation editor or math type for equations
- Save your file in docx or doc format

Manuscripts with mathematical content can also be submitted in LaTeX

Headings

Please use no more than three levels of displayed headings

Abbreviations

Abbreviations should be defined at first mention and used consistently thereafter

Footnotes

Footnotes can be used to give additional information, which may include the citation of a reference included in the reference list. They should not consist solely of a reference citation, and they should never include the bibliographical details of a reference. They should also not contain any figures or tables.

Footnotes to the text are numbered consecutively; those to tables should be indicated by superscript lower case letters (or asterisks for significance levels and other statistical data). Footnotes to the title or the authors of the article are not given reference symbols.

Always use footnotes instead of endnotes.

Acknowledgements

Acknowledgements of people, grants, funds, etc. should be placed in a separate section before the reference list. The names of funding organisations should be written in full.

Citation

Reference citations in the text should be identified by numbers in square brackets. Some examples:

1. Negotiation research spans many disciplines [3].
2. This result was later contradicted by Becker and Siligman [5].
3. This effect has been widely studied [1-3, 7].

Reference list

The list of references should only include works that are cited in the text and that have been published or accepted for publication. Personal communications and unpublished works should only be mentioned in the text. Do not use footnotes or endnotes as a substitute for a reference list.

The entries in the list should be numbered consecutively.

- Journal article

  Gamelin FX, Baquet G, Berthoin S, Thevenet D, Nourry C, Nottin S, Bosquet L (2009) Effect of high intensity intermittent training on heart rate variability in prepubescent children. Eur J Appl Physiol 105:731-738. doi: 10.1007/s00421-008-0955-8

  Ideally the names of all authors should be provided, but the usage of “et al” in long author lists will also be accepted:

  Smith J, Jones M Jr, Houghton L et al (1999) Future of health insurance. N Eng J Med 965:325-329

- Article by DOI

  Slifka MK, Whitton JL (2000) Clinical implications of dysregulated cytokine production. J Mol Med. doi:10.1007/s001090000086

- Book

  South J, Blass B (2001) The future of modern genomics. Blackwell, London

- Book chapter

Brown B, Aaron M (2001) The politics of nature. In: Smith J (ed) The rise of modern genomics, 3rd edn. Wiley, New York, pp230-257

- Online document

  Cartwright J (2007) Big stars have weather too. IOP Publishing PhysicsWeb. http://physicsweb.org/articles/newa/11/6/16/1. Accessed 26 June 2007

- Dissertation

  Trent JW (1975) Experimental acute renal failure. Dissertation, University of California

Always use the standard abbreviation of a journal's name according to the ISSN List of Title Word Abbreviations, see

www.issn.org/2-22661-LTWA-online.php

Tables

- All tables are to be numbered using Arabic numerals.
- Tables should always be cited in text in consecutive numerical order.
- For each table, please supply a table caption (title) explaining the components of the table.
- Identify any previously published material by giving the original source in the form of a reference at the end of the table caption.
- Footnotes to tables should be indicated by superscript lower case letters (or asterisks for significance values and other statistical data) and included beneath the table body

Artwork and illustrations guidelines

For the best quality final product, it is highly recommended that you submit all of your artwork – photographs, line drawings, etc. – in an electronic format. Your art will then be produced to the highest standards with the greatest accuracy to detail. The published work will directly reflect the quality of the artwork provided.

Electronic figure submission

- Supply all figures electronically.
- Indicate what graphics program was used to create the artwork.
- For vector graphics, the preferred format is EPS; for halftones, please use TIFF format. MS Office files are also acceptable.
- Vector graphics containing fonts must have the fonts embedded in the files.
- Name your figure files with "Fig" and the figure number, e.g., Fig1.eps.

Line art

- Definition: black and white graphics with no shading.
- Do not use faint lines and/or lettering and check that all lines and lettering within the figures are legible at final size
- All lines should be at least 0.1mm (0.3 pt.) wide.
- Scanned line drawings and line drawings in bitmap format should have a minimum resolution of 1200dpi
- Vector graphics containing fonts must have the fonts embedded in the files.

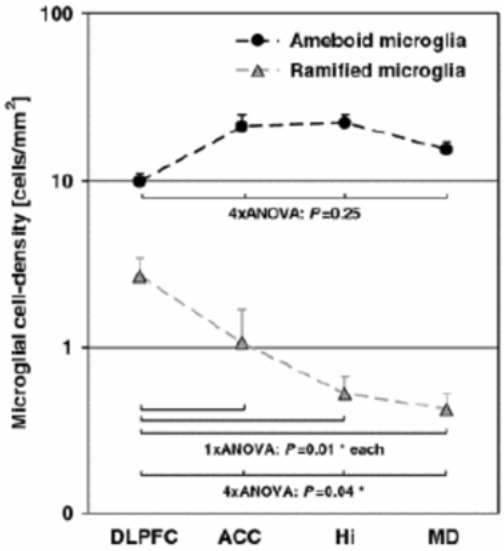

Halftone art

- Definition: Photographs, drawings, or paintings with fine shading, etc.
- If any magnification is used in the photographs, indicate this by using scaling bars within the figures themselves.
- Halftones should be a minimum resolution of 300dpi

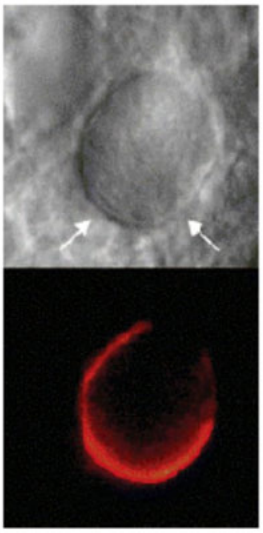

Combination art

- Definition: a combination of halftone and line art, e.g., halftones containing line drawing, extensive lettering, colour diagrams, etc.
- Combination artwork should have a minimum resolution of 600dpi

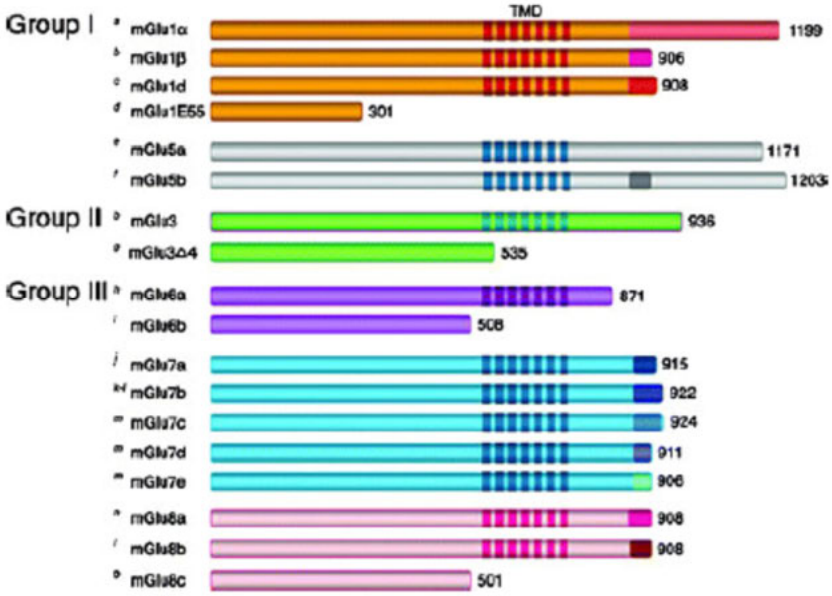

Colour art

- Colour art is free of charge for online publication.
- If black and white will be shown in the print version, make sure that the main information will still be visible. Many colours are not distinguishable from one another when converted to black and white. A simple way to check this is to make a xerographic copy to see if the necessary distinctions between the different colours are still apparent.
- If the figures will be printed in black and white, do not refer to colour in the captions.
- Colour illustrations should be submitted as RGB (8 bits per channel).

Figure lettering

- To add lettering. It is best to use Helvetica or Arial (sans serif fonts).
- Keep lettering consistently sized throughout your final-sized artwork, usually about 2-3mm (8-12pt).
- Variance of type size within an illustration should be minimal.
- Avoid effects such as shading, outline letters, etc.
- Do not include titles or captions within your illustrations.

Figure numbering

- All figures are to be numbered using Arabic numerals.
- Figures should always be cited in text in consecutive numerical order.
- Figure parts should be denoted by lowercase letters (a, b, c, etc.).

- If an appendix appears in your article and it contains one or more figures, continue the consecutive numbering of the main text. Do not number the appendix figures, “A1, A2, A3, etc.” Figures in online appendices (Electronic Supplementary Material) should, however, be numbered separately.

Figure captions

- Each figure should have a concise caption describing accurately what the figure depicts.
- Figure captions begin with the term Fig. in bold type, followed by the figure number, also in bold type.
- No punctuation is to be included after the number, nor is any punctuation to be placed at the end of the caption.
- Identify all elements found in the figure in the caption; and use boxes, circles, etc., as coordinate points in graphs
- Identify previously published material by giving the original source in the form of a reference citation at the end of the figure caption.

Permissions

If you include figures that have already been published elsewhere, you must obtain permission from the copyright owner(s) for both the print and online format. Please be aware that some publishers do not grant electronic rights for free and that Springer will not be able to refund any costs that may have occurred to receive these permissions. In such cases, material from other sources should be used.

Ethical standards

Manuscripts submitted for publication must contain a declaration that the experiments comply with the current laws of the country in which they were performed. Please include this note in a separate section before the reference list.

Conflict of interest

Authors must indicate whether or not they have a financial relationship with the organisation that sponsored the research. This note should be added in a separate section before the reference list.

If no conflict exists, authors should state: The authors declare that they have no conflict of interest.

Animal welfare

If applicable, the authors attest that experiments conducted on animal subjects complied with all applicable laws, regulations and standards in the country where the experiments were performed.

In general it is expected that animal experimentation published in the International Journal of Legal Medicine complies with prevailing standards in either the European Union or the United States

Scientific style

- Please always use internationally accepted signs and symbols for units, SI units.
- Genus and species names should be in italics.